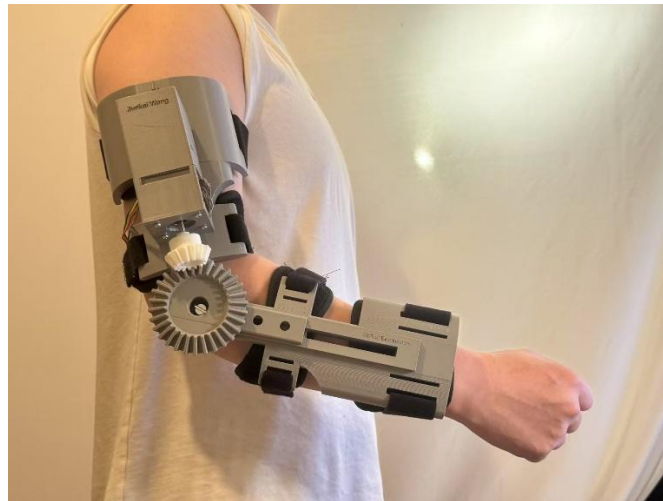




**EEEE3001**

## **Final Year Individual Project Dissertation**

### **Smart exoskeleton for patient rehab**



**AUTHOR:** **Mr Junkai Wang**

**DATE:** **May 1, 2025**

This third-year project Dissertation is submitted in part fulfilment of the requirements of the degree of Bachelor of Engineering.

## Abstract

This project focuses on the development of a 1-DOF optical sensor based exoskeleton to assist upper-limb rehabilitation, aiming to help patients regain muscle function. Traditional electromyography (EMG) systems often encounter issues such as sensitivity to electromagnetic interference, discomfort after long-term use, and high cost. To address these limitations, this work proposes and prototypes an alternative sensing method based on optical detection of muscle contractions. The resulting system aims demonstrate a functional platform that confirms the feasibility of optical sensing in wearable assistive devices and provides a modifiable foundation for future, more advanced implementations.

The prototype integrates three main subsystems: an optical sensing circuit, a real-time signal processing and control system, and a mechanical exoskeleton structure. First, the optical sensing system uses infrared LEDs and photodiodes to capture changes in muscle deformation during contraction. These signals are converted to voltages through a transimpedance amplifier (TIA) circuit and processed by a microcontroller (Feather M4). The signal is then filtered through a simple low pass filter and a Kalman filter to control the stepper motor accordingly. The mechanical structure was designed and 3D printed to provide lightweight support around the user's elbow joint, focusing on comfort, adjustability, and ease of assembly.

The research confirmed that the optical sensing system was able to detect meaningful muscle contraction signals and successfully trigger motor-driven exoskeleton movement in real time. However, due to the complexity of biological signals and the limitations of current low-cost sensing circuit, the data remained somewhat inconsistent under different conditions as expected, particularly in terms of signal amplitude and baseline drift. Nevertheless, through signal filtering, calibration, and control parameter tuning, the system demonstrated a stable and functional prototype suitable for 1-DOF upper-limb rehabilitation assistance. Risk management strategies, including tuning thresholds and limiting motor torque, were also applied to protect users and hardware.

Overall, the results successfully demonstrated the feasibility of using optical sensing in wearable rehabilitation devices. While this project remains an early-stage prototype, it highlights key advantages in terms of comfort, portability, and cost. More advanced signal processing algorithms, integration with machine learning and personalized calibration can be implemented in the future to achieve wider applications, including applying the system to a wider range of rehabilitation scenarios, such as assisting age-related motor function decline and full body support solutions.

# Contents

<b>ABSTRACT .....</b>	<b>II</b>
<b>LIST OF FIGURES .....</b>	<b>V</b>
<b>LIST OF TABLES.....</b>	<b>VI</b>
<b>1 INTRODUCTION.....</b>	<b>1</b>
1.1 BACKGROUND .....	1
1.2 PROJECT OVERVIEW.....	1
1.3 SPECIFICATION .....	2
1.3.1 <i>Optical System Design (Data Acquisition)</i> .....	2
1.3.2 <i>Signal Processing and Control System</i> .....	3
1.3.3 <i>Basic Exoskeleton Design and Construction</i> .....	3
1.4 METHODOLOGY .....	3
1.4.2 <i>Optical System Design (Data Acquisition)</i> .....	3
1.4.3 <i>Signal Processing and Control System</i> .....	4
1.4.3 <i>Basic Exoskeleton Design and Construction</i> .....	4
1.5 RISK MANAGEMENT AND MITIGATION .....	4
<b>2 PROJECT DESIGN BACKGROUND AND THEORY .....</b>	<b>6</b>
2.1 EXOSKELETON.....	6
2.1.1 <i>Actuators</i> .....	7
2.1.2 <i>Degree of Freedom</i> .....	8
2.1.3 <i>Exoskeleton Summary</i> .....	8
2.2 BIOMECHANICS OF HUMAN ARM .....	9
2.3 SIGNAL ACQUISITION TECHNIQUES (EMG AND OPTICAL SENSING) .....	10
2.3.1 <i>Electromyography (EMG) Signals</i> .....	11
2.3.2 <i>Optical Sensing Signals</i> .....	12
2.4 CONCLUSION OF PROJECT CONFIGURATION .....	14
<b>3 SYSTEM MODELLING AND DEVELOPMENT .....</b>	<b>15</b>
3.1 SYSTEM OVERVIEW AND ARCHITECTURE .....	15
3.1.1 <i>System Structure</i> .....	15
3.1.2 <i>Tool Use</i> .....	15
3.2 OPTICAL SENSOR CIRCUIT MODELLING AND DESIGN .....	16
3.2.1 <i>Requirements and Design Criteria</i> .....	16
3.2.2 <i>Optical System Design Considerations and Architecture</i> .....	17
3.2.3 <i>Detailed Design of Optical Sensor System</i> .....	19
3.2.4 <i>Implementation and Construction (Limitations and Challenges)</i> .....	24
3.3 SIGNAL PROCESSING AND CONTROL SYSTEM .....	29
3.3.1 <i>Overview System Architecture and Design requirement</i> .....	30
3.3.2 <i>Signal Processing and Filtering</i> .....	32
3.3.3 <i>Contraction Detection and Motor Control Algorithm</i> .....	34
3.3.4 <i>Real-Time Performance Testing and Tuning (Limitations)</i> .....	36
3.4 EXOSKELETON 3D MODEL DESIGN AND CONSTRUCTION .....	40
3.4.1 <i>Design Requirements and Exist System Review</i> .....	40
3.4.2 <i>3D Modelling</i> .....	41
3.4.3 <i>3D printing and Mechanical Testing (Limitations discussed)</i> .....	45
<b>4 FINAL SYSTEM TESTING AND VALIDATION .....</b>	<b>47</b>
4.1 TESTING SETUP AND PREPARATION.....	47
4.2 FINAL SYSTEM TEST .....	49

4.2.1	<i>Functional Test</i> .....	49
4.2.2	<i>Accuracy and Repeatability Evaluation</i> .....	50
4.2.3	<i>System Latency and Responsiveness</i> .....	51
4.3	SPECIFICATION COMPLIANCE REVIEW (CONCLUSION AND LIMITATIONS) .....	53
<b>5</b>	<b>CONCLUSION</b> .....	<b>54</b>
5.1	PROJECT CONCLUSION .....	54
5.2	FUTURE IMPROVEMENTS .....	55
5.3	CONSIDERATION OF SYSTEM WITHIN THE WIDER CONTEXT .....	55
5.4	REFLECTION ON PROJECT MANAGEMENT .....	56
<b>6</b>	<b>REFERENCES</b> .....	<b>58</b>
<b>APPENDICES</b> .....		<b>I</b>
<b>APPENDIX I – PROJECT PROGRESS FORMS</b> .....		<b>I</b>
<b>APPENDIX II – PROJECT GANTT CHART</b> .....		<b>VI</b>
<b>APPENDIX III – ARDUINO CONTROL CODE</b> .....		<b>VII</b>

## List of Figures

Figure 1. Project system diagram from proposal .....	2
Figure 2. Classification of Exoskeletons [2] .....	6
Figure 3. Actuators power and weight comparison [10] .....	8
Figure 4. (a) Joint Movement of Upper Limb; (b) Kinematic model of the human arm [2]0 .....	9
Figure 5. (a) Arm muscles; (b) Muscles used for flexion and extension on elbow [13][14] .....	9
Figure 6. The sEMG signals at two different movement: (a) continuous clenching to unclenching of the fist; (b) continuous up and down turning of the wrist [16] .....	11
Figure 7. (a) Muscle structure and movement of myofilaments; (b) Sensor working principle [18][19] .....	12
Figure 8. (a) signal corresponding to isometric; (b) isotonic contractions; (c) Two isometric contractions followed by two isotonic contractions [22] .....	13
Figure 9. Optical sensor distribution for muscle contraction detection. ....	13
Figure 10. Smart exoskeleton system overview .....	15
Figure 11. light penetration depths into the tissue for red and infrared light [21] .....	17
Figure 12. Comparison between the acquired data using three different light wavelengths [19] ....	18
Figure 13. Block Diagram of Optical sensing system .....	18
Figure 14. LED circuit schematic and simulation results.....	20
Figure 15. EPM-4001 photodiode characteristics [37] .....	20
Figure 16. TIA circuit.....	20
Figure 17. Schematic of TIA and filtering stage.....	22
Figure 18. Schemic of the Optical sensor circuit .....	23
Figure 19. placement of LEDs and photodiodes.....	23
Figure 20. Adafruit Feather M4 Express Pin configuration [23].....	24
Figure 21. LED Circuit build in Tinkercad .....	25
Figure 22. LED Circuit build in Breadboard .....	25
Figure 23. LED Circuit test result .....	26
Figure 24. MCP6292 amplifier [39].....	26
Figure 25. TIA and LP Filter circuit build in Tinkercad .....	26
Figure 26. TIA + LP Filter Circuit build on Breadboard .....	27
Figure 27. (a) Optical system test wrap; (b) The waveform of a biceps contraction .....	27
Figure 28. Schematic of second stage amplifier and filters.....	28
Figure 29. (a). Second stage amplifier added; (b) shortening the distance between the LED and the photodiode to 16mm muscle contraction test .....	29
Figure 30. Elbow torque and MMG signal during a complete flexion task in healthy adult males [26] .....	31
Figure 31. Block diagram of Control Process .....	32
Figure 32. ADC implementation .....	33
Figure 33. Open source simple Kalman Filter output [28].....	33
Figure 34. Kalman Filter implementation.....	34
Figure 35. Linear mapping of the muscle signals .....	34
Figure 36. Control system flowchart.....	35
Figure 37. Comparison of analogue output (oscilloscope) and digital output (serial plot).....	37
Figure 38. Motor FeatherWing and NEMA 17 connection .....	38
Figure 39. Example of motor control at different elbow flexion angles .....	38
Figure 40. Motor-controlled simulated arm positions at 0°, 30°, 60°, and 90°, with corresponding digital data from the Arduino Serial Monitor.....	39
Figure 41. Exoskeleton 3D model designed in Fusion 360.....	40
Figure 42. Types of common gears [33].....	42

Figure 43. Upper arm 3D model dimensions .....	43
Figure 44. Power transfer bevel gear system .....	44
Figure 45. Forearm arm design.....	44
Figure 46. Exported STL files for 3D print .....	45
Figure 47. Exoskeleton Parts: Upper arm, Forearm and pinion Gear .....	46
Figure 48. Fully assembled exoskeleton .....	47
Figure 49. Final assembled system.....	48
Figure 50. (a)PD output from Oscilloscope; (b) Serial Plotter output (Value 1: Raw; Value 2: Filtered) in test setup .....	48
Figure 51. Six frames showing one full cycle of elbow flexion and return ( $0^{\circ} \rightarrow 90^{\circ} \rightarrow 0^{\circ}$ ) .....	49
Figure 52. Exoskeleton output at target angles $0^{\circ}$ , $30^{\circ}$ , $60^{\circ}$ , and $90^{\circ}$ (forearm not fixed) .....	50
Figure 53. System response frame with time .....	52
Figure 54. Improved system response frame with time .....	52

## List of Tables

Table 1. Classification and comparison of actuators [9].....	7
Table 2. Muscles Responsible for Upper Limb Joint Movements [2].....	10
Table 3. Functional requirement of project .....	16
Table 4. Optical Sensor Design Specifications .....	17
Table 5. Key components for sensing system .....	19
Table 6. OP240 Electrical Characteristics [38] .....	19
Table 7. design parameters for TIA and LP filter .....	26
Table 8. Mean Segment Weight as Percentage of Total Body Weight [26] .....	30
Table 9. Mean Segment length as Percentage of Total Body Length[26] .....	30
Table 10. NEMA 17 stepper motor [28] .....	31
Table 11. Stepper motor operation mode .....	31
Table 12. LP and Kalman Filter parameters .....	37
Table 13. Obtained voltage and motor target angles at elbow of $60^{\circ}$ .....	39
Table 14. Robotic rehabilitation systems used for upper limb.....	41
Table 15. Mean Segment length as Percentage of Total Body [26] .....	42
Table 16. Comparison of PLA and ABS Properties [35] .....	46
Table 17. Accuracy and repeatability test results .....	50
Table 18. Specification Compliance Summary .....	54

# 1 Introduction

## 1.1 Background

Every year, millions of individuals experience severe motor impairments due to various diseases or accidents, significantly impacting their daily lives. For example, in 2023, approximately 15 million people worldwide suffered a stroke, with 5 million deaths and another 5 million left permanently disabled [1]. One of the most common consequences of stroke is upper limb weakness, affecting approximately 77% of stroke survivors [2]. It is also important to note that stroke is not the only condition that leads to upper limb weakness, other disorders such as muscular dystrophy, arthritis, and diabetes can also cause similar results [2]. In the past decades, worldwide increase of cardiometabolic diseases lead to elevated number of patients suffer from upper limb motor dysfunction, creating an unmet need for rehabilitation. Although medical treatments have greatly reduced the patients' life risk, limited options are available to restore the life quality for those who lost proper muscle function. Rehabilitation approach is an effective method for these individuals to regain muscle function and mobility. However, physical therapy can be a time-intensive and demanding process for both patients and therapists. Robotic-assisted rehabilitation has therefore emerged as a promising alternative, offering consistent support while reducing the burden on patients and therapists [2][3].

Currently, robotic rehabilitation devices can be generally classified into three categories: end effectors, exoskeletons, and hybrid systems [2]. Among these, exoskeletons are worn by the user and provide support throughout the full range of motion, enabling more natural movement patterns. Despite the significant potential of exoskeletons to mimic natural movement and deliver targeted assistance, most development efforts have focused on lower-limb rehabilitation, with relatively fewer solutions available for the upper limbs [2][3][6].

## 1.2 Project Overview

To address this gap, this project aims to develop a smart exoskeleton arm brace for upper-limb rehabilitation. This device will use an optical sensing system to detect muscle contractions and adjust the brace accordingly. By aiming to "amplify" the patient's movements and strength, rather than forcing motion, this approach will provide a more intuitive and supportive experience, ultimately benefiting patients with impaired muscle memory regain functional abilities.

This project specifically focuses on designing a single-degree-of-freedom (1 DOF) exoskeleton for the elbow, targeting relevant muscles for flexion and extension, including the Biceps Brachii, Brachioradialis, Brachialis, and Triceps Brachii [2][11]. Unlike traditional surface electromyography (sEMG) systems, an optical sensing system will be developed, offering advantages such as reduced sensitivity to sweat, immunity to electromagnetic interference, and the ability to detect deeper muscle activity compared with sEMG [4]. However, since optical sensing technology essentially detects changes in reflected light signals caused by changes in muscle shape and blood flow, complex interactions bring additional complexity and challenges. The interaction between light signals and human muscle responses can lead to complex and potentially unstable outputs, which will be discussed in later chapters. Considering the time and cost constraints of the project, this project will focus on the development and verification of a rehabilitation exoskeleton prototype based on optical sensors. Its main goal is to demonstrate the feasibility of optical sensing technology for rehabilitation equipment, lay a solid foundation for future research and development.

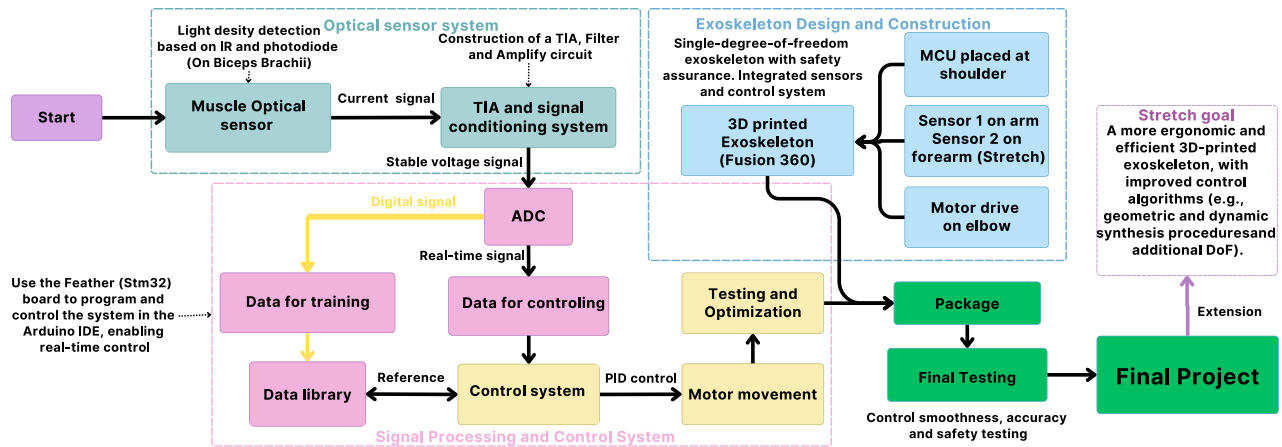


Figure 1. Project system diagram from proposal

To fill the above-mentioned gaps, the project will consist of three main sections as shown in Figure 1: optical sensor design, signal conditioning and processing, control system design, and exoskeleton design and construction. The first three parts are critical to building the system and present significant challenges, each requiring substantial time and research. Since these components are highly interconnected, a simple yet complete and well tested system design would be the most effective approach.

## 1.3 Specification

The project is divided into three main subsystems: Optical System Design (3.2), Signal Processing and Control System (3.3), and Basic Exoskeleton Design and Construction (3.4). As indicated in the overall aim, the exoskeleton design is a lower-priority goal compared to the development of the core sensing and control system. Allt the points are given by decreasing priority.

### 1.3.1 Optical System Design (Data Acquisition)

**Optical muscle signal sensing:** The key and the most challenging part of this project is the design and construction of the optical sensor for the muscle flexion and extension detection. The general idea is using LED emitters and photodetectors to measure the changes in LED light passing through muscles [5]. The density of the detected light indicates muscle contractions. After that, record the outputs of the muscle signals and compare them with traditional sEMG to ensure the accuracy of the sensor under various conditions [4]. The goal is to achieve an accuracy of 70% or the system shows reasonable outputs which can reflect the muscle activities.

**Signal filter and amplification:** The proposal of the signal filter and amplification circuit is to condition the raw photodiode signals so they can be used by the control system. First, the transimpedance amplifier (TIA) will convert photodiode current signals to voltage. Then, the filtering circuit is using to improving the signal-to-noise ratio. A bandpass filter with a cutoff frequency of 6Hz and 60Hz will be implemented, where 6Hz is used to filter other noisy environments and 60Hz is used to filter noise from interference of electronic devices. Afterwards, the filtered signal is amplified for further processing. The goal is ensuring the outputs of the optical system are stable with small noise interference under oscilloscope or similar tool.



### 1.3.2 Signal Processing and Control System

This part of the project focuses on real-time signal processing and motor control, using a Microcontroller Unit (MCU) that is compact, lightweight, and capable of supporting all required functionalities. The Feather M4 Express was selected for its balance of processing power, size, and compatibility with embedded control applications.

**Data conversion:** The first step is coding an ADC module that converts the analogue muscle signals from the optical sensors into digital form suitable for the MCU processing.

**Data for training data library:** Then, to precisely control the motor responding to the muscle activities, the dataset for muscle activity is required [2]. The library should include at least 50 samples of different contraction states obtained through experiments. This data will be critical for refining the control system's response.

**Motor control system based on data library:** Finally, develop a control system using the muscle activity data from the library to drive the motor in real-time. Implement a PID control algorithm or other suitable methods that use the processed signals to achieve smooth motor movement. The motor should be able to smoothly control the elbow joint with minimal delay and provide assistance consistent with muscle contraction.

The goal is to achieve a motor response within 0.5s following a change in muscle activity, and to actuate the exoskeleton in a coordinated manner without overcorrection or noticeable lag.

### 1.3.3 Basic Exoskeleton Design and Construction

The exoskeleton is designed provide 1-DoF for elbow flexion and extension support, focusing on lightness, safety, and user comfort. The motor will be at the elbow, sensors on the upper arm and forearm, and the MCU at the shoulder. The design includes motor torque transmission, adjustable straps and proper cable management.

**Stretch goal:** If the primary goal of designing a basic rehabilitation exoskeleton system that responds to muscle activity and controls the motor is achieved, the extended goal would involve completing the 3D printing of a robust exoskeleton to house the system, as well as improving the control algorithm to enhance the system's response speed and overall performance.

## 1.4 Methodology

### 1.4.2 Optical System Design (Data Acquisition)

This method for detecting muscle activity uses photodiodes to measure the light intensity from IR LEDs passing through the muscle. Infrared light is selected because it penetrates muscle tissue effectively and the light source which wavelengths shorter than 600nm will be absorbed by red skin pigmentation [4]. The LEDs and sensors will be embedded in a flexible, wearable band that can be easily worn on the arm. By placing the LED and photodiode at around 20mm apart, and multiple sensor pairs will be distributed reasonably across the arm and forearm to account for muscles thickness variations of different wearer, with their data averaged for more accurate detection of muscle contractions. The photodiode's current signal will then be processed through a TIA to voltage, followed by a 6Hz to 60Hz bandpass filter and amplifier to remove environmental noise and electronic interference for a stable output with acceptable noise interference.

One challenge is managing interference from tissues in the arm, as well as determining the optimal distribution of LEDs and sensors to achieve the most accurate readings. This will require considerable experimentation and research. Additionally, due to limited budget and knowledge of optical systems, more time will be needed for research and optimization of sensor distribution. However, for the TIA and signal conditioning circuit, less time will be required, as this is similar to the circuit design used in the Year 2 pulse oximeter project.

Although this method reduces sensitivity to sweat and electromagnetic interference [4], the system may be less accurate compared to sEMG due to project budget and time constraints, as well as the complexity of reflected light behaviour caused by the intricate structure of human physiology.

### 1.4.3 Signal Processing and Control System

The Feather M4 microcontroller was chosen for its small size and lightweight design, making it ideal for wearable device design like this project. An ADC module will be used to convert the analogue signal of the optical sensor into digital form for the MCU. The programming will be conducted using the Arduino IDE, ensuring compatibility with the system's hardware. After setup the environment, muscle contraction data will be collected in a reference data library with at least 50 samples of different muscle states. This library will be used to drive the motor based on detected muscle activity. A PID control algorithm will be implemented to ensure smooth motor movements, allowing fine-tuned adjustments to motor speed and torque.

The challenge will be ensuring real-time processing of muscle signals but avoid delays in motor response. Additionally, the control system is complex for smooth movement without overcorrection will require careful adjustment which need long time testing and a fully developed system [6]. However, the experience gained from previous motor control projects (Year 1) will help minimize development time.

Limitations are time and design level constraints, which may prevent the control system from being fully optimized within the project timeline. However, the system is still able to respond to basic arm movements. Continued improvements will be required to perfect the control system over time (Applying geometric and dynamic synthesis procedures [6]). Nonetheless, safety will be prioritized during development to ensure the motor control system operates within parameters that are safe for the user.

### 1.4.3 Basic Exoskeleton Design and Construction

The 3D modelling for the exoskeleton will be carried out using Fusion360 for its ease of use, robust features, and support for rapid prototyping. However, some time will be needed to familiarize with the software. Since the project focuses on a 1-DoF exoskeleton for elbow movement, the design will be relatively simple compared to more complex exoskeletons, such as those for hand or finger movement. The motor will be placed at the elbow to assist with flexion and extension, while the MCU will be positioned at the shoulder for minimal obstruction. The sensors will be placed on the upper arm and forearm to accurately detect muscle contractions.

## 1.5 Risk Management and Mitigation

**Delay in Receiving Components:** Components may not arrive until late November, potentially delay project start-up and system assembly, putting the project timeline behind schedule. The likelihood and impact will be medium, as the impact of hardware delays, sensor and system development timeline delays can be reduced through adequate preparation.

Mitigation: Begin simulations and design early. Borrow lab equipment to perform preliminary tests, ensuring that once components arrive, assembly can proceed immediately.

**Optical Sensor Inaccuracy:** At the first part of the project, optical sensors may not provide the accuracy required to detect muscle contractions, rendering subsequent work impossible or producing erroneous results. The likelihood is medium, but the impact is high, and the accuracy of the sensor data can affect the function of the control system and the final results of the project.

Mitigation: Integrate EMG electrodes to supplement the optical system and improve accuracy. Hybrid setup will allow for better muscle signal detection.

**System Development (Software Learning and Safety Concerns):** Limited familiarity with software tools (e.g. Feather M4, Fusion360) can affect the progress and quality of the project and disrupt the plan. Learning these software will consume a lot of time, and unfamiliarity and limited experience with these key software will seriously affect the project progress. The likelihood is low, the impact is high. Since this risk may happen at MCU processing part, while the work at software is the main job. Mitigation: Start learning the software early and look for online resources such as YouTube. Also plan ahead what software will use and learn those software in parallel at preparation stage. If necessary, use another more familiar or simpler software.

**Sensor and System Integration:** Integrating motor, sensors, and MCU may take longer than expected due to complexity or the initial design is not working. Potentially leading to redesigns which will waste a lot of time and the whole-time plan will be influenced. This risk could happen in the mid to late project. The likelihood is low, and the impact is High.

Mitigation: Test subsystems individually before full integration. Early testing allows for smooth final assembly with fewer errors. Always have a plan B when doing any part, and communicate fully with the supervisor to try to find possible solutions

**Data loss:** Potential data loss due to improper file management or software crashes. Low likelihood high impact.

Mitigation: Set up automatic backups and manually back up critical project files regularly to prevent loss of data.

**Safety Considerations:** Because this project is an exoskeleton that assists the human arm, if the exoskeleton is worn on the arm and excessive pressure is applied or it is moved unexpectedly, the motor may fail or operate with excessive force, resulting in injury. The possibility should be zero, because this is the first thing to consider, and once it happens, the impact will be serious.

Mitigation: Implement safety limits in the motor control system to prevent excessive torque or speed. Include an emergency stop function that can immediately halt motor operation if an unsafe condition is detected. Add a safety feature to the exoskeleton frame design to prevent any posture that is not safe for the human body.

## 2 Project Design Background and Theory

With an increasingly ageing population and higher incidences of neurological disorders, the global demand for effective rehabilitation solutions is rapidly growing. Among various medical conditions, stroke is one of the leading causes of long-term disability, significantly impairing motor functions and reducing the quality of life [1][2]. According to the World Health Organization (WHO), over 15 million people worldwide suffer from stroke each year, of whom approximately 5 million remain permanently disabled, requiring prolonged rehabilitation treatment and continuous assistance in daily activities [1]. Such statistics underline the urgency and importance of developing efficient and accessible rehabilitation therapies.

Conventionally, rehabilitation for stroke patients heavily relies on manual physical therapy administered by trained therapists. While this approach can be effective, it comes with considerable limitations, such as high cost, limited availability and therapy duration [2]. To address these limitations, robotic rehabilitation solutions, particularly exoskeleton technology, have emerged as promising alternatives. Exoskeletons are wearable robotic systems designed to assist or augment human limb movements, offering consistent rehabilitation interventions. Developing such systems involves integrating knowledge across several disciplines, including mechanical engineering for structural design and actuation, biomechanics to understand human movement dynamics, and sensing technologies to accurately detect muscle activities. The following sections will discuss these key elements for this project.

### 2.1 Exoskeleton

In the field of robotics, exoskeletons represent one of the most representative wearable devices, which can help people easily achieve motor functions and therefore play a vital role in rehabilitation and functional assistance. Exoskeletons can generally be classified into two main categories: rehabilitation exoskeletons and assistive exoskeletons.

Rehabilitation exoskeletons focus primarily on therapeutic interventions aimed at restoration of impaired motor functions through repeated movements and controlled exercises. As the name suggests, assistive exoskeletons provide long term or continuous support to enhance the physical capabilities for individuals with disabilities or diminished muscle strength [8]. Based on their anatomical application and actuators, exoskeletons can also be classified into upper-limb or full-body and active or passives exoskeletons depending on the target as shown in Figure 2.

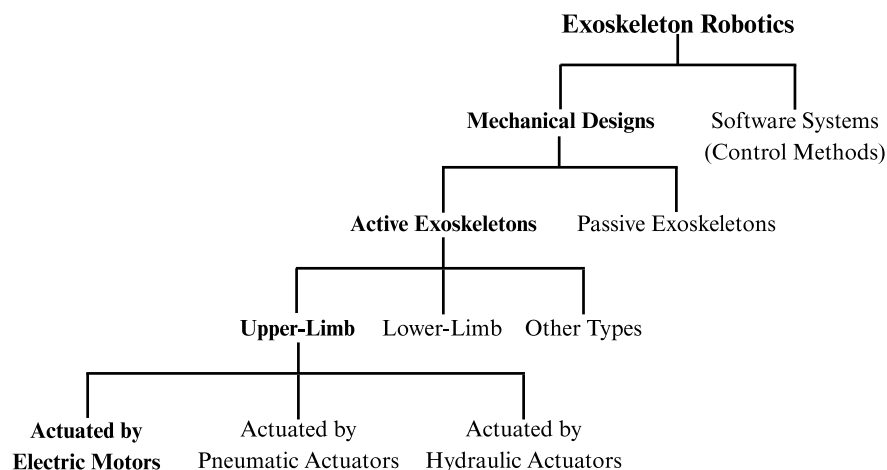


Figure 2. Classification of Exoskeletons [2]

The aim of this project is to develop an exoskeleton focused on upper-limb rehabilitation, specifically targeting the Biceps Brachii muscle for assisting elbow flexion and restoring arm motor function. Therefore, the system can be categorized as an active upper-limb exoskeleton, in which movement is driven by powered actuators rather than passive mechanisms.

### 2.1.1 Actuators

Actuator is the key component in robotics field that used to conduct movements. A variety of actuation technologies are available for exoskeleton development, including electric motors, pneumatic actuators, and hydraulic actuator, each with distinct advantages, limitations, and control strategies. For example, electric motors, especially stepper and servo motors, are the most widely used due to their high precision, relatively simple control, compact size, and cost-effectiveness [9]. They are particularly suitable for portable, lightweight applications like this project. The brief conclusion of the actuators is illustrated in Table 1.

Table 1. Classification and comparison of actuators [9]

Property	Electric motors	Pneumatic actuator	Hydraulic actuator
Force	Low	Moderate	High
Initial cost	High	Low	High
Operating and maintenance costs	Low	Moderate	High
Precision control	High	Moderate	Moderate
Operating conditions	Not suited for applications with extreme operating conditions	Best suited for applications with high temperatures and hazardous environments	Cannot operate in some hazardous environments
Environmental effects	No fluid leaks hence environmental hazards are eliminated	Risk of environmental hazards due to contamination of compressed air by lubricants or other fluids	Hydraulic fluid leaks lead to environmental hazards
Size	Small	Moderate	Large
Noise	Quiet operation	Noisy due to the presence of the compressor	Noisy due to the presence of a hydraulic pump
Speed	Smooth, variable speed with controlled acceleration	More susceptible to stick-slip and varying load. Well-suited for light high-speed applications.	Difficult to control accurately. Varies with temperature and wear. Stick slip can be a problem
Repeatability	Repeatable, reproducible performance during the entire product life	Very contamination sensitive. Require regular maintenance. Seals are prone to leak.	Very contamination sensitive
Efficiency	High	Low	Moderate

According to Table 1, and considering the project's time, cost, and portability constraints, electrical actuation using a stepper motor was chosen. Stepper motors allow for precise angular control without requiring a precise closed-loop feedback system, which simplifies the design and reduces development time. Additionally, they are readily available, inexpensive, and easy to interface with standard microcontrollers (Adafruit Feather M4 Express). In contrast, while hydraulic actuators provide higher force output and faster response, their complexity, cost, and maintenance needs make them unsuitable for a lightweight wearable prototype. Similarly, pneumatic system is fast and inexpensive, but it requires bulky external air supplies and lack the positional precision needed for joint rehabilitation. The three actuators' weight and power comparison is shown in Figure 3.

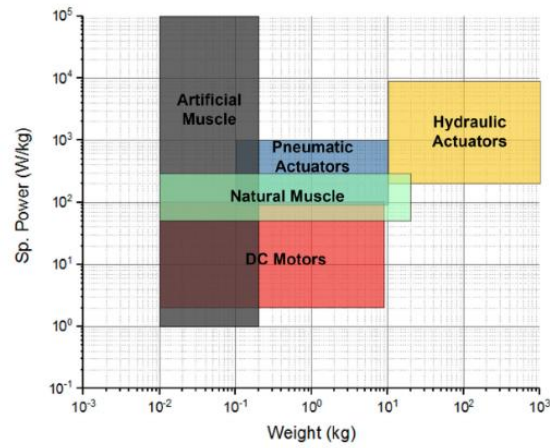


Figure 3. Actuators power and weight comparison [10]

Furthermore, a comparative study by Pustavrh et al. evaluated hydraulic, pneumatic, and electric linear actuator systems under similar load conditions. The study found that electric systems achieved the smoothest response and the lowest energy consumption, highlighting their efficiency and suitability for applications requiring precise and consistent motion control. In contrast, hydraulic systems, while capable of high force output, were noted for their potential environmental hazards due to fluid leakage and higher maintenance requirements. Pneumatic systems, although lightweight and fast, lacked the positional accuracy and required external air supplies, making them less ideal for precise rehabilitation tasks [10]. Therefore, stepper motors represent the most balanced and practical choice for this project's application.

### 2.1.2 Degree of Freedom

Next, since an exoskeleton can be regarded as a type of articulated robotic system composed of interconnected segments, it is essential to consider the types of joints and motions that define its degrees of freedom (DOF) [2]. Each joint in an exoskeleton allows specific types of movement, typically classified as translational, rotational, or mixed. The number and arrangement of these joints determine the DOF of the system, which directly influence the complexity and capability of the exoskeleton. A higher DOF provides more natural and flexible movement and moves more similarly to human biomechanics, but it also increases the difficulty in mechanical design and control. For example, a typical human upper limb possesses seven DOF that three at the shoulder (flexion/extension, abduction/adduction, internal/external rotation), one at the elbow (flexion/extension), and three at the wrist (flexion/extension, radial/ulnar deviation, and pronation/supination) [2]. In this project, one DOF exoskeleton that focuses on the elbow rotation joint will be developed.

### 2.1.3 Exoskeleton Summary

In conclusion, from the perspective of structural and functional classification, the proposed design can be defined as a one DOF upper-limb rehabilitation exoskeleton actuated by an electric motor. As a wearable robotic device, its mechanical structure and movement must align with human arm biomechanics, ensuring safe and effective support during rehabilitation exercises. Furthermore, to enable a responsive control, the actuation should be driven by related muscle activity signals. Therefore, a proper understanding of human biomechanics and muscle behaviour is essential and was illustrated in section 2.2.



## 2.2 Biomechanics of Human Arm

Biomechanics is the science of applying mechanical principles to understand the movement and structure of living organisms and can be seen as the application of Newtonian mechanics to the neuromuscular skeletal system [11]. In the context of rehabilitation exoskeleton, biomechanics is essential for a design that can safely and effectively interact with the human body. It enables engineers to model natural human motions, determine joint limitations, and evaluate the forces and torques generated during movement [11].

There are three important types of biomechanics. Medical biomechanics (clinical applications), sports biomechanics (aimed at improving athletic performance) and occupational biomechanics (supports workplace ergonomics and safety) [2]. In this project, the focus lies within medical biomechanics, particularly the kinematics and muscle dynamics of the arm, to guide the exoskeleton design for rehabilitation (detailed in section 3.4).

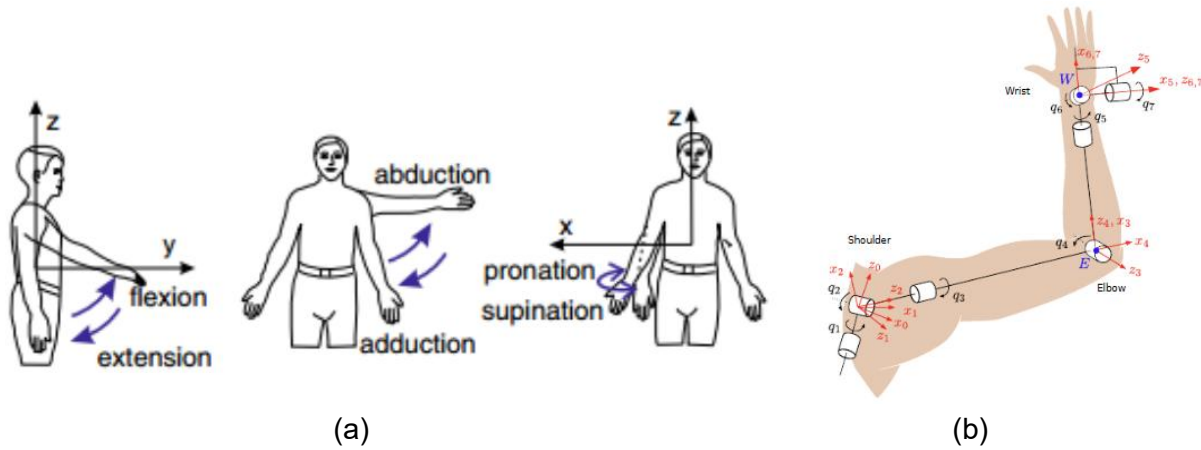


Figure 4. (a) Joint Movement of Upper Limb; (b) Kinematic model of the human arm [2][12]

The human arm is considered a highly developed system for performing complex movements in nature, and its motion is defined by how the bones and joints are structured and connected. The arm consists of three primary segments: the upper arm (humerus), the forearm (radius and ulna), and the hand [2]. These segments are connected by several joints, each providing different ranges and types of movement (DOF). Together, these joints provide up to seven degrees of freedom (7 DOF) in the upper limb. This wide range of motion is what enables humans to reach, grasp, lift, and manipulate objects in complex ways [13]. A diagram representing these movements is shown in Figure 4. To recreate such movements, exoskeletons are typically designed based on abstract models that mimic human limb kinematics, rather than directly replicating biological joints [2]. These designs aim to provide a simplified functional representation of the body's natural capabilities, with a focus on enhancing motion within therapeutic or assistive contexts.

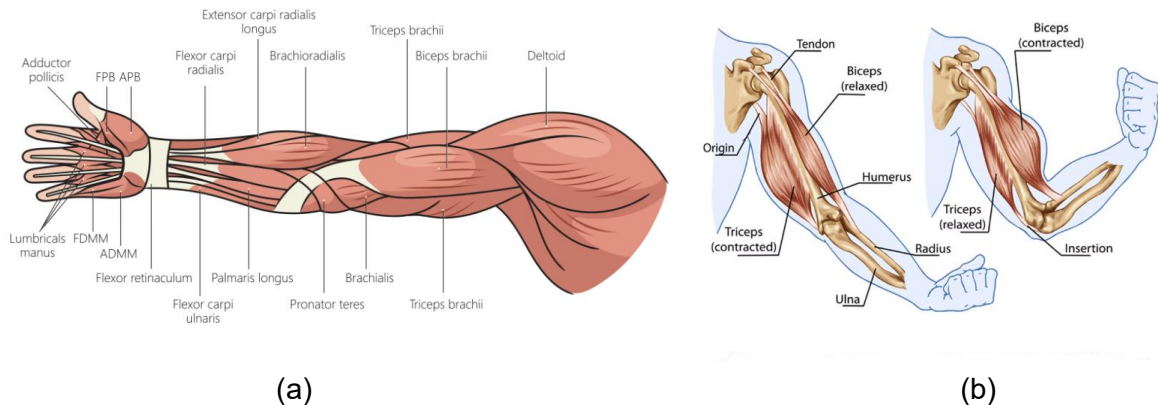


Figure 5. (a) Arm muscles; (b) Muscles used for flexion and extension on elbow [14][15]

Figure 5a shows the Muscles distributed on human arm, the movements of the human arm are executed through the coordinated action of multiple muscles working across the joints. Each joint in the upper limb is associated with specific muscles responsible for generating particular motions such as flexion, extension, rotation, and deviation. For example, as shown in Figure 5(b) the elbow joint primarily enables flexion and extension, movements controlled by major muscles such as the biceps brachii, triceps brachii, and brachialis. Understanding the roles of these muscles is crucial in both rehabilitation and the development of sensor-based control systems. Table 2 summarizes the key joints in the upper limb, their associated movements, and the primary muscles responsible for those actions.

Table 2. Muscles Responsible for Upper Limb Joint Movements [2]

Joints		Movements	Associated Muscles
Elbow	1	Flexion	<ul style="list-style-type: none"> <li>• Biceps brachii (Upper arm)</li> <li>• Brachioradialis (Forearm)</li> <li>• Brachialis (Upper arm)</li> </ul>
		Extension	<ul style="list-style-type: none"> <li>• Triceps Brachii (Upper arm)</li> </ul>
Wrist (Hand movements)	2	Flexion	<ul style="list-style-type: none"> <li>• Flexor carpi radialis (Anterior part of forearm)</li> </ul>
		Extension	<ul style="list-style-type: none"> <li>• Extensor carpi radialis longus (forearm)</li> <li>• Extensor carpi radialis brevis (forearm)</li> </ul>
	3	Abduction (Radial Deviation)	<ul style="list-style-type: none"> <li>• Flexor carpi ulnaris (Forearm)</li> <li>• Extensor carpi ulnaris (ulnar side of forearm)</li> </ul>
		Adduction (Ulnar Deviation)	<ul style="list-style-type: none"> <li>• Extensor carpi radialis brevis (Forearm)</li> <li>• Extensor carpi radialis longus (proximal end of above muscle)</li> <li>• Flexor carpi radialis (Anterior part of forearm)</li> </ul>
	4	Supination	<ul style="list-style-type: none"> <li>• Biceps brachii (long head) (Upper arm)</li> </ul>
		Pronation	<ul style="list-style-type: none"> <li>• Pronator quadratus (adjacent to wrist)</li> </ul>
Fingers (Hand Grasping)	5	Flexion	<ul style="list-style-type: none"> <li>• Flexor digitorum profundus (Forearm)</li> </ul>
		Extension	<ul style="list-style-type: none"> <li>• Extensor digitorum communis (Posterior forearm)</li> </ul>

In this project, the focus is on the elbow joint, specifically on 1 DOF corresponding to flexion and extension of the forearm, as shown in Table 2. These movements are primarily governed by the contraction and relaxation of the biceps brachii and triceps brachii muscles. During flexion, the biceps contract and shorten, pulling the forearm upward, while during extension, the triceps engage to push the forearm back to its resting position. These muscle contractions are accompanied by measurable physiological changes, including changes in muscle shape, stiffness, and electrical activity. Monitoring these changes allows the system to infer movement intention, even in the absence of visible motion, and those signals are the key elements for the control of the exoskeleton.

To acquire this muscle activity data, various sensing technologies can be employed. The traditional method is electromyography (EMG), which measures the electrical activity produced by muscle fibres. However, EMG systems often suffer from electrical noise, skin irritation, and high cost [4]. To minimise those limitations, in this project, an alternative optical sensing approach is adopted and will be introduced in section 2.3, which uses infrared (IR) light and photodiodes to detect deformation during muscle contraction (by checking the intensity of reflected light).

## 2.3 Signal Acquisition Techniques (EMG and Optical sensing)

This rehabilitation exoskeletons rely on muscle activity signals to understand the user's movement intentions. Muscle signal provides the basis for interpreting movement intention and initiating the



corresponding actuation of the exoskeleton system. For example, a real-time muscle signal can be obtained by applying sensors on the bicep and the real-time control can be realized by processing this signal to MCU. Over the years, various sensing methods have been developed for this purpose. Traditionally, surface electromyography (EMG), which measures the electrical signals produced by muscles, has been used as the interface to control exoskeleton devices [2]. However, EMG-based control can face practical challenges (like electrical noise and sensor complexity) [4]. Optical muscle sensing generally involves detecting the physical changes in a muscle (such as shape or size) using light-based sensors, rather than measuring electrical activity. This section explains how EMG and optical muscle sensing work and listed their advantages and disadvantages for this exoskeleton project, including factors like comfort, signal quality, cost, and reliability.

### 2.3.1 Electromyography (EMG) Signals

The generation of electromyographic (EMG) signals begins in the central nervous system. When the brain initiates the intention to move a specific muscle, it sends electrical impulses through motor neurons to the targeted muscle fibres [16]. This results in the formation of motor unit action potentials (MUAPs), during which the electrical excitation leads to the contraction of the muscle fibres [2]. In this way, multiple muscles coordinate to facilitate limb movement. This bioelectrical activity can be captured using EMG sensors placed either on the surface of the skin or inserted within the muscle tissue. The higher the muscle contraction, the higher the EMG signal level read.

Among various EMG methods, surface electromyography (sEMG) is the most commonly used due to its non-invasive nature. It uses electrodes placed on the skin to detect the sum of electrical signals generated by underlying muscle fibres [17][18]. EMG therefore provides a direct measurement of the electrical signals responsible for muscle contractions, making it a valuable tool for detecting neural activation related to voluntary movement. An example of a typical sEMG setup is shown in Figure 6, where surface electrodes are placed on the head to capture electrical activity during hand movement. The signal is then amplified, filtered, and digitized for processing.

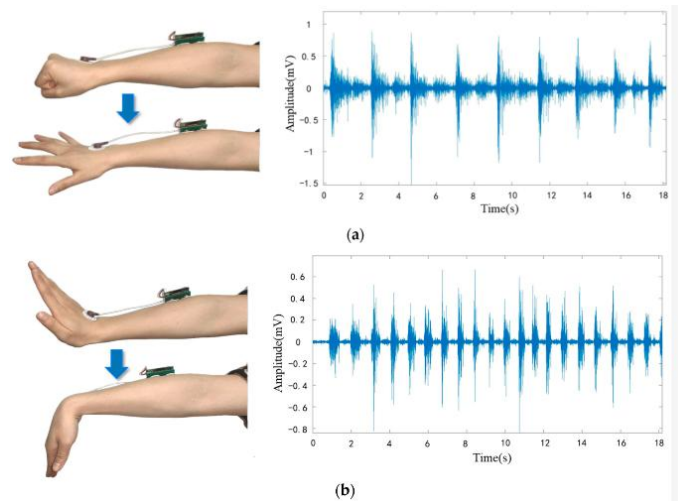


Figure 6. The sEMG signals at two different movement: (a) continuous clenching to unclenching of the fist; (b) continuous up and down turning of the wrist [17]

The raw EMG signal is stochastic and can be statistically modelled using a Gaussian distribution function [2]. The amplitude of EMG signals typically ranges from 0 to 10 mV peak-to-peak or up to 1.5 mV RMS. While the usable frequency range extends from 0 to 500 Hz, the majority of relevant signal energy is concentrated in the 50–150 Hz band [17]. Only components above the electrical noise floor are considered meaningful for further processing and interpretation in control systems.

However, EMG signals are susceptible to a variety of noise sources that may degrade signal quality. These include inherent noise from the electrode, motion artifacts, electromagnetic interference (EMI), and physiological or internal noise [17][18]. The severity of these noise types depends on various factors such as individual skin structure, blood flow velocity, local skin temperature, and the composition of tissue (muscle, fat, etc.) at the measurement site. For instance, all electronic components generate a certain degree of intrinsic electrical noise, with frequency components ranging from 0 Hz up to several kilohertz. With respect to electromagnetic interference, the human body can act like an antenna, continuously exposed to surrounding electromagnetic radiation. These environmental sources of EMI can introduce interfering signals or distort the muscle signals being recorded. In some cases, the amplitude of environmental noise can exceed that of the actual EMG signal by a factor of one to three [17].

In conclusion, EMG is a widely used method to detect muscle signals by measuring the tiny electrical activity in muscles. It gives direct information about muscle movement and is useful in rehabilitation control systems. However, it also has some problems, such as being easily affected by noise, needing careful electrode placement, and not being very comfortable for daily use. Because of these issues, other ways like using optical sensors have become popular as a simpler and cheap option.

### 2.3.2 Optical Sensing Signals

Optical muscle sensing is an alternative method to EMG for detecting muscle activity. Instead of measuring electrical signals, it uses light (usually from infrared LEDs) to detect physical changes in the muscle surface when the muscle contracts. This makes it a non-invasive, accurate and cheap sensing technique, which is more comfortable and stable in many daily use situations.

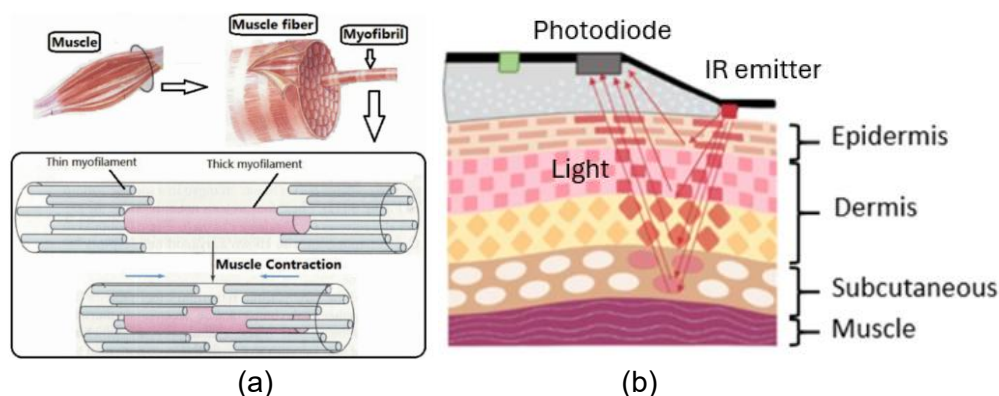


Figure 7. (a) Muscle structure and movement of myofilaments; (b) Sensor working principle [19][20]

The basic idea of an optical sensing system is to shine light onto the skin above a muscle and then detect the reflected light using a photodiode as shown in Figure 7b [4]. When a muscle contracts, its shape and thickness change slightly, meanwhile the blood flow density also changes. More specifically, the muscle fibre is a bundle of myofibrils composed of thick filaments and thin filaments as shown in Figure 7a [19]. During contraction, the thin filaments slide inward across the thick filaments, causing them to overlap and compress. This overlapping shortens the muscle fibre and increases its density. As a result, the muscle becomes more compact and influences reflection due to the change in internal structure [16]. The amount of force generated by a muscle depends on how many muscle fibres are activated. For example, lifting a sheet of paper requires fewer fibres compared to lifting a heavy object like a book [19].

These changes affect the amount of light reflected or absorbed. For example, during contraction, the muscle may become slightly thicker, more firm, which reduces the space between the light source

and the surface, leading to a change in reflection. Additionally, some studies also suggest that muscle contractions can affect local blood flow, when muscle contract the intramuscular pressure increases and thus reducing the blood flow, which can also influence how light travels through or bounces off the tissue. The photodiode then detects these light changes and converts them into a voltage signal [19]. However, the behaviour of infrared (IR) reflection is complex and influenced by a variety of physiological and physical factors. These include the type of muscle contraction, such as isometric versus isotonic contractions, the muscle's oxygenation dynamics during deformation, the relative placement and spacing of the photodiodes and LEDs with respect to muscle fibre orientation, and even external factors like skin tone and surface conditions [19][20][21].

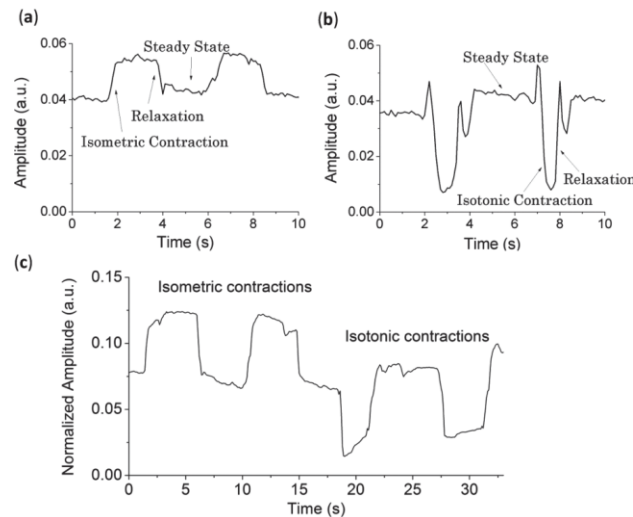


Figure 8. (a) signal corresponding to isometric; (b) isotonic contractions; (c) Two isometric contractions followed by two isotonic contractions [23]

For example, Figure 8 shows the optical signal of the biceps muscle under isometric and isotonic contractions. The opposite signal behaviour observed in isometric and isotonic contractions can be explained by the differences in how the muscle changes during each contraction. In isometric contractions, the muscle length remains almost constant. Therefore, the initial signal change is mainly due to changes in light scattering, but then, as blood flow decreases slightly, the signal increases due to reduced absorption. In contrast, during isotonic contractions, the muscle shortens at the beginning and loses blood more quickly. This first causes a signal drop, and only later does the effect of increased light scattering by the compressed muscle fibres become apparent [23].

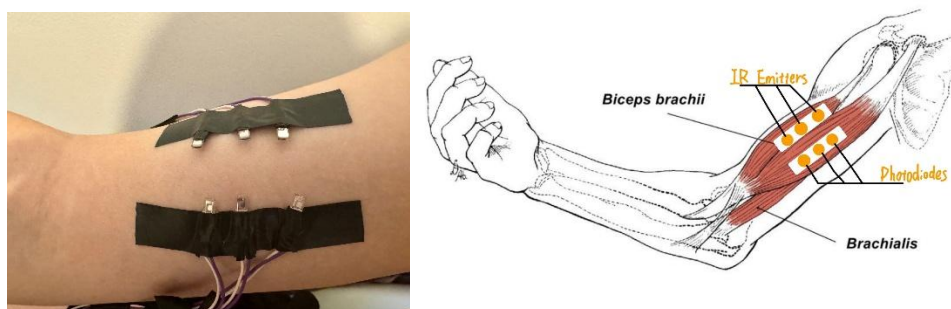


Figure 9. Optical sensor distribution for muscle contraction detection.

Therefore, since the aim of the project is to help patient rehabilitation, the isotonic contractions are the most important. To simplify the system design and focus on reliable signal acquisition, this project specifically targets isotonic contractions of the biceps brachii, which are most relevant during elbow flexion. The infrared LEDs and photodiodes are arranged perpendicular to the muscle fibres and

spaced 20mm (balance depth sensitivity and signal to noise ratio [23]) apart on the skin surface to detect muscle surface deformation as shown in Figure 9 (will be detailed in Section 3.2).

In this configuration, when the muscle contracts and the surface curvature increase, the tissue absorbs more infrared light due to changes in density and blood flow, or scatter the reflected light away from the photodiode. This results in less reflected light reaching the detector, and consequently, a lower output voltage from the photodiode circuit. This signal is often very small and needs to be amplified using a special type of amplifier called a transimpedance amplifier (TIA). The TIA converts the small current produced by the photodiode into a readable voltage. To reduce noise and unwanted fluctuations, the signal is passed through a low-pass filter (usually below 50 Hz), which helps remove fast, random changes that are not related to muscle movement. After that, the signal is read by a microcontroller (such as the Feather M4 used in this project) for further processing and motor control.

Finally, compared to EMG, optical sensing has several advantages. First, it does not need direct electrical contact with the skin. There is no need for conductive gel or worrying about sweat affecting electrode contact. This makes it more suitable for long-term use in wearable device like this project. Second, it is not affected by electromagnetic noise from nearby electronics as EMG. The sensor is built into a soft band that wraps around the upper arm, making it more comfortable and less noticeable. However, the challenges are obvious too. Since it detects changes based on reflected light, it can be sensitive to motion or shifting of the sensor on the skin, or even the tightness of the wrap [5]. Also, optical signals are not as direct as EMG because they do not come from neural activation itself, but from the mechanical or blood flow changes caused by contraction. However, many studies have shown that optical signals can still closely match EMG signals in timing and pattern and are accurate enough for controlling exoskeletons or other assistive systems. For example, one study found that infrared reflectance showed a sharp increase at the start of a muscle contraction, with timing very similar to EMG spikes [5][6].

## 2.4 Conclusion of Project Configuration

In conclusion, this project proposes the design and development of a smart upper-limb rehabilitation exoskeleton prototype aimed at assisting stroke patients or individuals with impaired arm mobility. The system is configured to provide 1-DOF movement support at the elbow joint, enabling flexion and extension of the forearm. By detecting biceps brachii muscle activity, the exoskeleton mimics natural arm movement through an active assistive exoskeleton. The main components of the project include a sensing module for muscle activity detection, a stepper motor actuation system, an embedded control system, and a exoskeleton structure.

To detect muscle activity, the project adopts an optical sensing system as an alternative to traditional EMG electrodes. This system uses infrared LEDs and photodiodes positioned on the biceps surface to monitor changes in muscle thickness and blood flow during isotonic contraction. The analogue signal is conditioned using a transimpedance amplifier (TIA) and a low-pass filter to suppress noise, before being digitized by the MCU for real-time processing. For actuation, a stepper motor was selected due to its accuracy, ease of control, and affordability. The motor is driven using the Adafruit Motor Shield and controlled by a Feather M4 Express microcontroller. Building upon this framework, the next section will detail the modelling, implementation, and development process of each subsystem to realise the complete functional prototype.

### 3 System Modelling and Development

This chapter introduces the design background and details the design and implementation of the exoskeleton. It discusses the methodologies adopted, alternative techniques considered, and their limitations. The chapter covers the optical sensing system, signal processing and control algorithms, and mechanical design, including 3D modelling and material selection, highlighting key design choices and challenges encountered.

#### 3.1 System Overview and Architecture

##### 3.1.1 System Structure

The designed system is a wearable, optical sensor driven motorized 1 DOF exoskeleton aimed at assisting upper-limb rehabilitation, specifically for restoring elbow flexion and extension. The prototype includes three primary subsystems as shown in Figure 10, the optical muscle sensing system, signal processing and control system (including actuation system), and mechanical structure. These subsystems are integrated into a compact and portable design suitable for user friendly rehabilitation support.

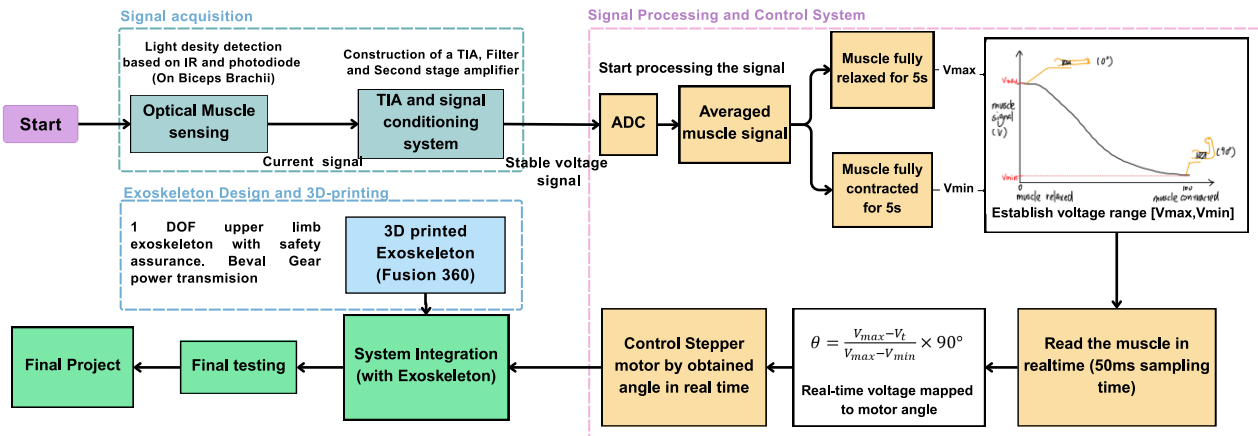


Figure 10. Smart exoskeleton system overview

The optical sensing unit is placed over the biceps brachii muscle and consists of infrared (IR) LEDs and photodiodes that monitor changes in muscle contraction. When the muscle contracts, changes in tissue density and blood flow reduce the intensity of received light, which is converted into electrical signals by a photodiode. These weak analogue signals are then amplified and filtered by a transimpedance amplifier (TIA) circuit with a low-pass filter to reduce noise. The processed signal is sent to a microcontroller (Feather M4 Express), which interprets the signal using a threshold-based control algorithm to determine the appropriate motor response. The motor control algorithm was implemented in Arduino IDE using the Adafruit\_MotorShield library, enabling easy configuration of motor speed, direction, and step size. The motor then drives the mechanical structure of the exoskeleton to assist the user's arm movement in real time.

##### 3.1.2 Tool Use

For the tools use, this project focuses primarily on practical experimentation and real-time testing rather than simulation, due to its reliance on complex, variable biological signals from human muscles. Since the core of the system involves detecting physiological changes such as muscle contraction using infrared (IR) LEDs and photodiodes, these signals are difficult to simulate accurately in software alone. The unpredictability of biological tissues, differences between subjects, and the sensitivity of optical sensing components introduce many uncontrollable factors. Therefore,



considering the time cost and budget of the project, the development process prioritized hardware prototyping and empirical testing to obtain reliable results. In addition, analogue circuit design was performed using LTspice to simulate the behaviour of the transimpedance amplifier and low-pass filter. The microcontroller programming was written in C language using Arduino IDE, where the Adafruit\_MotorShield library was used to control the stepper motor based on real-time sensor input. The mechanical structure of the exoskeleton, including the motor bracket and arm support, was designed using Fusion 360 and manufactured using 3D printing technology. Table 3 shows the functional Requirement of Exoskeleton.

Table 3. Functional requirement of project

Components	Function
MCU (Feather M4 Express)	Reads Analogue signals from the optical sensors, process them and apply control algorithms to control the stepper motor. Serves as the central control unit.
Power supply	Powers the MCU, IR LEDs, and amplifier circuits. Drawn from MCU pin or laptop USB (Can use batteries with buck converter).
Optical sensor system	Consists of IR LEDs, photodiodes and signal conditioning circuit to detect muscle contraction by monitoring reflected light intensity changes.
Actuator (Stepper Motor + Driver)	Provides mechanical movement to assist elbow flexion and extension based on processed muscle signals.
Exoskeleton (3D-Printed Frame)	Mechanically supports the user's arm, transmits torque from the motor, and ensures ergonomic and safe rehabilitation motion.

## 3.2 Optical Sensor Circuit Modelling and Design

The optical sensing circuit is the first priority in this project, which is used to detect the biceps muscle activity in real time and try to provide fast, accurate and stable data for the control system. This section will first list the design requirements with reference to the design specifications. Then, the selection of components and their reasons are explained. Finally, the design details and implementation are explained in detail, and the limitations are pointed out.

### 3.2.1 Requirements and Design Criteria

Designing an optical biosensor for muscle activity requires setting realistic goals that can be achieved within the time, cost, and equipment constraints of this project. The sensor must be able to detect when the muscle contracts and how strongly and then output a clear voltage signal that the microcontroller (MCU) can read through its analogy-to-digital converter (ADC). The target output swing was set to within 1V to ensure the signal stays within the 3.3V ADC range and avoids clipping, while still showing clear differences between relaxed and contracted muscle states.

The system is designed to provide real-time feedback of biceps activity to control a stepper motor. Since the exoskeleton should respond quickly to assist arm movement, the sensor needs to detect muscle activation with minimal delay. Human muscle force typically develops within 50–200 ms, so the sensor should have a bandwidth of at least 20–50 Hz to keep up with these changes [7]. Although the time needed for optical signal acquisition is very short, unnecessary delays must still be avoided to ensure smooth and timely control. In addition, because the changes in photodiode current are very small (in the nanoamp to microamp range), a high-gain transimpedance amplifier (TIA) is required to convert them into measurable voltages. However, higher gain also increases noise. To maintain reliable detection, a signal-to-noise ratio (SNR) of at least 20 dB (signal 10 times stronger than noise) is targeted. In practice, this means keeping noise below 50 mV while aiming for signal

changes of a few hundred millivolts during contraction. Achieving this is possible with basic components like op-amps and resistors, as long as the circuit is carefully designed with proper filtering and layout. The system runs on a 3.3V supply from the MCU. LEDs are driven with a forward current of around 20 mA, and the design ensures that all components operate safely within their ratings. The sensor must also be safe and comfortable for users, with IR light levels kept well below eye safety limits and mounted using a soft, adjustable strap that can be worn for extended periods.

Table 4. Optical Sensor Design Specifications

Specification	Target / Requirement
Output Voltage Swing	0.1V (rest) to 1.0V (full contraction), matched to MCU ADC range (0–3.3V)
Response Time (Sampling frequency)	$\leq 500$ ms
Sensor Bandwidth	$\geq 20$ –50 Hz (to track contraction dynamics accurately)
Signal-to-Noise Ratio	$\geq 20$ dB (signal at least 10 $\times$ stronger than noise; noise < 50 mV)
LED Drive Current	$\leq 20$ mA forward current at 1.8V per IR LED (EPM-4001)
Power Supply	3.3V from MCU (Feather M4 Express)

In summary, the sensor must produce a stable, responsive, and readable analogue voltage that reflects muscle activity. It must match the ADC range, respond within 500 ms, and maintain enough SNR to distinguish real signals from noise as shown in Table 4. These goals form the basis for the circuit and mechanical design decisions that follow.

### 3.2.2 Optical System Design Considerations and Architecture

#### 3.2.2.1 Wavelength Selection and Sensing Principle

In designing the optical sensing system, first selecting the appropriate LED wavelength is critical for ensuring effective penetration into muscle tissue and strong signal contrast between relaxed and contracted states. Two common choices are red light ( $\sim 660$  nm) and infrared (IR) light ( $\sim 850$ – $950$  nm) [20]. While red LEDs offer high surface reflectance, they are more sensitive to surface noise and skin tone variability. In contrast, IR light penetrates deeper into tissue and is less affected by pigmentation or superficial artifacts, making it more suitable for sensing underlying muscle deformation during contraction (as shown in Figure 11), especially for patients with motor deficits [22].

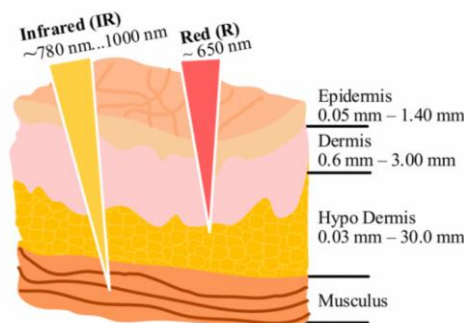


Figure 11. light penetration depths into the tissue for red and infrared light [22]

A research study investigated the responses of three common LED wavelengths: green (~530 nm), red (~630 nm), and infrared (~850–935 nm). The results showed that green light has the shallowest penetration depth and is highly responsive to small changes on the skin surface, which makes it sensitive to superficial muscle deformation. While this leads to large signal variations during movement, it also makes the signal more vulnerable to external interference such as ambient lighting, sweat, or skin pigmentation [20]. Red light provides a moderate balance between penetration and sensitivity but may still struggle to detect changes that occur deeper within the muscle tissue [20]. Infrared light, especially in the 850–950 nm range, has the deepest penetration of the three. It is less sensitive to pigmentation and provides a more consistent response across different user groups. Although the amplitude of the signal change during muscle contraction may be smaller than that of green or red light, infrared signals are more reliable for sensing deeper tissue changes [20]. The responses of the three LEDs are shown in Figure 12.

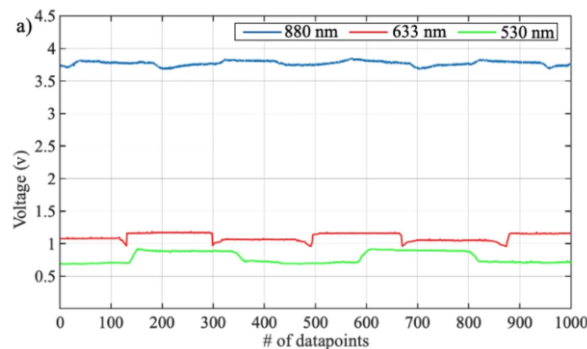


Figure 12. Comparison between the acquired data using three different light wavelengths [20]

Since this project targets rehabilitation for individuals with limited or impaired muscle function, the primary goal is to detect deeper muscle contractions that may not result in significant surface movement. Therefore, infrared LEDs were selected for this optical system.

### 3.2.2.2 System Structure and Component Selection

To implement a functional and responsive optical sensing system, the configuration shown in Figure 13 was developed. This block diagram outlines the signal flow from LED driver circuit to the Microcontroller, highlighting each key hardware module and its function in the system.

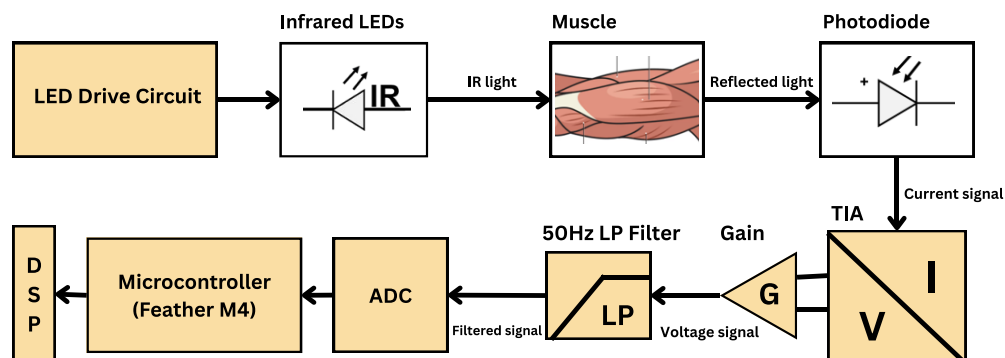


Figure 13. Block Diagram of Optical sensing system

The process begins with the LED Drive Circuit, which powers the infrared LEDs that emit light into the surface of the biceps brachii. When the muscle shows isotonic contractions, the shape, thickness, and internal structure of the muscle change, which affects the amount of reflected or transmitted light. This light is then detected by a photodiode, which converts the varying light intensity into a



small current. The Transimpedance Amplifier (TIA) with enough gain is used to convert this current into a usable voltage signal, which is then passed through a low-pass filter (LP) to reduce high-frequency noise and motion artifacts. This filtered voltage is then amplified with proper gain to increase the signal's clarity and readability.

After that, the analogue signal is then digitized by an Analog-to-Digital Converter (ADC) integrated within the Feather M4 microcontroller. The microcontroller reads the real time signal and applies the control algorithm to determine whether muscle contraction has occurred. Based on the signal pattern and level, appropriate commands are issued to the motor driver (Adafruit Motor Shield) to control the stepper motor for assisting the elbow movement.

Table 5. Key components for sensing system

Subsystem	Component	Specification / Model
Light Source	IR LED	OP240(935 nm wavelength)
Light Detector	Photodiode	EPM-4001
TIA	Amplifier	MCP6292

Based on the system flow shown in Figure 12, the key components required for each stage of the optical sensing system are summarized in Table 5.

### 3.2.3 Detailed Design of Optical Sensor System

This section provides a detailed breakdown of the optical sensor hardware design and calculations, including LED circuit design, photodiode signal conditioning with a TIA, and low pass filtering stages.

#### 3.2.3.1 LED Circuit

First, the muscle sensing system employs four infrared LEDs (OP240) positioned over the biceps brachii. Each of them was supplied by 3.3V MCU input voltage. The LED circuit should provide a suitable forward voltage and current for LEDs. The OP240 LED is selected for its emission peak at 890 nm and the key specifications are summarized in Table 6 under 25°C.

Table 6. OP240 Electrical Characteristics [38]

Parameter	Value
Forward Voltage ( $V_{F\_IR}$ )	1.8 V
Forward Current ( $I_{F\_IR}$ )	20 mA
Peak Wavelength	890 nm
Storage and Operating Temperature Range	-40°C to +100°C

The supply voltage is 3.3 V, provided by the Feather M4 microcontroller. To provide a suitable work condition to 1.8V and 20mA, a series resistor is used to limit the LED current. According to Ohm's Law:

$$R_{IR} = \frac{V}{I} = \frac{V_{MCU} - V_{F\_IR}}{I_{F\_IR}} = \frac{3.3V - 1.8V}{0.02A} = 75\Omega \quad (1)$$

Thus, a 75  $\Omega$  resistor is selected in series with each LED as obtained in Eqn (1). A schematic and simulation results of the LED drive circuit is developed and tested using LTspice as shown in Figure 14.

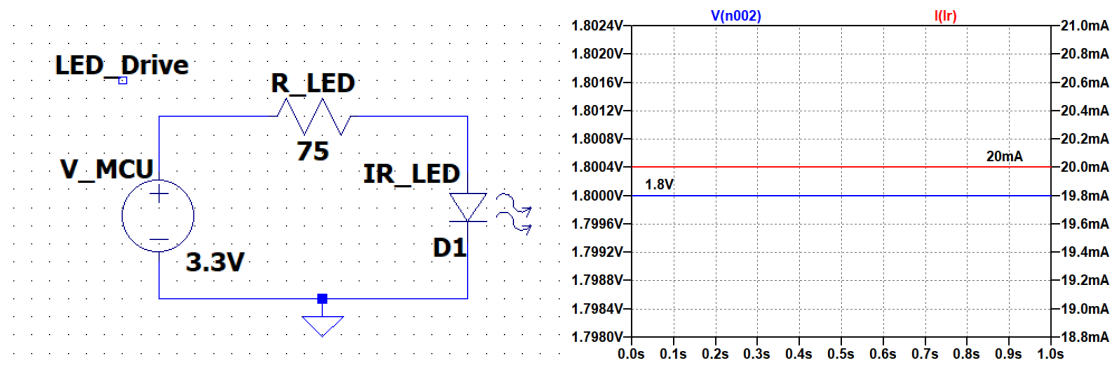


Figure 14. LED circuit schematic and simulation results

### 3.2.3.2 Transimpedance Amplifier (TIA) and LP filter

To capture the changes in light intensity reflected from the contracting biceps muscle, a silicon photodiode was selected due to its high sensitivity in the near-infrared region. In this design, the EPM-4001 photodiode was used, which provides optimal responsivity at wavelengths around 880–935 nm shown in Figure 15, aligning well with the OP240 IR LEDs used in the previous subsection.

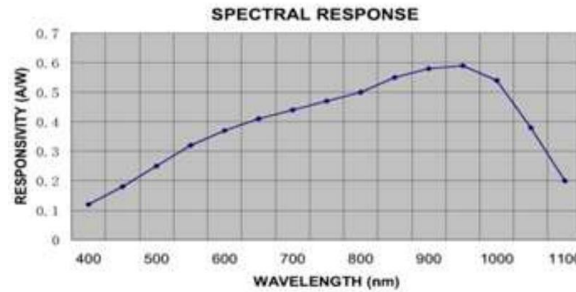


Figure 15. EPM-4001 photodiode characteristics [37]

The photodiode operates in photovoltaic mode, where incoming photons generate a current proportional to the light intensity. Under typical lighting from the IR source and reflection off the human arm, the expected photodiode current ranges from tens of nanoamperes to a few microamperes.

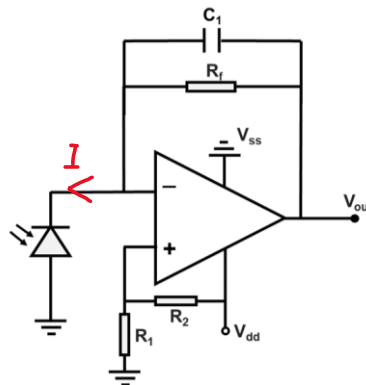


Figure 16. TIA circuit

Because this current is extremely small, a transimpedance amplifier (TIA) is required to convert it into a readable voltage. The basic TIA configuration involves an op-amp with a feedback resistor  $R_f$  (Figure 16), which defines the gain of the circuit. Three parameters should be considered before designing the circuit, select a suitable feedback resistor, offset voltage and LP filter dealing stability and noise.

First, for the suitable feedback resistor, the output voltage of the TIA can be approximated by Eqn (2):

$$V_{out\_TIA} = I_{PD} \times R_f \quad (2)$$

where  $I_{PD}$  is the photodiode current (PD is working under Reverse Bias, and the current is in reverse direction), and  $R_f$  is the feedback resistor. According to the datasheet, the maximum photodiode current can reach up to  $I_{PD} = 100 \mu A$  under strong illumination. However, in practical use, when light is reflected off human tissue, especially during muscle contraction, the received light intensity decreases significantly. Additionally, variations in skin tone, muscle mass, and sensor placement can lead to large differences in output current between users. Therefore, to achieve a measurable voltage swing in the range of 0–1 V suitable for the microcontroller's ADC, a feedback resistor of 1 M $\Omega$  was selected. This high resistance allows even small currents to produce readable voltage signals. For example, a tested current of 0.21  $\mu A$  measured on a healthy subject in the lab resulted in an output voltage of approximately 0.21 V, which falls well within the ADC input range and provides sufficient resolution for signal processing and control:

$$V_{out\_TIA} = I_{PD} \times R_f = 0.93 \mu A \times 1 M\Omega = 0.21 V \quad (3)$$

After the TIA stage, the output signal may exhibit both positive and negative voltage swings, especially since the photodiode response can vary depending on the type of muscle contraction. As illustrated in Figure 8, isotonic and isometric contractions can produce signals with opposite polarity due to differences in blood flow and muscle fiber scattering. This causes parts of the signal to drop below 0 V, which is not suitable for microcontroller ADCs such as the one on the Feather M4 Express (0–3.3 V input range). To solve this, a DC offset is introduced to shift the entire signal upward and center it within the ADC's input range. This is achieved by using two resistors,  $R_1 = 1 k\Omega$  and  $R_2 = 10 k\Omega$ , forming a voltage divider connected to the 3.3 V supply. The resulting midpoint voltage is approximately:

$$V_{offset} = \frac{R_1}{R_1 + R_2} \times 3.3 V = \frac{1k}{1k + 10k} \times 3.3 V = 0.3 V \quad (4)$$

This offset voltage is applied to the non-inverting input of the op-amp, effectively shifting the signal upwards and promise the output voltage never lower than zero. It ensures the entire analog output always remains positive and within range (Lowest voltage after test is 0.18V), preventing clipping and allowing accurate digital conversion by the ADC. It also prepares the signal for subsequent filtering and control processing stages.

Finally, a low-pass filter with a cutoff frequency of 125 Hz is implemented in the feedback loop of the transimpedance amplifier (TIA) circuit. This filter is achieved by placing a capacitor in parallel with the feedback resistor  $R_f$ . Its purpose is to suppress high-frequency noise that may be introduced by ambient light, motion artifacts, or electronic interference, especially given the high gain nature of the TIA stage.

The cutoff frequency of this first-order RC low-pass filter is given by:

$$f_c = \frac{1}{2\pi R_f C_f} \quad (5)$$

With  $R_f = 1 M\Omega$ , to achieve a cutoff at approximately 125 Hz, the required capacitor value  $C_f$  is calculated as:

$$C_f = \frac{1}{2\pi \times 1 \times 10^6 \times 125} \approx 1.27 \text{ nF} \quad (6)$$

In practice, a standard capacitor value of 1nF was used, depending on availability. This cutoff frequency was chosen to preserve the majority of muscle contraction signal energy, which typically falls in the 0–150 Hz range, while effectively attenuating higher frequency noise. Placing the capacitor in the feedback loop ensures that the gain of the TIA decreases at higher frequencies, improving signal clarity and reducing the impact of unwanted interference before the signal is passed on for further processing.

In fact, after initial testing in the lab, noticeable noise around 50–60 Hz was observed in the TIA output signal, which is likely caused by ambient electromagnetic interference, particularly from power-line sources. Since the primary frequency content of muscle deformation signals lies between 0–30 Hz, a second stage low pass filter was implemented following the TIA output. This filter complements the filtering already provided by the TIA's feedback loop and ensures that the signal reaching the microcontroller is stable and free of unnecessary noise. To set the cutoff frequency slightly above 50 Hz (to retain most of the useful muscle signal content but remove high-frequency noise), the following values, R=33kΩ and C=100nF of LP filter were selected:

$$f_c = \frac{1}{2\pi R_{lp} C_{lp}} = \frac{1}{2\pi \times 33 \times 10^3 \times 100 \times 10^{-9}} \approx 48 \text{ Hz} \quad (7)$$

A simplified LTspice schematic of the TIA and filtering stage is shown in Figure 17.

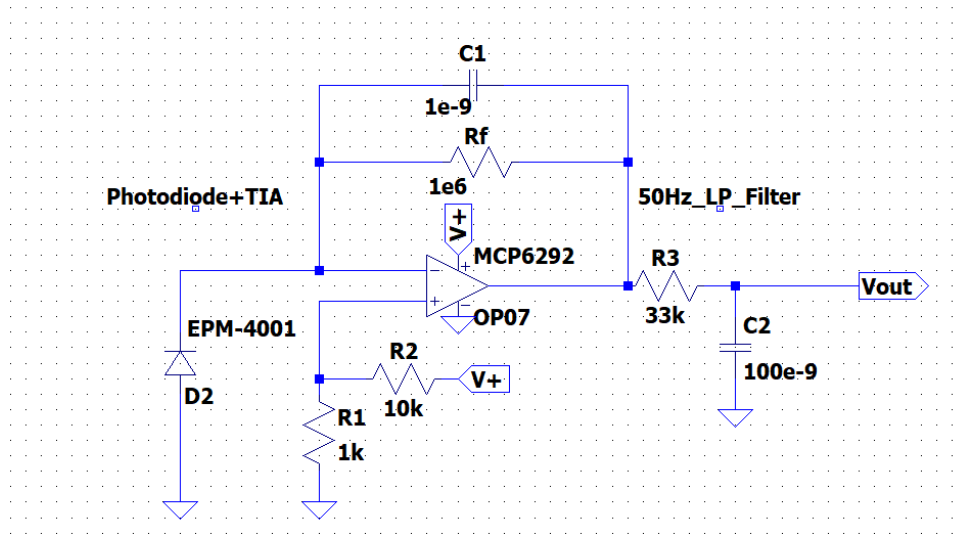


Figure 17. Schematic of TIA and filtering stage

### 3.2.3.3 Integration of LED Drive and Sensing Circuit

To form a complete optical muscle sensing system, both the infrared LED drive circuit and the TIA circuit must be integrated onto a single breadboard. This integration ensures compactness, physical stability, and ease of prototyping. The overall schematic of the sensing system, including the LED circuit, TIA, and associated filters, is shown in Figure 18.

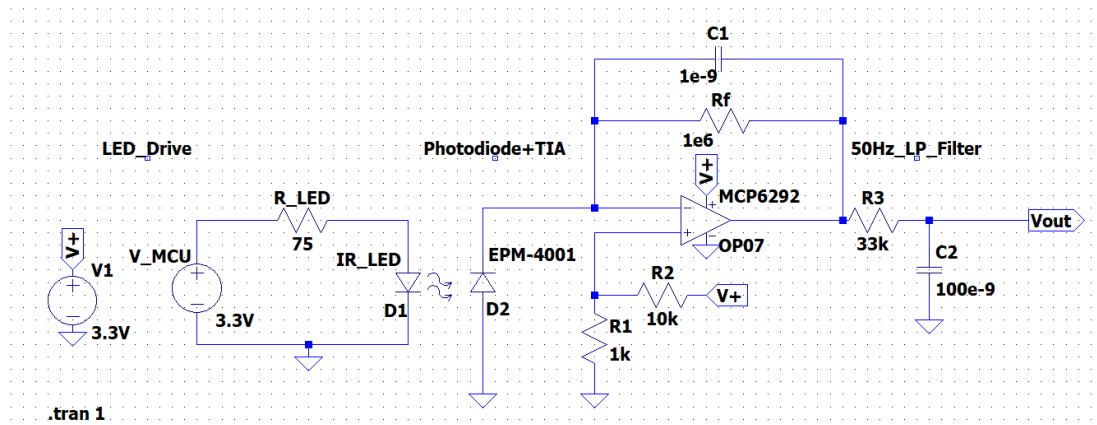


Figure 18. Schematic of the Optical sensor circuit

In this project, three infrared LEDs are designed to deliver sufficient light intensity across the central region of the biceps brachii. This setup ensures that enough reflected light reaches the photodiodes for detection. As discussed in Section 2.3.2, optical muscle sensing is highly sensitive to several factors, including LED/photodiode orientation relative to muscle fibres, sensor placement, and skin surface conditions [23]. To reduce surface-level artifacts such as those caused by sweat, hair, or pigmentation, infrared light is selected due to its deeper tissue penetration and reduced sensitivity to superficial variation.

Therefore, the LEDs and photodiodes are placed perpendicular to the muscle fibres and spaced approximately 20 mm apart on the skin surface. This configuration strikes a balance between depth sensitivity and signal-to-noise ratio, in accordance with findings in prior optical sensing literature [20]. It allows the system to effectively track surface deformation and internal changes associated with isotonic contraction of the muscle.

Then, to improve signal robustness and reduce localized errors, three photodiodes are placed along the sensor array. The output signals from these photodiodes are independently processed and averaged to generate the final control signal in MCU. This averaging process minimizes the effect of small local disturbances, such as inconsistent skin contact or pressure differences, and leads to a more stable and accurate representation of muscle activity. This is essential for ensuring smooth and responsive control of the exoskeleton.

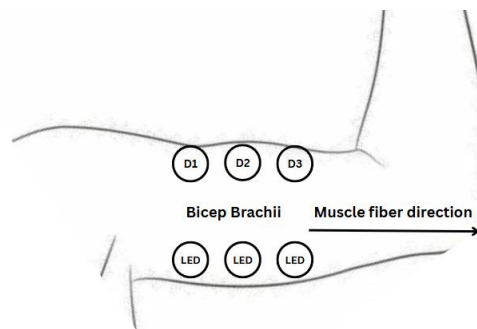


Figure 19. placement of LEDs and photodiodes

A visual representation of the actual placement of LEDs and photodiodes on the arm is shown in Figure 19, illustrating the setup of the sensing array.

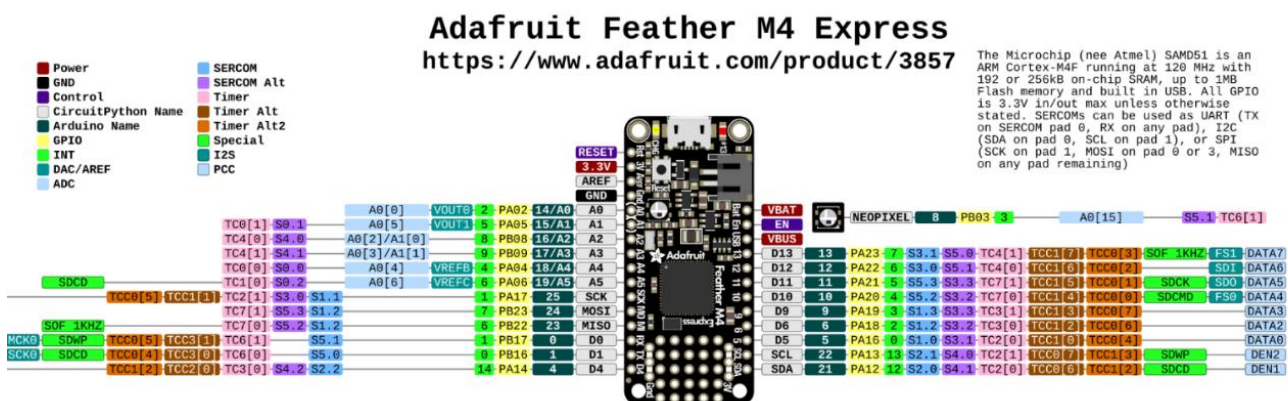
### 3.2.4 Implementation and Construction (Limitations and Challenges)

The complete optical sensing circuit was built and tested on a breadboard, integrating the LED driver and photodiode amplifier into a unified system. For convenience, the LED emitter and its current-limited drive circuit were placed on the same board along with the photodiode and transimpedance amplifier (TIA). Resistor values and component positions were adjusted based on the theoretical model in Section 3.2.1. The LED and photodiode were positioned opposite the muscle, and a soft, light-proof cuff was used to wrap around the arm. Preliminary experiments confirmed that the circuit produced a measurable voltage output corresponding to the photodiode current.

Since the behaviour of muscle tissue and optical sensor responses is difficult to simulate accurately, the design, testing, and adjustments were primarily conducted in the laboratory. Breadboard implementation provided a flexible platform for real-time tuning, such as adjusting amplifier gain by swapping feedback resistors and integrating the planned filtering stages. This approach ensured that the circuit's actual performance aligned closely with the theoretical calculations and performance targets described in Sections 3.2.1 and 3.2.3.

#### 3.2.4.1 Microcontroller Configuration

The microcontroller chosen for this project is the Adafruit Feather M4 Express, based on the ATSAMD51 chip. This board was selected for its high-speed 120 MHz Cortex-M4 processor, built-in ADC (Analog-to-Digital Converter), ample GPIO pins, and compatibility with the Arduino IDE, which made programming and hardware interfacing more efficient [24]. Additionally, its compact form factor and USB programmability make it ideal for its light weight and size, make it rapid prototyping in wearable and sensor-based applications like this exoskeleton system.





### 3.2.4.2 LED Circuit

According to Figure 14, the schematic of the OP240 infrared LED circuit consists of a single 3.3 V power supply, a 75  $\Omega$  series resistor, and the LED. Theoretically, this configuration delivers approximately 1.8 V across the LED with a forward current of 20 mA, which falls within the recommended operating range, ensuring stable and efficient LED performance.

Based on the Pin configuration shown in Figure 20, the three LED circuit is constructed in Figure 21 with parameters labelled using Tinkercad.

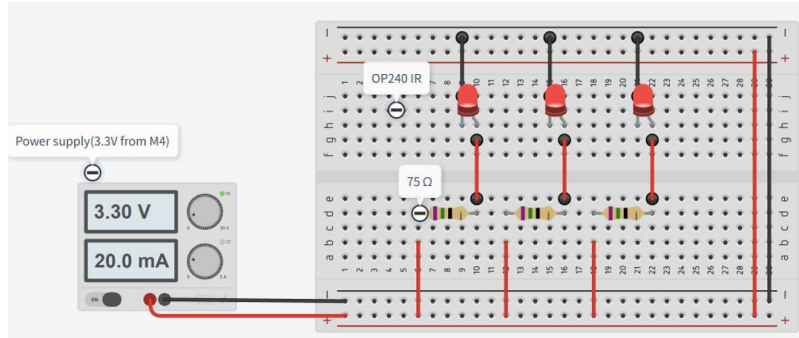


Figure 21. LED Circuit build in Tinkercad

Therefore, the test circuit was then built on a breadboard, as shown in Figure 22. Due to the unavailability of 75  $\Omega$  resistors in the laboratory, 82  $\Omega$  resistors were used instead. This substitution still provided adequate current limiting to protect the LEDs while ensuring their correct operation. The IR emitters were soldered with extension wires, purple for ground (negative) and white for power (positive), to allow easier integration with the wearable cuff. Electrical insulation tape was applied to the exposed terminals to prevent short circuits and ensure safety during testing.

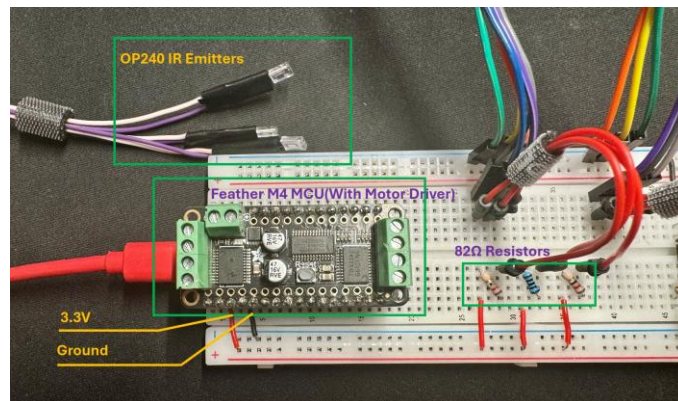


Figure 22. LED Circuit build in Breadboard

After that, to verify the LED circuit performance, the voltage and current across the IR LEDs were measured using a multimeter. The readings were approximately 1.56 V and 20 mA, as shown in Figure 23, confirming that the LEDs were operating within their specified range. Additionally, the infrared light emitted by the LEDs was successfully captured using a standard smartphone camera. This provided a quick and simple method to visually confirm LED operation during testing and alignment.



Figure 23. LED Circuit test result

### 3.2.4.3 Transimpedance Amplifier (TIA) and LP filter

The design parameters determined in the previous section are summarized in Table 7, which includes the selected feedback resistor and capacitor  $R_f$ ,  $C_f$ , the offset resistor values  $R_1$  and  $R_2$ , and the filtering components  $C_{LP}$  and  $R_{LP}$ . Additionally, the amplifier used is the MCP6292, a dual low-noise operational amplifier suitable for low-level signal amplification. It operates well under a 3.3 V supply and offers rail-to-rail output, making it ideal for battery-powered analogue circuits like this project [25]. The configuration of the TIA and filter circuit is shown in Figure 24.

Table 7. design parameters for TIA and LP filter

Component	$R_f$	$C_f$	$R_1$	$R_2$	$R_{LP}$	$C_{LP}$
Value	1M $\Omega$	1nF	1k $\Omega$	10k $\Omega$	33k $\Omega$	100nF

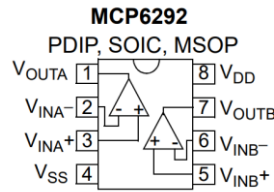


Figure 24. MCP6292 amplifier [39]

Based on these values and schematic Figure18, the transimpedance amplifier (TIA) circuit was constructed virtually using Tinkercad as shown in Figure 25.

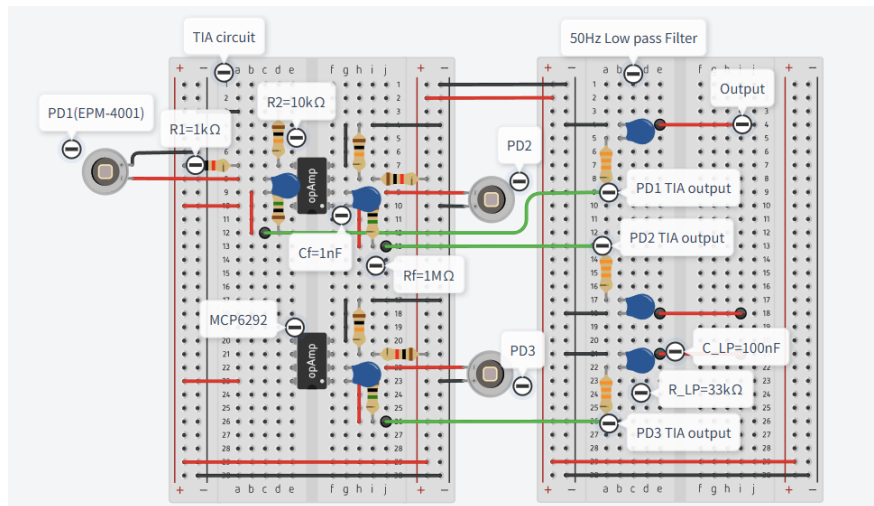


Figure 25. TIA and LP Filter circuit build in Tinkercad



Following the schematic design in Tinkercad, the TIA and LP filter circuit was physically constructed on a breadboard using the MCP6292 operational amplifier, resistors, and capacitors defined in Table 6. Figure 26 shows the actual hardware implementation used for signal testing.

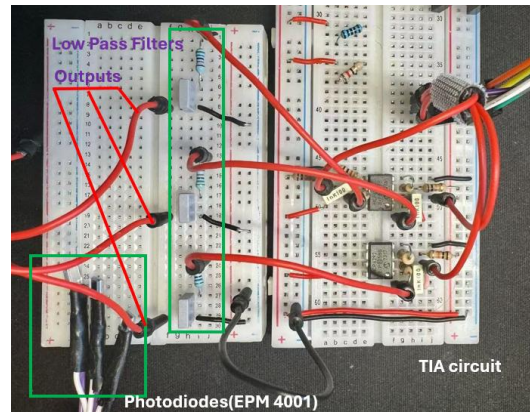


Figure 26. TIA + LP Filter Circuit build on Breadboard

#### 3.2.4.4 Complete System Test and Summary

After that, the circuit was tested on a healthy volunteer with the optical sensor array 20mm LED to photodiode distance attached to the biceps brachii (as shown in Figure 19) and wrapped by a cuff to prevent light leakage and ambient light influences. During the test, all three infrared LEDs were powered on, and the volunteer was instructed to first relax the arm and then perform a single full elbow flexion and return to rest, which corresponding to one complete contraction of the biceps.

The output from one of the photodiode channels was monitored using an oscilloscope. Figure 27 displays the test environment and captured waveform. A noticeable voltage drop was observed during the contraction phase and is align with the isotonic contraction's behaviour, confirming successful detection of muscle activity. At rest, the average output voltage was approximately 0.220 V, which dropped to around 0.190 V at peak contraction. This corresponds to a signal variation of about 30 mV. The shape and timing of the waveform were consistent with the theoretical response of isotonic contraction as discussed in Figure 8, validating the effectiveness of the sensor design.

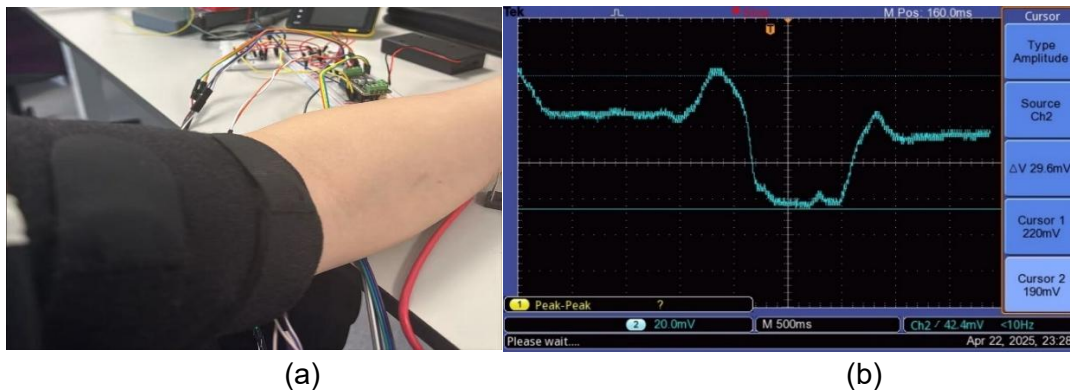


Figure 27. (a) Optical system test wrap; (b) The waveform of a biceps contraction

However, two key limitations were observed during testing. First, the signal amplitude was relatively small, with only about 30 mV of change between resting and contraction states. The 30mV swing is smaller than the 0.9V design specification, while the trend is still clear but small vary range might lead to unstable sensing result and thus reducing the control accuracy in Control section. Second, a

noticeable 50 Hz interference was present (likely from power line noise). While the noise did not overwhelm the main muscle signal, it was clearly visible in the waveform. Nevertheless, the signal-to-noise ratio (SNR) was still acceptable for identifying contraction events that large than 20dB (noise <2mV), and the overall waveform exhibited a consistent and interpretable pattern.

It is important to note that this result represents only a single healthy test data. In practical applications, individual differences such as skin tone, muscle mass, fat tissue thickness, and sensor placement can significantly affect the photodiode output. Therefore, this system might require further calibration and testing when used by diverse users. However, for now, this baseline dataset will be used as the reference for adjusting the signal processing system in the next stage.

To increase the output voltage range, one potential solution is to reduce the LED to photodiode distance, thereby enhancing the amount of reflected light detected. However, reduce the distance will increase the noises thus reduce the signal quality [23]. Alternatively, the feedback resistor value in the TIA can be increased to boost signal gain, although this may also amplify noise. another approach would involve adding a second amplification stage after the TIA to increase voltage swing while incorporating additional filtering to maintain signal integrity. Therefore, two methods of reducing the sensor spacing and applying a second stage amplifier were tested and compared below.

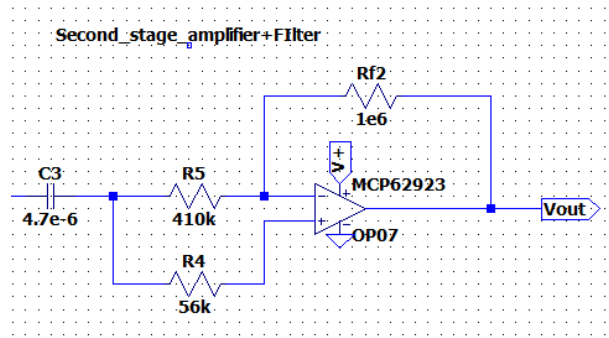


Figure 28. Schematic of second stage amplifier and filters

As shown in Figure 28, a second stage amplification and filtering circuit was integrated into the design with a 0.6Hz high pass filter and a gain of 2. This enhancement specifically focuses on increasing the signal swing while reducing high frequency noise, thereby improving the robustness and reliability of the optical sensing system. The calculations are listed in in Eqns (8) to (11).

$$f_c = \frac{1}{2\pi RC} \quad (8)$$

Using R4=56 kΩ and C3=4.7 μF, the calculated cutoff frequency is:

$$f_c = \frac{1}{2\pi RC} = \frac{1}{2\pi \times 56k \times 4.7u} = 0.6Hz \quad (9)$$

The gain of the amplifier is:

$$G_2 = -\frac{R_{f2}}{R_5} \quad (10)$$

Given Rf2=1 MΩ and R5=50 kΩ, the gain becomes 20:

$$G_2 = -\frac{R_{f2}}{R_5} = -\frac{1M}{410k} = -2.4 \quad (11)$$

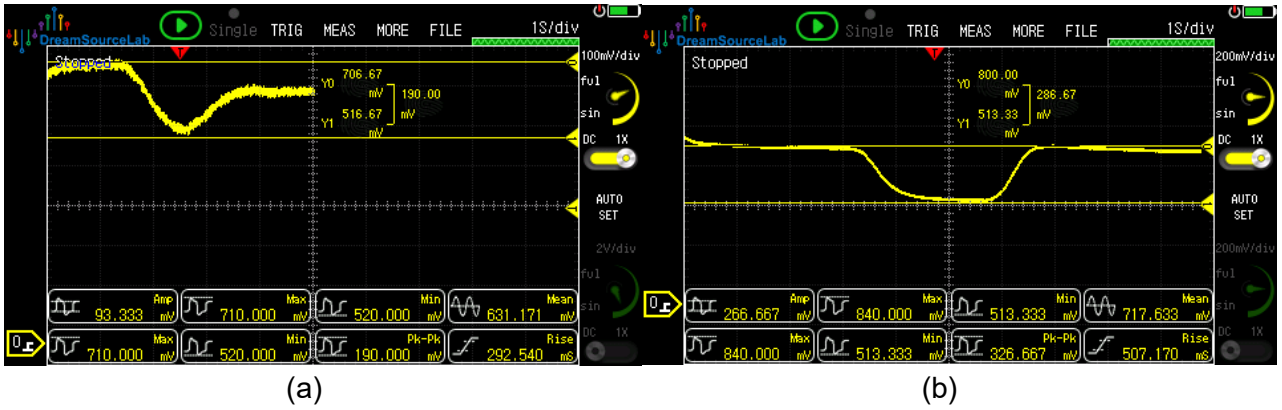


Figure 29. (a). Second stage amplifier added; (b) shortening the distance between the LED and the photodiode to 16mm muscle contraction test

The observed result of this enhancement during a muscle contraction test is shown in Figure 29a. The output signal from the second-stage amplifier clearly captured the contraction phase, with a significantly increased voltage swing of approximately 0.2 V, compared to the original 30 mV before amplification. However, Figure 29b shows the result of shortening the distance between the LED and the photodiode to about 16 mm (The noise increased keep decrease distance) and replace the  $R_{LF}$  to  $4.7 \mu F$ . Better results were observed, with clear signals and less noise. The output swing was also increased to 300 mV. Therefore, it was decided to use the second method to improve the design.

To further reduce the 50 Hz interference, which is likely caused by ambient power-line noise, a digital notch filter or an adaptive software filter can be implemented in the signal processing stage. These improvements, along with the application of Kalman filtering techniques (discussed in Section 3.4), can further enhance the signal stability and ensure accurate and real-time control of the exoskeleton system.

In summary, most of the experimental results successfully met the design specifications outlined in Table 3. The sensor demonstrated a functional bandwidth within the target range of 0–50 Hz, and the measured signal-to-noise ratio (SNR) exceeded 20 dB, ensuring reliable detection of muscle contractions under typical conditions. However, the output voltage swing observed during testing was smaller than the initial design expectation of 0.1 V to 1 V, with actual swings closer to 300mV. This deviation highlights the need for further signal amplification or digital compensation in subsequent development stages. Despite this limitation, the system effectively captured muscle activity patterns and provided usable data for the later control system.

### 3.3 Signal Processing and Control System

To effectively assist upper limb rehabilitation, the exoskeleton must respond to the user's muscle activity in real time (with small latency). This section aims to design a control system to process muscle signals and then calculate the corresponding motor control angle according to the changes in muscle signals. Specifically, when the user tries to move the arm, the system will detect the degree of muscle contraction and processes the signal through a microcontroller (Feather M4). The system then activates the stepper motor (NEMA 17) according to the designed threshold control algorithm to generate relative movement in the exoskeleton. This process ensures that the movement response is synchronized with the user's movement intention, thereby achieving natural and safe rehabilitation. All the code used in control system is presented in Appendix III, some of the key codes are shown as figure for explanation.

### 3.3.1 Overview System Architecture and Design requirement

#### 3.3.1.1 Motor Torque Requirements and Actuator Selection

To ensure the system aligns with the project goal of assisting rehabilitation for patients with impaired muscle function, the selection of the motor model and corresponding motor driver will be first carefully analysed.

To select a suitable motor for this rehabilitation exoskeleton, it is important to first estimate how much torque is needed to support the user's arm movement. Since the purpose of the system is to assist, not completely replace, muscle effort, the motor only needs to provide partial support, just to help users with weakened muscles perform elbow flexion and extension comfortably. Using a motor that is too strong may cause discomfort or even harm to users, especially those in recovery. Therefore, this section will first figure out the required torque to rise the forearm on elbow and then based on that select the appropriate stepper motor and analyse the reason.

To calculate the required torque elbow, the arm length and weight is need. The calculation of body segment weights and lengths is based on reference data that relate body segment mass to a person's overall body weight [26]. According to national averages in the UK, the typical male weighs about 83.6 kg and is 175.3 cm tall, while the average female weighs around 70.2 kg with a height of 161.6 cm[2]. Taking both into account, the average adult has a body weight of approximately 76.9 kg and a height of 168.45 cm. The following calculations are based on these average values.

Table 8. Mean Segment Weight as Percentage of Total Body Weight [26]

Segment	Males (%)	Females (%)	Average (%)	Average weight (Kg)
Forearm	1.87	1.57	1.72	1.32
Hand	0.65	0.5	0.575	0.442
Forearm + hand	2.52	2.07	2.295	1.765

Table 9. Mean Segment length as Percentage of Total Body Length[26]

Segment	Males (%)	Females (%)	Average (%)	Average length (cm)
Forearm	15.7	16	15.85	26.7
Hand	11.5	11.5	11.5	19.37
Forearm + hand	21.45	21.75	21.6	46

Then, to estimate the torque required to assist forearm movement, a simplified static biomechanical model is used. In this model, the forearm and hand are treated as a single rigid segment rotating about the elbow joint. The torque ( $\tau$ ) needed is the product of the gravitational force acting on the segment and the horizontal distance from the elbow to the segment's center of mass.

$$\tau = F \cdot d = mgL = 1.765 \times 9.81 \times \frac{46}{2} = 3.97 \text{ Nm} \quad (12)$$

Based on the simplified static model, the estimated torque required to support the human forearm and hand during elbow flexion is approximately 4.0 Nm. To validate this estimation, Figure 30 presents experimental results from a referenced study based on six healthy adult volunteers ( $22.24 \pm 2.94$  years; height  $172 \pm 0.5$  cm; and weight,  $67.01 \pm 7.22$  kg), where elbow torque was recorded during a complete flexion task [27]. As shown, the peak torque reached just under 5 Nm, which is consistent with the estimated value above. This supports the reliability of the torque calculation used for motor selection in this system.

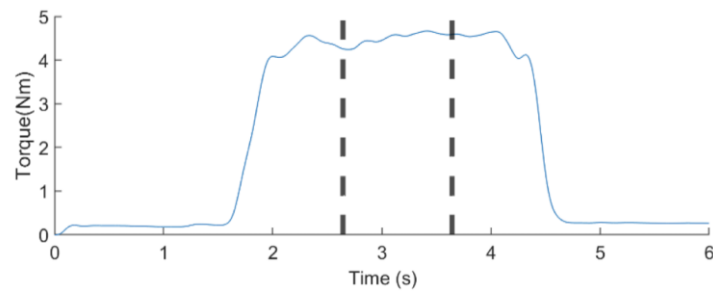


Figure 30. Elbow torque and MMG signal during a complete flexion task in healthy adult males [27]

Since this project is designed to assist rather than fully drive the user's arm, the motor does not need to produce the entire torque, it should provide partial support that complements the patient's muscle activity, particularly for individuals with limited strength. Using a lower torque motor is also safer and reduces the risk of injury, especially when working with patients who may have weakened or recovering muscles.

Based on these criteria, a NEMA 17 stepper motor was chosen for the system. The standard holding torque of a NEMA 17 is around 0.45 to 0.5 Nm, which is approximately 20% of the required torque. In addition, the NEMA 17 motor is compact and relatively lightweight, its built-in step resolution allows for smooth and precise movement, which works well with the voltage-based control algorithm introduced in the previous section. The motor is also compatible with the 8V supply (relatively safe working voltage for human) and can be easily driven by the Adafruit Motor Shield used in the project. The key specifications of the selected motor are summarized in the table below:

Table 10. NEMA 17 stepper motor [28]

Parameter	Value
Size	42.3mm× 42.3mm × 58mm
Weight	220g
Step Angle	1.8°
Holding Torque	0.59Nm

For driving the motor, the Stepper FeatherWing Add-on board was chosen. This driver is fully compatible with all Feather series microcontrollers, including the Feather M4 used in this project. Stepper motors can be operated under several stepping modes as shown in Table 11. In this project, Double Coil mode was selected. Since the chosen NEMA 17 motor is lightweight and compact but has limited holding torque (0.59 Nm), using double coil mode ensures maximum available torque output for assisting elbow movement.

Table 11. Stepper motor operation mode

Stepper Mode	Description	Advantages	Disadvantages
Single Coil	Only one coil is energized at a time	Low power consumption	Low torque
Double Coil	Two coils energized simultaneously	Higher torque, good stability	Higher power consumption
Interleaved	Alternating between single and double coil steps	Smoother motion	Slightly lower torque than double
Microstepping	Current controlled in fine increments	Very smooth, precise motion	Reduced torque per microstep

### 3.3.1.2 System Structure

Considering the time and budget limits, a threshold-based linear mapping control method was implemented to achieve simple but effective movement assistance in this project (Improved method induced in Last section).

As shown in Figure 31, the TIA outputs will first be read by ADCs and averaged to form a control signal  $V_t$ , the control process then begins with a 5s baseline calibration phase, during which the user holds their arm relaxed. The system collects 50 voltage samples and calculates their average as the baseline voltage  $V_{max}$ , corresponding to a fully relaxed muscle state. Afterwards, the user fully flexes his arm for another 5 seconds and records  $V_{min}$ , representing a fully contracted muscle.

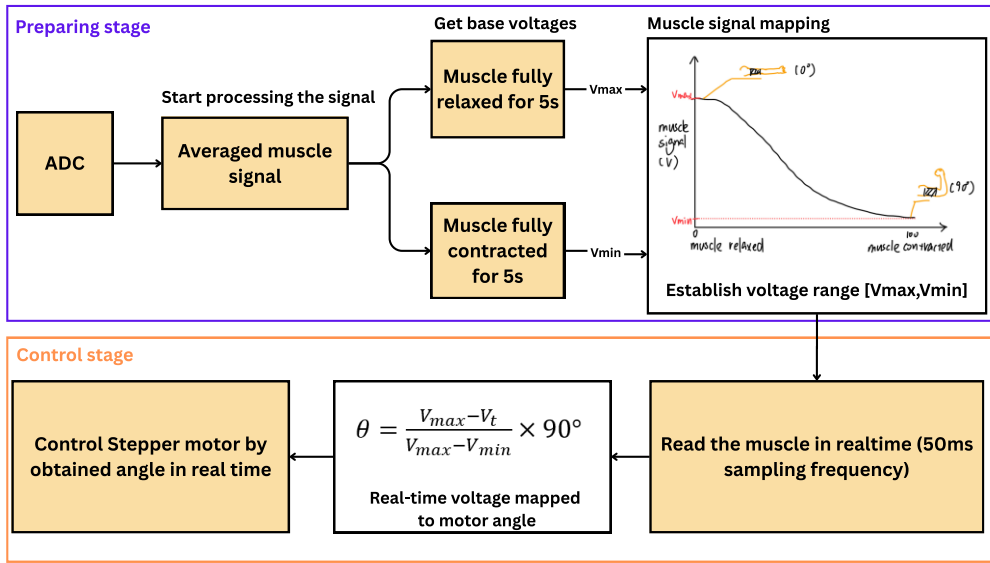


Figure 31. Block diagram of Control Process

This establishes a voltage range  $[V_{max}, V_{min}]$  which is linearly mapped to a  $90^\circ$  elbow motion range. For any real-time sensed voltage  $V_t$ , the control system calculates the intended motor rotation angle  $\theta$  using the formula (13). For example, the target motor angle will be  $45^\circ$  with  $V_t = 650\text{mV}$  if muscle signal range from  $500\text{mV}$  to  $800\text{mV}$ .

$$\theta = \frac{V_{max} - V_t}{V_{max} - V_{min}} \times 90^\circ \quad (13)$$

This calculated angle is then transmitted to the stepper motor controller, which drives the mechanical exoskeleton in real time to support elbow flexion or extension accordingly.

### 3.3.2 Signal Processing and Filtering

According to the control block diagram, as the first step of control system, the purpose of this stage is to accurately acquire muscle activity signals using the optical sensing system described earlier. Some of the key code used are presented as figures refer to Appendix III.

First, the analogue voltage outputs from three photodiodes (PDs) that attached along the biceps brachii are read through the microcontroller's ADC channels A0, A1, and A2. To ensure robust signal collection, the microcontroller first reads the voltage from each of the three channels separately, then calculates their average. The implemented code for this operation is shown in Figure 32:



```
// Read average voltage from A0, A1, A2
float readAverageVoltage() {
    int adcA0 = analogRead(A0);
    int adcA1 = analogRead(A1);
    int adcA2 = analogRead(A2);

    // Convert ADC to voltage
    float voltageA0 = adcA0 * (3.3 / 1024.0);
    float voltageA1 = adcA1 * (3.3 / 1024.0);
    float voltageA2 = adcA2 * (3.3 / 1024.0);

    return (voltageA0 + voltageA1 + voltageA2) / 3.0;
}
```

Figure 32. ADC implementation

During earlier circuit testing (see Section 3.2.4), it was observed that a noticeable 50 Hz noise appeared in the signal, mainly caused by power line interference. To address this, a simple 50 Hz digital low-pass filter was added. This filter smooths out 50Hz power line components, ensuring that the majority of the useful muscle signals (which are mainly below 30 Hz) are preserved. The digital low-pass filter uses a basic smoothing formula:

$$\text{filtered\_value} = \text{previous\_filtered\_value} + \alpha \times (\text{new\_reading} - \text{previous\_filtered\_value}) \quad (14)$$

Where  $\alpha$  is a small smoothing factor of 0.2, higher the  $\alpha$ , higher the response but also higher high frequency noise.

Despite the low-pass filter, small random fluctuations were noticeable in the muscle signal, which could affect motor control stability. Therefore, the further signal processing method Kalman filter is considered for this project. It provides an advanced method for reducing random noise while maintaining the ability to quickly track true signal changes. Unlike a simple low-pass filter that smooths all rapid changes, the Kalman filter dynamically adjusts its filtering based on estimated noise levels and signal behaviour, making it ideal for applications where both stability and responsiveness are required [29]. It predicts the next signal value and corrects it based on the new measurement, effectively balancing between following real changes and rejecting noise.



Figure 33. Open source simple Kalman Filter output [29]

The working principle of the Kalman filter can be complex, involving prediction and correction steps based on system dynamics and noise statistics. However, in this project, a simplified basic Kalman filter is implemented manually based on an open-source development (the performance is shown in Figure 33). It assumes a constant system model and updates the estimated muscle signal using a weighted average between the previous estimate and the current noisy measurement [29]. The weights depend on the expected process noise ( $Q$ ) and measurement noise ( $R$ ), which were tuned

experimentally. Specifically, lower Q values assume smoother muscle signals, while higher R values account for noisy sensor readings. The update equations are shown in Eqn (15) (16) (17):

$$Kalman\ Gain(K) = \frac{error\_estimate}{error\_estimate + R} \quad (15)$$

$$Estimate = Estimate + K \times (Measurement - Estimate) \quad (16)$$

$$error\_estimate = (1 - K) \times error\_estimate + Q \quad (17)$$

Where Estimate is the filtered output, Measurement is the latest noisy sensor reading, error\_estimate is the internal estimate of uncertainty, Q is the process noise covariance (small for smoother signals) and R is the measurement noise covariance (larger for noisier signals) [29]. In the Arduino implementation, the Kalman filter was applied to the averaged muscle voltage readings as shown in Figure 34. The processed muscle signal will then be used as the input for control loop.

```
// Kalman Filter function
float kalmanFilter(float measurement) {
    kalmanGain = errorEstimate / (errorEstimate + errorMeasure);
    estimate = estimate + kalmanGain * (measurement - estimate);
    errorEstimate = (1 - kalmanGain) * errorEstimate;
    if (errorEstimate < 1) {
        errorEstimate = 1;
    }
    return estimate;
}
```

Figure 34. Kalman Filter implementation

### 3.3.3 Contraction Detection and Motor Control Algorithm

After obtaining stable and accurate signals, the control algorithm is then be implemented in Arduino IDE to generate control commands for the stepper motor, enabling the exoskeleton to assist elbow movements in real time. The output will be the target angle for the motor drive relative to the actual angle of the arm.

#### 3.3.3.1 Control Strategy

The control algorithm is as illustrated in Figure 30, first, the user is asked to keep their arm relaxed for 5 seconds. During this period, the system samples the muscle signal at a rate of 10 samples per second, collecting a total of 50 samples. These readings are averaged to establish a baseline voltage, corresponding to the muscle's fully relaxed state. Next, the user performs a full biceps contraction for another 5 seconds. The lowest signal value during this phase is recorded, corresponding to the maximum contraction state. These two values define the range within which the muscle signal varies. And Eqn (13) is then applied to estimate the arm movement in digital style.

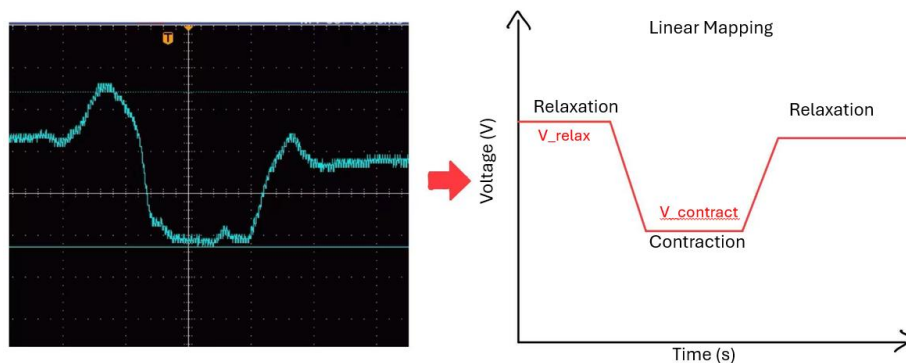


Figure 35. Linear mapping of the muscle signals



To translate muscle signal changes into motor commands, a linear mapping is applied. As shown in the mapping diagram (Figure 35), a fully relaxed muscle (highest voltage) corresponds to an elbow angle of 0°, while a fully contracted muscle (lowest voltage) corresponds to an elbow angle of 90°. Intermediate voltages are linearly mapped to angles between 0° and 90°, assuming a one-to-one linear relation between signal strength and muscle contraction effort. The mapping Equation is shown in Eqn (18).

$$\theta = \frac{V_{max} - V_t}{V_{max} - V_{min}} \times 90^\circ \quad (18)$$

In fact, the muscle signal is more complexed and can't be simply mapped into linear relationship. More advanced method such as machine learning should be implemented. However, considering the time limit for this project, linear relationship will be assumed. While this might not be perfectly accurate, it is sufficient for basic elbow movement assistance and proof-of-concept validation. The main objective of this project is to demonstrate the feasibility of using optical muscle signals for real-time rehabilitation control. As a first prototype, assuming a linear mapping simplifies the algorithm, reduces computational load, and ensures faster system response. Future improvements could involve collecting more muscle signal datasets and applying regression analysis or machine learning models to build a more accurate, nonlinear mapping between muscle activity and joint movement.

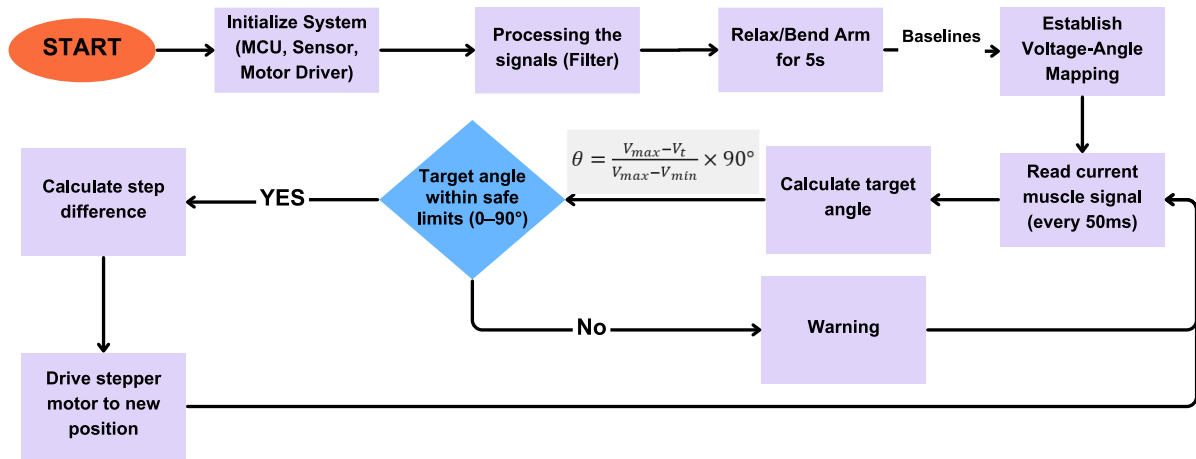


Figure 36. Control system flowchart

For safety considerations, maximum motor rotation is limited to 90°, even if the signal fluctuates unexpectedly. Furthermore, to ensure the patient's arm is not subjected to excessive forces, the stepper motor is configured to operate in high torque mode (double coil activation per step). In addition, the sampling frequency of the optical sensor was set at 50 ms per reading (20 readings per second), balancing real-time response with signal stability. This allows the system to follow the user's intention promptly without noticeable lag, fulfilling the goal of real-time rehabilitation assistance. The overall system flowchart is presented Figure 36.

### 3.3.3.2 Code Implementation

Based on the control structure outlined above, the system was implemented in Arduino IDE as shown below. The code is put in Appendix III. The program is responsible for calculating the intended elbow angle based on the voltage change and controlling the stepper motor movement accordingly.

First, the necessary libraries are included to interface with the Adafruit Motor Shield, and a stepper motor object is initialized. The motor speed is set to 20 RPM for smooth but not harmful (for patient) movement.

During the `setup()` function, a calibration phase is performed: The user is asked to hold their arm relaxed for 5 seconds each. During this period, 50 samples are collected from the optical sensor, averaged, and stored as the baseline voltage representing the fully relaxed muscle state. Next, the user fully contracts their muscle for another 5 seconds, and the minimum voltage during this phase is recorded as the `contractionMin` voltage. These two reference points (baseline and contraction minimum) are then used to map real-time muscle activity into elbow joint angles ranging from 0° (relaxed) to 90° (fully contracted).

In the `loop()` function: The optical signal is read and processed using the digital low-pass filter and Kalman filter described previously to reduce noise and stabilize the readings. Then, the filtered voltage is mapped linearly between the baseline and `contractionMin` to compute a target elbow angle. The target angle is compared to the current motor position. The system calculates the step difference needed and drives the stepper motor either forward or backward to follow the user's muscle movement. Motor movement is constrained within 0° to 90° to ensure user safety and appropriate rehabilitation assistance. All voltage readings, mapped angles, and motor actions are displayed in the Serial Monitor for visualization and debugging purposes. A detailed explanation of the motor behaviour testing will be presented in Section 3.3.4.

### 3.3.4 Real-Time Performance Testing and Tuning (Limitations)

Based on the above system, a control system was built. In this section, the control system will be evaluated and debugged to meet the specifications of the real-time control of the exoskeleton. To test the system, it should first integrate with sensing system which provide the signal input. Then, to verify the real-time performance of the combined system, a series of combined tests were performed on a healthy volunteer. The goal was to evaluate whether the optical sensor can reliably detect muscle contraction and whether the stepper motor can respond correctly to provide timely and smooth rehabilitation assistance. By testing, the parameters of the Kalman filter should be tuned to the appropriate level, as well as the modification of the control algorithm.

#### 3.3.4.1 Signal Processing and Filtering Test

The functions of the ADC and digital filter will be first tested. In order to ensure the generation of accurate control signals, motor is not powered in this test.

The user first calibrates the system by relaxing the arm and then fully contracting the biceps for 5 seconds each (as described in Section 3.3.3.2) to obtain the reference voltages  $V_{max}$  and  $V_{min}$ . After calibration is complete, the system will enter the control loop, which continuously reads and processes real-time signals and calculates the motor target angle.

After that, the performance is tested by doing the elbow flexion and extension movement, each lasting 2 seconds, record and compare the detected and processed muscle signals. In theory, the ADC signal should align with the TIA input, and the filtered control signal was expected to smooth the raw ADC input. In this experiment, oscilloscope was used to record the analogue signal output by the optical system, and Arduino serial plotter was used to record the signal converted by the ADC in the MCU, as well as the final control signal after being processed by the LP and Kalman filters. The analogue output of the oscilloscope and plotter output are shown in the figure 37:

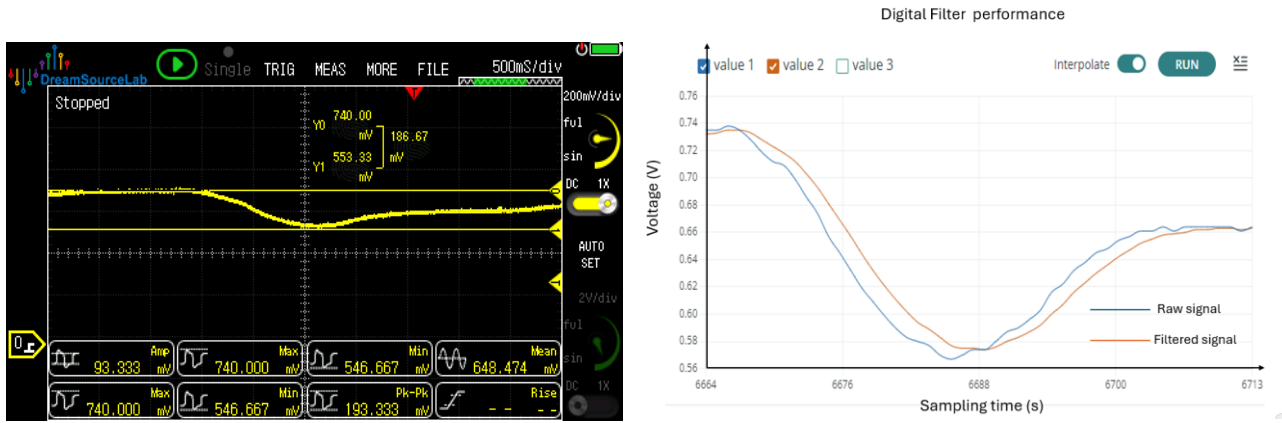


Figure 37. Comparison of analogue output (oscilloscope) and digital output (serial plot)

As shown in Figure 37, the analogue signal captured by the oscilloscope and the digital signal read by the microcontroller (after ADC sampling and simple filtering) exhibited similar trends. Both signals clearly reflected the elbow flexion and extension movements during the 2-second test window. The voltage dropped during muscle contraction and recovered during relaxation, which matched the expected behaviour described in Section 2.3.4.

In addition, Figure 27 clearly demonstrates the smoothing effect of the filters while preserving the essential muscle signal trend. Although slight delays and minor amplitude differences were observed, these discrepancies are reasonable. They mainly result from the finite ADC resolution (10 bits), the limited sampling rate (20 Hz), and the intentional smoothing introduced by the digital filters, which help enhance system stability. The tuned filter parameters are summarized in Table 11, where `errorEstimate` represents the expected uncertainty (variation) in the filter's current estimate of the signal. A lower value makes the filter more stable but slower to react to changes. `ErrorMeasure` represents the expected noise level in the incoming measurements, a lower value makes the filter follow the measurements more closely.

Table 12. LP and Kalman Filter parameters

Parameter	Value
<code>errorEstimate</code> (Kalman)	0.1
<code>errorMeasure</code> (Kalman)	0.005
<code>Alpha</code> (Low Pass)	0.2

Overall, the signal acquisition and filtering system performed as expected. It successfully captured the muscle activity waveform with sufficient fidelity and real-time responsiveness, validating both the optical sensor circuit and the signal processing approach developed in Section 3.2.

### 3.3.4.2 Realtime Motor Control Test

After confirming that the muscle signal acquisition and filtering were working correctly, the next stage involved testing the real-time control of the stepper motor based on muscle activity. The aim was to validate whether the system could accurately interpret muscle signals and drive the exoskeleton movement smoothly and stably.

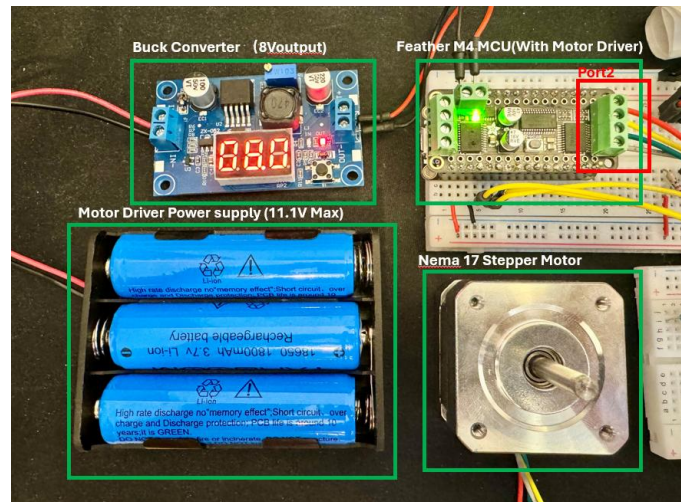


Figure 38. Motor FeatherWing and NEMA 17 connection

Figure 38 shows the hardware setup for motor control, where the Feather M4 is connected to the Adafruit Stepper FeatherWing and a NEMA 17 stepper motor, powered by an 8 V buck converter. The FeatherWing driver board, chosen for its compatibility and integrated safety features, includes a dedicated PWM driver with I<sup>2</sup>C control, thermal and overcurrent protection, and automatic motor disable on startup. The Adafruit MotorShield Arduino library enabled seamless software integration.

Then, to evaluate the motor response accuracy, a series of controlled elbow flexion tests were conducted at approximately 0°, 30°, 60°, and 90°. For each target angle, the actual arm position was recorded via photograph, along with the corresponding motor angle displayed on the Arduino Serial Monitor and a photo of the NEMA 17 stepper motor movement. If control theory and signal processing works well, the motor was expected to perform a similar position or movement with the actual arm. For example, when arm moved from 0-30°, the simulated arm should also move from original degree to 30°. The basic functional test was conducted to verify the control algorithm first, and then accuracy test.

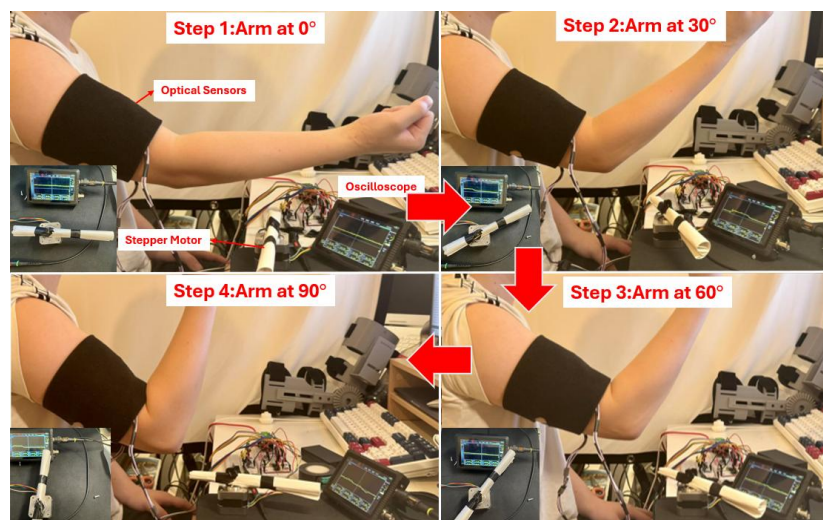


Figure 39. Example of motor control at different elbow flexion angles

As illustrated in Figure 39, the test began by activating the optical sensors and initializing the system. The user then gradually moved their arm in four stages from full extension (0°) to full flexion (90°). At each step, the arm was held stationary until both the Serial Monitor readings and motor rotation



stabilized. Once stable, the data were recorded, and photographs of the motor position (with a simulated arm to amplify motor motion results) and oscilloscope readings were taken.

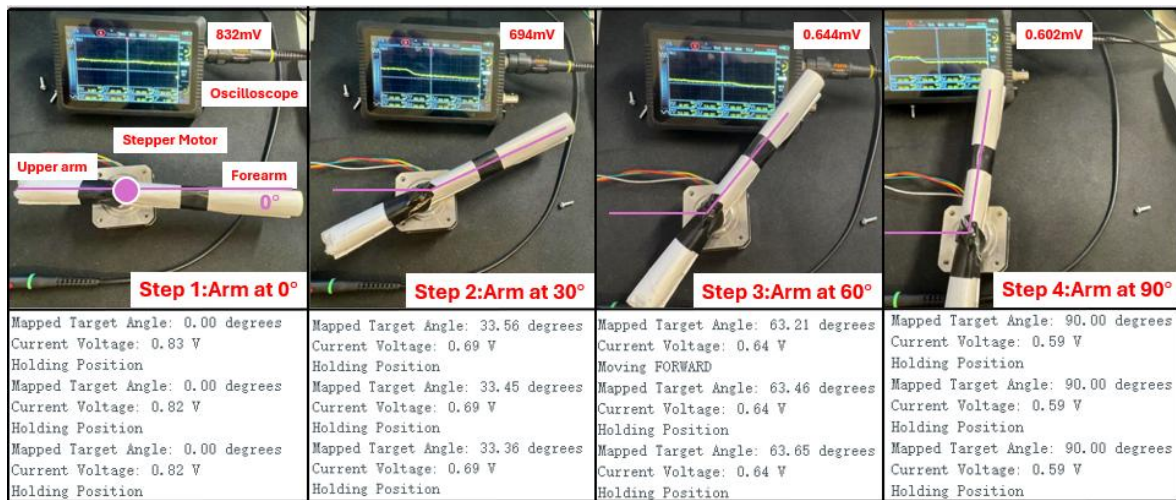


Figure 40. Motor-controlled simulated arm positions at 0°, 30°, 60°, and 90°, with corresponding digital data from the Arduino Serial Monitor.

Figure 40 shows the test result of the motor control system, it successfully demonstrated the control system performance, with the stepper motor reliably responding to the user's muscle contractions and relaxation in a controlled laboratory setting. The overall trend of motor movement closely matched the arm's actual position changes but with small different, validating the fundamental control logic implemented in the previous section.

To further evaluate accuracy and repeatability, the user repeated flexion movements from 0° to approximately 60° five times. For each attempt, the filtered voltage and corresponding mapped angle were recorded (Table 13). While the motor followed the trend of arm movement, the recorded angles showed fluctuations, reflecting limitations in signal consistency and mapping precision.

Table 13. Obtained voltage and motor target angles at elbow of 60°

Test	Filtered Voltage (V)	Target Angle (°)
1	0.64	63.21
2	0.58	61.2
3	0.75	63.5
4	0.61	57.33
5	0.59	62.1

Overall, the control system performed as expected and was able to respond to muscle activity correctly. However, during testing, several practical limitations were observed. First, a noticeable delay occurred between muscle activation and motor response. This was primarily caused by the signal filtering process, including a Kalman filter and low-pass filter. While these filters effectively reduced signal noise, they also introduced latency. However, in rehabilitation scenarios, a moderate delay can be beneficial for safety and user comfort, allowing users to engage muscles gradually and avoid abrupt movements.

Second, the initially configured 50 ms sampling interval introduced hardware issues. Although faster sampling improves responsiveness, it caused excessive current fluctuations and overheating in the motor and driver. Continuous micro-adjustments of the holding position stressed the hardware and

eventually led to MCU burnout. To mitigate this, the sampling interval was increased to 200 ms, reducing power demand and improving thermal stability.

Lastly, accuracy and repeatability were constrained by the use of a simplified linear voltage-to-angle mapping model. Due to natural variability in muscle signals, sensor placement, and arm posture, the system could not always reproduce consistent motor output for identical muscle contractions. For instance, skin tension, fatigue, or minor sensor shifts affected voltage readings significantly [5]. To address this, the target angle tolerance was set to  $\pm 5^\circ$ , so that repeated trials within a range (e.g.,  $55^\circ$ – $65^\circ$  for a  $60^\circ$  target) were considered acceptable. While this adjustment improved practical usability, it highlighted the limitations of a rule-based mapping system. Achieving higher precision would require more advanced approaches, such as machine learning-based pattern recognition or adaptive control algorithms. These improvements are reserved for future development, as this project focused on demonstrating the basic feasibility of an optical-sensing rehabilitation control system.

### 3.4 Exoskeleton 3D Model Design and Construction

After verifying that the optical muscle sensing and real-time motor control system worked as expected, the next step was to integrate these functions into a wearable mechanical structure. The purpose of this stage was to design and construct a lightweight upper limb exoskeleton (Shown in Figure 41) that could incorporate with the constructed sensing and control system to achieve a correct elbow flexion and extension movements based on the detected muscle activity.

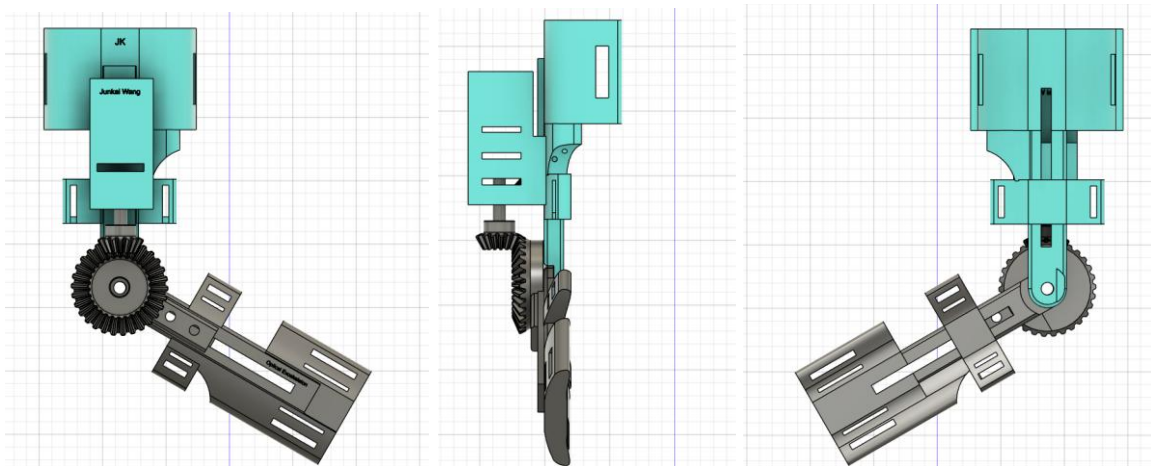


Figure 41. Exoskeleton 3D model designed in Fusion 360

Given the project's aim to develop a simple, low-cost rehabilitation prototype, the exoskeleton design prioritized ease of construction, comfort, and safe interaction with the user. The structure was focused on providing 1-DOF assistance at the elbow joint. This section outlines the design requirements, conceptual development, 3D modelling, material selection, and construction process of the exoskeleton, followed by basic mechanical validation tests.

#### 3.4.1 Design Requirements and Exist System Review

##### 3.4.1.1 Design Requirement

The design of the exoskeleton needed to satisfy several important requirements to ensure it was suitable for a rehabilitation application, safe for users, and compatible with the control system developed in previous sections. The main design criteria are summarized below:

First ensure comfort and safety. Soft straps and adjustable components used to adapt to different arm sizes while preventing excessive pressure on the skin. And restrict the move degree ensure safety. Keep exoskeleton as light as possible while maintaining sufficient strength. 3D-printed plastic materials should be chosen to achieve a balance between weight and strength. The mechanical design was focused on elbow flexion and extension. Finally, the design should be able to case all the sensing and control system, such as position to put optical sensors and stepper motors.

Based on these requirements, the design approach emphasized practicality and simplicity, aiming to deliver a functional demonstration model rather than a fully optimized medical device or product. The tool used for 3D modelling are AutoDesk Fusion 360. The following sections describe the concept development, detailed design, and construction process of the exoskeleton.

### 3.4.1.2 Review of Existing Exoskeleton Systems

To better inform the design process, several existing upper limb rehabilitation exoskeleton systems were reviewed. These systems vary in complexity, control strategies, mechanical structure, and intended application areas. A summary of representative examples is provided in Table 14.

Table 14. Robotic rehabilitation systems used for upper limb

System	DOF	Supported Movement	Actuators	Further Description
Intelligent Upper-Limb Exoskeleton [30]	1	Elbow flexion/extension	Soft pneumatic artificial muscles (PAMs)	Integrates soft, thin-film sensors and electronics with PAMs, offering immediate assistance based on muscle activation. Lightweight and wearable design.
Cable-Driven Upper Limb Exoskeleton [31]	1	Elbow flexion/extension	DC motor with cable transmission	Features a compact and lightweight design using Bowden cables for remote actuation
Robotic Arm Orthosis [32]	1	Elbow flexion/extension	DC brushed motor	Provides assistive torque during elbow flexion-extension tasks, designed for stroke rehabilitation with a focus on portability.
3D Printed Exoskeleton [33]	1	Elbow flexion/extension	Servo motor	An affordable solution optimized for portability and modularity, utilizing 3D printing techniques for ease of manufacturing and customization.

Compared to the reviewed systems, this project follows a similar design philosophy by targeting single-DOF elbow movement and prioritizing lightness and simplicity. However, instead of pneumatic or cable-driven systems, a compact electric motor with a simple optical sensing control strategy was chosen to balance performance and budget constraints.

## 3.4.2 3D Modelling

### 3.4.2.1 Design Parameters

Fusion 360 was selected as the CAD software for designing the exoskeleton due to its user-friendly interface, integrated mechanical simulation tools, and compatibility with 3D printing workflows. The designed exoskeleton consists of three major sections: the upper arm support, the forearm support, and the drivetrain assembly.

Before modelling, the dimensions of the human arm must be defined first. Although adjustable length designs are considered initially, because it commonly used to accommodate different users, but



achieving smooth adjustability through 3D-printed parts can be challenging due to friction and precision. Therefore, a fixed length design was designed for this prototype instead. The dimensions were based on anthropometric data. Table 15 summarizes the mean segment lengths as a percentage of total body height, combined with forearm and hand measurements derived from Table 9 [26].

Table 15. Mean Segment length as Percentage of Total Body [26]

Segment	Males (%)	Females (%)	Average (%)	Average length (cm)
Upper Arm	17.2	17.3	17.25	29.05
Forearm	15.7	16	15.85	26.7
Hand	11.5	11.5	11.5	19.37
Forearm + hand	21.45	21.75	21.6	46

From Table 15, the average forearm length in the UK population is approximately 26.7 cm. Considering ergonomics, ease of wearing, and reference to commercial exoskeletons. Both the upper arm and forearm sections were each designed with a fixed length of 20 cm, starting from the elbow. This mid-range value supports a wide range of users without making the device bulky or restrictive.

Regarding the connection method, referring to the similar exoskeleton design in table 14, the strap-type fixation can effectively adapt to different arm circumferences while maintaining stability. Therefore, soft straps are added to the design to ensure that the exoskeleton is firmly fixed to the user's arm. In addition to structural considerations, the motor, microcontroller, and battery housing are mainly arranged along the upper arm part. This design reduces the load on the forearm and makes arm movement easier and more natural, which is consistent with the rehabilitation goal of focusing on assisting elbow flexion.



Figure 42. Types of common gears [34]

For transmission, a bevel gear mechanism was designed (Figure 42) to convert the motor's rotational motion into the elbow joint's flexion/extension movement. Straight bevel gears are conical gears with straight teeth that are used to transmit motion between intersecting shafts, typically at a 90° angle. In this design, the motor axis is mounted along the upper arm, and the gear redirects the motion to drive the forearm rotation around the elbow [34]. The pinion gear was designed with 15 teeth and the driven gear with 30 teeth. This configuration achieves a mechanical advantage of 2, as calculated by Eqn (19):

$$\text{Mechanical Advantage (MA)} = \frac{N_{\text{Gear}}}{N_{\text{Pinion}}} = \frac{30}{15} = 2 \quad (19)$$

where  $N_{Gear}$  and  $N_{Pinion}$  represent the number of teeth on the driven gear and driving pinion, respectively. This 2:1 ratio results in an output torque that is twice the input torque, while the rotational speed is reduced by half, as shown in Eqn (20). That means that the motor output range should be adjusted to 0-180° to drive the exoskeleton to achieve a range of 0-90°.

$$Speed\ Ratio = \frac{\omega_{output}}{\omega_{motor}} = \frac{N_{Pinion}}{N_{Gear}} = \frac{1}{2} \quad (20)$$

$$Motor\ operation\ degree\ range = \frac{1}{2} \times exoskeleton\ range \quad (21)$$

Such a design is particularly beneficial for rehabilitation exoskeletons because it allows the motor to operate with lower load stress while still providing sufficient torque to assist the patient's forearm movement. At the same time, the reduced output speed ensures safer and smoother motion, preventing abrupt or aggressive movements that might harm users with weakened muscles.

Finally, to reduce weight and improve thermal dissipation, material was selectively removed from some less important areas, introducing ventilation holes and cutout patterns without compromising structural integrity. The following section details the final 3D models and provides explanations for each major design feature.

### 3.4.2.2 Model Design and Explanation

As shown in Figure 40, the exoskeleton is divided into three primary modules: the upper arm support, forearm support, and the bevel gear actuation mechanism. Each module was specifically designed to meet the functional and safety requirements identified for rehabilitation applications.

#### Upper arm:

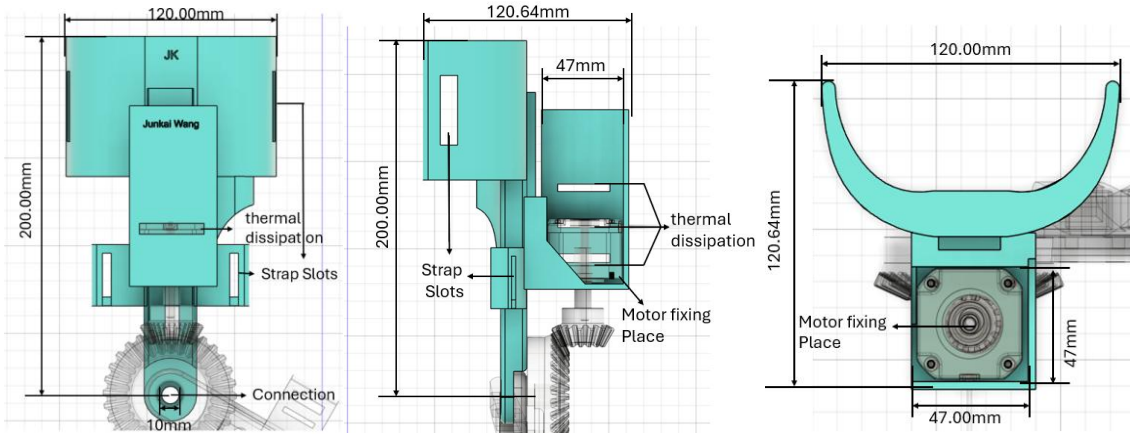


Figure 43. Upper arm 3D model dimensions

First, the designed 3D model for the upper arm section is shown in Figure 43. According to the design specifications, the main structural length was set to 200 mm to match the anthropometric data and support the mechanical requirements. To secure the exoskeleton onto the user's upper arm, four strap slots were incorporated symmetrically on the sides of the structure. These elongated slots allow adjustable Velcro straps to pass through, providing stable and comfortable fixation across a range of arm sizes.

At the center of the upper arm support, a motor fixing platform was designed to accommodate the NEMA 17 stepper motor. Based on the typical motor dimensions (42.3 mm × 42.3 mm × 58 mm) listed in table 11, a reserved space of 47 mm × 47 mm was implemented to ensure sufficient

clearance for installation and stabilization. In addition to motor mounting, space was reserved along the outer side of the structure for placing the optical sensor circuits and the battery packs. To further enhance performance, ventilation holes were introduced both along the main shaft and around the motor fixing area. These holes ensure thermal dissipation during continuous motor operation. In addition, a 10mm connect hole was designed for strong enough support between two parts.

### Bevel Gear power transmission and connection:

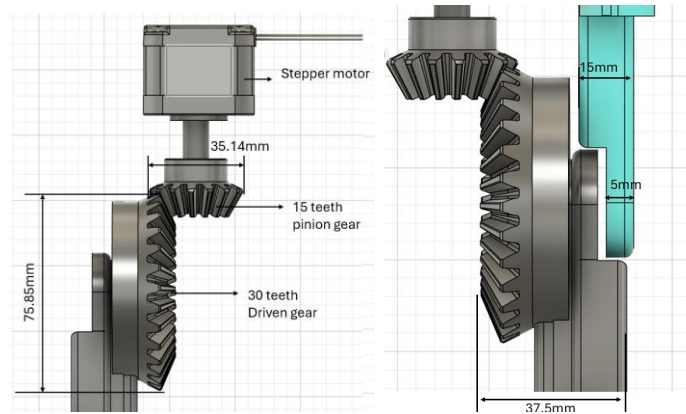


Figure 44. Power transfer bevel gear system

The transmission of motor power to the forearm rotation is achieved through a bevel gear system, as illustrated in Figure 44. This system converts the rotational output of the stepper motor, which is mounted along the upper arm support, into the rotational movement needed around the elbow joint. A 15-teeth pinion gear with centre empty is directly attached to the motor shaft (but 3D printed individually), while a 30-teeth driven gear is mounted orthogonally to it. The bevel gear arrangement allows efficient transfer of torque between two shafts positioned at approximately 90 degrees to each other, aligning with the human elbow axis.

The selected gear sizes were based on the exoskeleton supports size. The motor-to-pinion shaft distance was set at 35.14 mm, and the driven gear diameter was approximately 75.85 mm, ensuring sufficient engagement while maintaining compactness. The system achieves a 2:1 gear reduction ratio, which can double the output torque and a halving of the output rotational speed. The driven gear was rigidly fixed to the forearm support, therefore the motor's torque to be directly transferred to the forearm brace. This mechanical integration provides both actuation stability and structural strength, supporting repeated flexion-extension motions without significant mechanical play or deformation. The rigid connection also improves the precision and responsiveness of the system.

### Forearm:

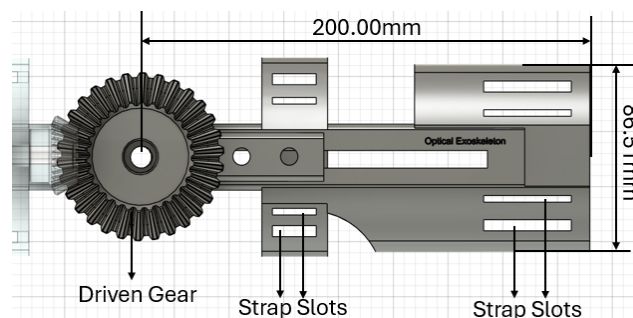


Figure 45. Forearm arm design

The design of the forearm section is presented in Figure 45. The forearm support was modelled with an overall length of 200 mm and a maximum width of 86.51 mm, which can provide sufficient

coverage for supporting a range of forearm size. However, it might be large for some groups. To securely attach the forearm support to the user's arm, two strap slots were incorporated at both the proximal (near the elbow) and distal (near the wrist) sections. This dual-slot configuration allows the Velcro straps to tightly secure the structure even for users with slimmer forearms, ensuring both stability and user comfort during operation.

In addition, longitudinal cuts have been added to the main axis of the forearm structure. This can effectively reduce the overall weight of the forearm section without compromising its mechanical integrity. By minimizing the use of unnecessary materials, the design achieves two key goals: reducing the burden on the patient's forearm, thereby improving comfort and safety during rehabilitation training; reducing motor load, helping to maintain system efficiency, extend motor life, and improve overall control responsiveness.

### 3.4.3 3D printing and Mechanical Testing (Limitations discussed)

After completing the 3D modelling of the exoskeleton, the next step was to make the physical components using 3D printing. The key considerations in this stage included parameter selection for optimal print quality, material choice based on mechanical and thermal requirements.

#### 3.4.3.1 Printing Process and Parameter Settings

In preparation for 3D printing the exoskeleton components, multiple STL export parameters were manually adjusted to ensure printability and mechanical properties. The design process still considered how different settings and structural arrangements would affect the quality of the final part [36]. For example, increasing the wall thickness and filling density of load-bearing areas (such as the gear seat and actuator interface) helped improve overall strength. However, overly stiff structures increase the risk of warping and make post-processing more difficult. Specifically, the bevel gear components were exported with higher surface resolution and thicker wall thickness to improve strength and precision under torque transmission. This design decision ensured that the gear teeth maintained meshing integrity during motor-driven elbow flexion. However, these improvements also made printing more challenging due to increased material usage and the need for precise support locations.

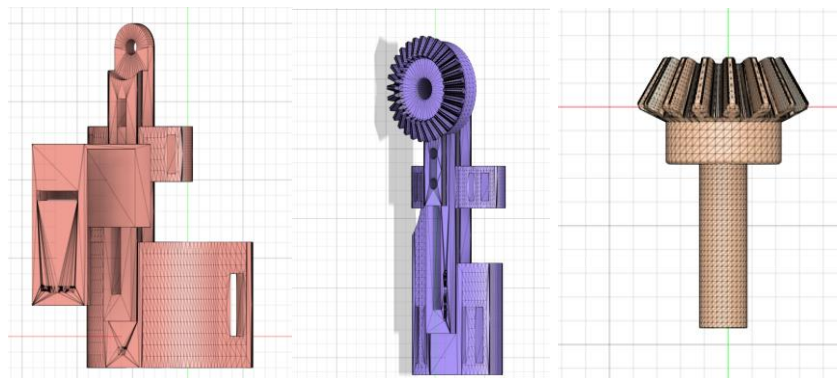


Figure 46. Exported STL files for 3D print

Tree-like support structures were used to simplify post-processing, especially around internal cutouts and under overhangs. These supports reduce material consumption and are easier to remove without damaging critical components. For the two largest components, the upper arm and forearm structures, their height exceeded the horizontal limit of the print bed, so they needed to be placed vertically. Although printing at a 45° angle could theoretically improve interlayer bonding strength, it was not feasible in this case due to space limitations and stability issues during printing.

### 3.4.3.2 Material Selection and Comparison

Two materials were considered for printing the exoskeleton, PLA (Polylactic Acid) and ABS (Acrylonitrile Butadiene Styrene). Table 16 provides a comparison of their key properties.

Table 16. Comparison of PLA and ABS Properties [35]

Property	PLA	ABS
Strength	Good tensile strength	Higher impact resistance
Thermal Resistance	Low (60 °C softening point)	High (100 °C softening point)
Flexibility	Brittle	Tough and more flexible
Printability	Easy to print	Requires heated bed; more prone to warping
Surface Finish	Smooth, good detail	Slightly rougher, may require post-processing
Environmental Stability	Poor (deforms under heat/sunlight)	Good

While PLA offers excellent printability and surface finish, it might be suitable for mechanical structures exposed to dynamic loads or elevated temperatures. For this project, the printed parts must withstand motor heat, friction, and repeated movement, especially around the gear and motor mounting points. Therefore, ABS was selected for all components due to its greater mechanical durability, higher thermal resistance, and better long-term stability in wearable rehabilitation applications.

### 3.4.3.3 Printed Part Evaluation and Assembly Testing

Figure 47 shows the three primary components after printing: the upper arm support, the forearm support with the integrated driven gear, and the pinion gear. Upon inspection, all parts were printed successfully with no major dimensional issues. The gear teeth remained well-defined and meshed properly during manual testing, motor can be fixed on firmly and all strap slots and mounting interfaces were preserved as designed.

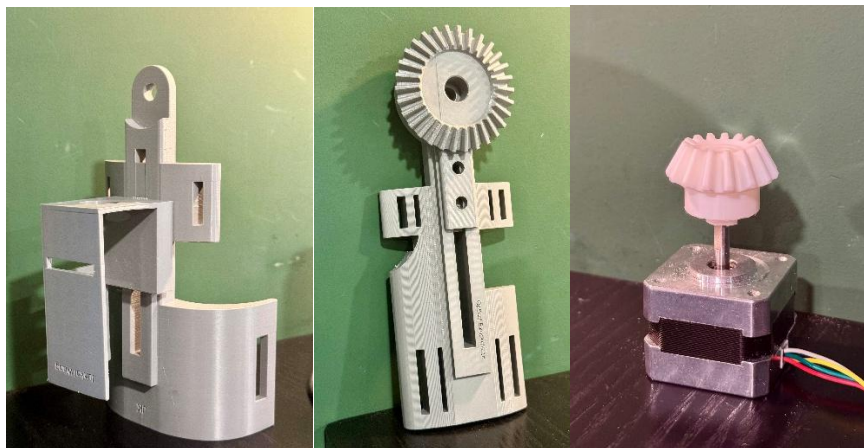


Figure 47. Exoskeleton Parts: Upper arm, Forearm and pinion Gear

Among the three, the upper arm part revealed a design-related issue. The slot for housing the stepper motor was too tightly enclosed, which limited airflow and caused concern for potential heat buildup during extended operation. To address this, the inner wall of the motor cavity was partially removed after printing, leaving the motor partially exposed on one side. This modification improved



thermal dissipation while preserving mechanical strength, as the unsupported region was non-load bearing.

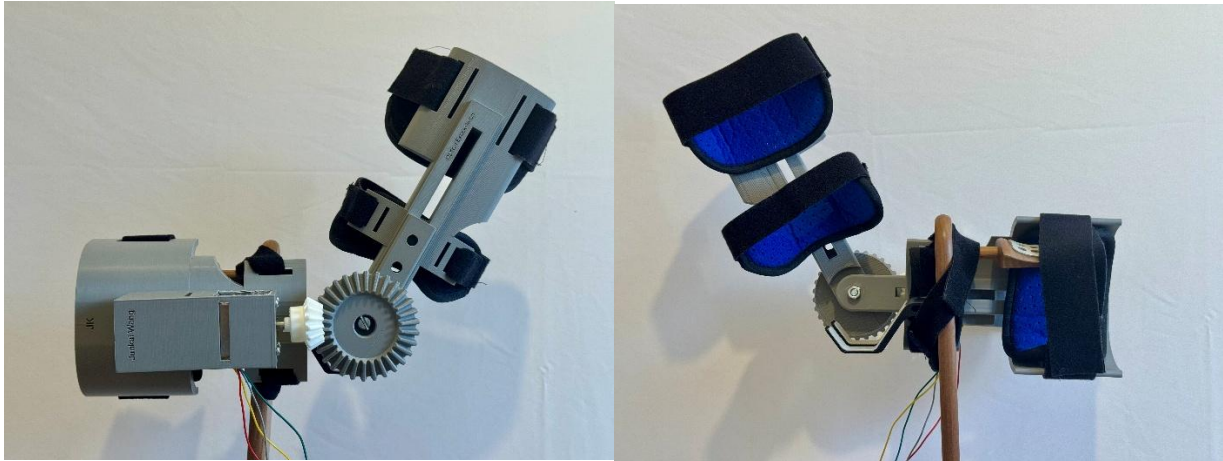


Figure 48. Fully assembled exoskeleton

Figure 48 illustrates the fully assembled exoskeleton, including integrated Velcro straps and soft padding. Padding was applied both inside the strap regions and between the outer exoskeleton and the user's arm to enhance comfort and improve conformity to different arm shapes. This addition also helped the optical sensor maintain better surface contact during muscle activity, which is crucial for signal reliability.

## 4 Final System Testing and Validation

This section will focus on testing the entire integrated system. The wearable exoskeleton prototype will be evaluated under real-world use conditions to assess its overall performance in terms of response accuracy, repeatability, and compliance with project specifications. The following analysis will present the test methods, results, and comparisons to expected performance goals to determine the effectiveness and reliability of the final prototype.

### 4.1 Testing Setup and Preparation

As described in the System Modelling and Implementation section, each subsystem of the exoskeleton, including the optical sensing circuit, signal processing algorithms, and motor control logic, was independently developed and thoroughly tested. These tests confirmed that the individual modules functioned as expected under controlled conditions. Although some deviations were observed during the early testing phase, they are considered as acceptable elements. For example, the muscle contraction signal swing produced by the optical sensing module was approximately 0.3V, slightly lower than the initially expected 0.9V. However, the signal was still within a usable and consistent range, with a clear response to muscle activation. In control system testing, this signal range was successfully used to drive the motors to the target angle with an average tracking error of approximately  $\pm 5^\circ$ , indicating that its response speed was acceptable for the intended application.

To begin testing the full system, all the components were assembled and tested. The stepper motor was mounted into the dedicated slot on the 3D-printed upper arm section and ensure that it was aligned with the bevel gear system. The motor wires were connected to the breadboard, where the motor driver and the Feather M4 microcontroller were placed. This allowed easy adjustment and debugging during the test phase.

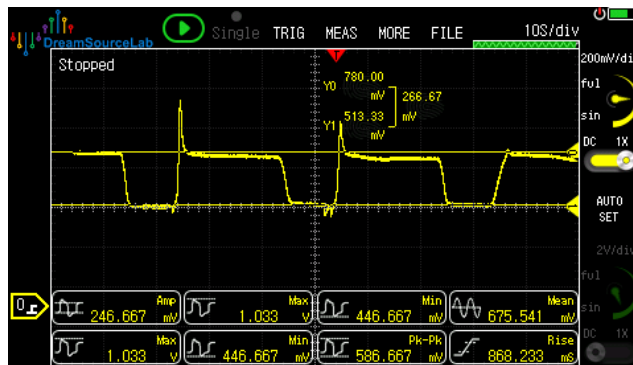


Next, the optical sensing module, was positioned over the user's biceps on the right arm. An elastic wrap was used to hold the sensor in place firmly so that it maintained good contact with the skin during movement and prevented the light leakage and influences. After that, the exoskeleton was worn over the arm. The adjustable straps were tightened to keep the structure stable, and soft foam pads were added at contact points to improve comfort and help the sensor stay in position. A photo of the fully assembled system worn on the arm is shown in Figure 49.

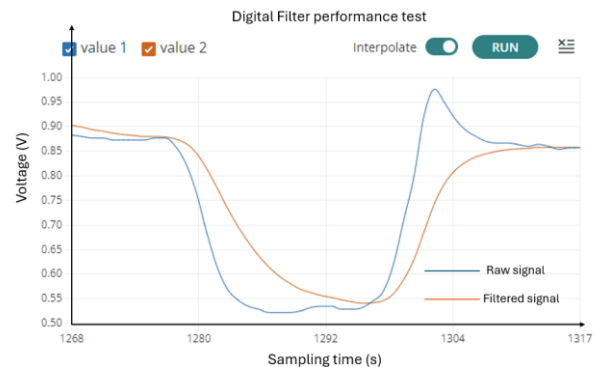


Figure 49. Final assembled system

Before testing the full system with motor actuation, an initial signal acquisition test was carried out without powering the motor. This was done to check whether the optical sensor and signal processing system were working properly. For this test, the user wore the exoskeleton and kept their arm relaxed. Then, they were instructed to perform three complete cycles of elbow flexion and extension. First, the arm is completely relaxed, then contracted for 10s, and then relaxed again. There is a 20s interval between each movement. The entire test lasts about 100s. During this time, the signal output from the photodiode array was recorded using the oscilloscope, as shown in Figure 50a.



(a)



(b)

Figure 50. (a)PD output from Oscilloscope; (b) Serial Plotter output (Value 1: Raw; Value 2: Filtered) in test setup

The results demonstrate that the optical sensing system was able to produce stable and repeatable voltage signals in response to muscle activity, with voltage levels ranging of 0.27V from approximately 513 mV (full contraction) to 780 mV (fully relaxed). This confirms that the sensor could reliably detect muscle contractions and produce clear voltage changes for each movement. The expected voltage swing was around 0.3 V, and the observed output was within this range. The aim of this test was to verify that the signal was consistent and stable across multiple movements, and suitable for further processing as input to the motor control system.

Finally, the behaviour of the ADC and the digital filtering algorithm (the Kalman filter and averaging steps) was evaluated using the Arduino Serial Plotter, as shown in Figure 50b. The raw voltage signal and the filtered output were plotted for one contraction. The filtered signal shows the smoother results, but with approximately 0.08s delay. This test verified that the signal processing system could operate continuously without crashing or producing unstable output. After confirming that both the optical sensing and signal processing systems were functioning as expected, the motor was connected for the full system tests described in the following sections.

## 4.2 Final System Test

In this section, the performance of the integrated exoskeleton system is evaluated through Four tests. These include functionality validation, accuracy and repeatability measurements, and latency analysis. The purpose of these tests is to assess whether the system can reliably respond to muscle activity, follow the user's intended motion, and provide smooth and timely actuation. The limitations of system's performance as a functional rehabilitation prototype will be discussed.

### 4.2.1 Functional Test

First, this test was designed to verify the overall functionality of the integrated exoskeleton system that whether it could detect the user's muscle activity in real time and drive the motor accordingly to produce coordinated movement. In theory, the motor actuated exoskeleton should be able to follow the user's arm movement, but definitely have some delay and derivation as observed in motor control test (Section 3.3)

To test the basic system function, the user wears the optical sensor on the right arm and fixes it on the biceps using an elastic wrap to achieve stable contact, as shown in the test setup. Then, in order to show the results more clearly, the exoskeleton was positioned close to the user but not worn during this test. Then, the user was instructed to perform a full elbow movement starting from full extension ( $0^\circ$ ), flexing to approximately  $90^\circ$ , and then returning to  $0^\circ$  (The controlled target angle was increased to  $0$ - $180^\circ$  because of the 2:1 gear reduction ratio). To visually demonstrate the continuous motor response, a 60FPS video recording was made. six frames were extracted from the full motion ( $0^\circ \rightarrow 90^\circ \rightarrow 0^\circ$ ) and are shown in Figure 51.

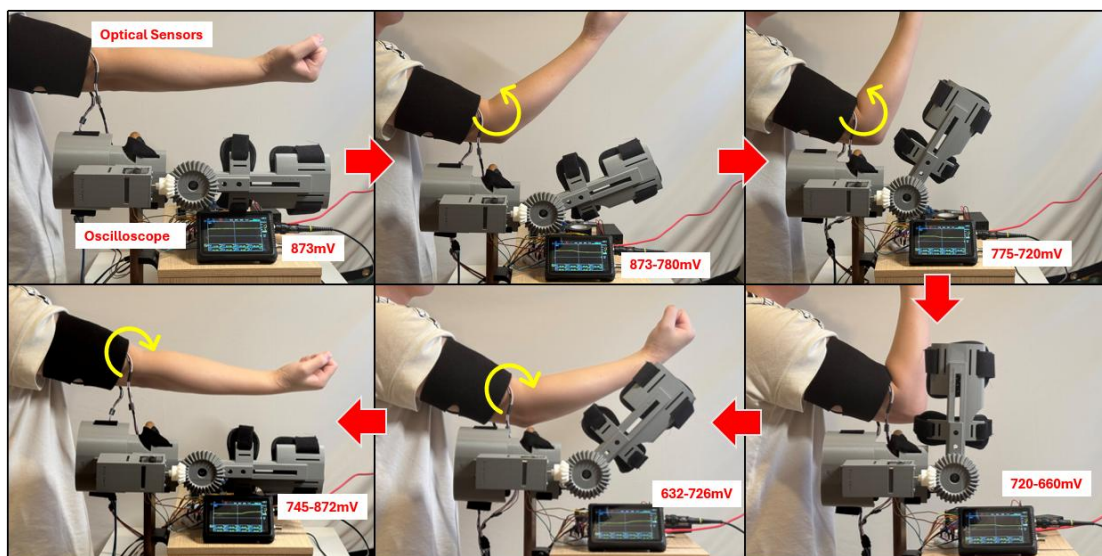


Figure 51. Six frames showing one full cycle of elbow flexion and return ( $0^\circ \rightarrow 90^\circ \rightarrow 0^\circ$ )

The results show that the system can detect muscle activation and move the exoskeleton in a smooth and responsive way. The exoskeleton support moved closely with the user's arm, which means the signal and motor worked together well in real time. However, some small delays and angle differences were noticed during the movement. Even so, the test proves that the system meets the basic goal of working as a wearable assistive device, and the specific values of delays and accuracy will be tested as follows.

#### 4.2.2 Accuracy and Repeatability Evaluation

Since the exoskeleton was tested responsive to muscle activation but with delays and angle differences, the next step was to evaluate the accuracy it could match with the arm angle. The test used four predefined elbow positions: 0°, 30°, 60°, and 90°. For better visibility of control accuracy, the user wore the exoskeleton on at upper arm but without fixing the forearm, so that the motor driven support motion could be visually compared with the user's actual elbow position.

At each target angle, the user held and waited for the exoskeleton to stabilize and then captured a frame to record the motor output. These frames are shown in Figure 52, which shows the mechanical response at each target position.

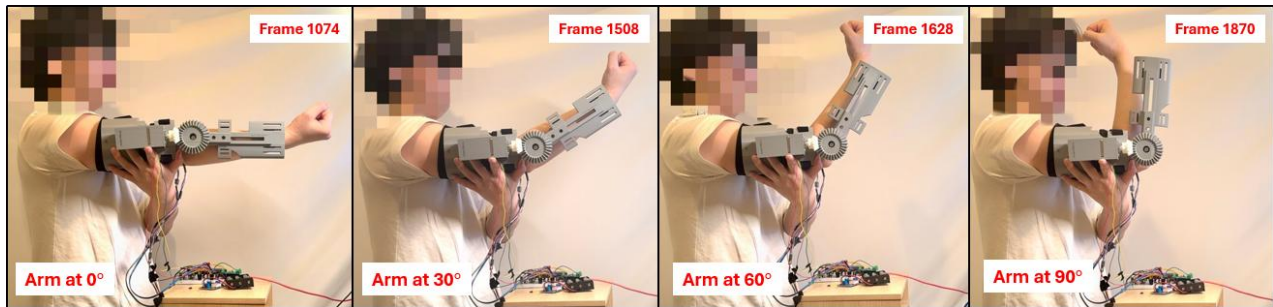


Figure 52. Exoskeleton output at target angles 0°, 30°, 60°, and 90° (forearm not fixed)

In this experiment, the exoskeleton demonstrated good overall performance in following the user's intended elbow angles. The motor output closely matched the arm position, particularly in mid-range angles around 30° and 60°, where the optical signal was more stable and the mapping relationship was more reliable. However, at the extremes, such as below 20° and above 70°, noticeable deviations were observed between the motor angle and the actual elbow position. This can be attributed to the limitations of the current control logic, which uses a simple linear voltage-to-angle mapping. In reality, muscle signals vary non-linearly across different contraction intensities, and this causes higher error at the low and high ends of the motion range.

To further assess accuracy and consistency, the same four angle test was repeated six times under same conditions (continuously do six four angle tests in one experiment). The resulting motor angles were recorded and compared with the target angles, and the maximum deviation for each target angle was summarized in Table 17.

Table 17. Accuracy and repeatability test results

Target Angle	Avg Measured Angle	Max Deviation	Mean Error
0°	0°	0°	0°
30°	29.4°	-4.9°	2.58°
60°	62.4°	+6.1°	4.56°
90°	89.1°	-0.88°	0.18°

The results show that the system achieved good accuracy at both 0° and 90°, with only small deviations observed. At 30°, the motor response also closely followed the expected position with minimal error. However, the largest deviation was recorded at 60°, where the average error increased slightly. This could be due to a less stable signal in mid-range contractions, where muscle activation is not as distinct as at full extension or full flexion. Despite this, the overall error across all four target positions remained within an acceptable range for a low cost assistive device.

There are one issue that careful setup and calibration are essential before each test, as the tightness and position of the elastic strap, as well as the initial orientation of the arm, significantly affect signal accuracy. This is because the current control logic relies on a simple linear mapping between the maximum and minimum voltage values recorded during the initial calibration phase. However, the signal range and voltage swing can vary depending on the arm posture. For example, when the arm is hanging vertically rather than held horizontally (as in the current test setup), the optical sensor output will change. As a result, the same control logic will become inaccurate if the user changes posture during operation. In addition, the system isn't heavily damped, so the response might not look super smooth, but that's acceptable. In human robot interaction, especially in rehab or assistive use and collaborative robotics, the system is needed to respond quickly to user input. Because human behaviour is not totally damped, too much damping would make it feel sluggish and uncomfortable.

Those highlights a key limitation of the current system that it performs reliably under controlled and fixed conditions but may not generalize well to dynamic or varying use cases. The solution will be considered in future improvement. Therefore, for this project, this situation will not be considered for next tests. Following this, the next section evaluates system latency based on the video took in this section.

#### 4.2.3 System Latency and Responsiveness

To evaluate the system's real-time responsiveness, two types of latency were assessed. The signal processing delay introduced by the filtering algorithm, and the total system latency from muscle contraction to motor response. The design specification for latency was set to be 0.5s.

The optical sensing system applies a combination of a Kalman filter and a low-pass filter to smooth the photodiode voltage signal. While this improves signal stability and reduces noise, it also introduces a certain level of processing delay. To quantify this delay, both the raw input voltage and the filtered output signal during a single muscle contraction event were visualized using the Arduino Serial Plotter, as already shown in Figure 50b. In that test, the sampling interval was set to 200 ms, meaning the system updated the signal at 5Hz. Therefore, the delay in signal processing should be 0.2s. however, as shown in the plot, when arm move quickly, the rising edge of the filtered signal appeared maximum five samples later than that of the raw signal. This corresponds to a processing delay of about  $5 \times 200ms = 1s$ . Which means if quick movement are made the system would spent a long-time approach to the target position as shown in Figure 53. Three frames were shown in Figure 53, the frame when arm start move, the frame when exoskeleton start move and the frame when exoskeleton approached target position. Since the frames were obtained from 60fps video, each frame corresponds to 0.017s.



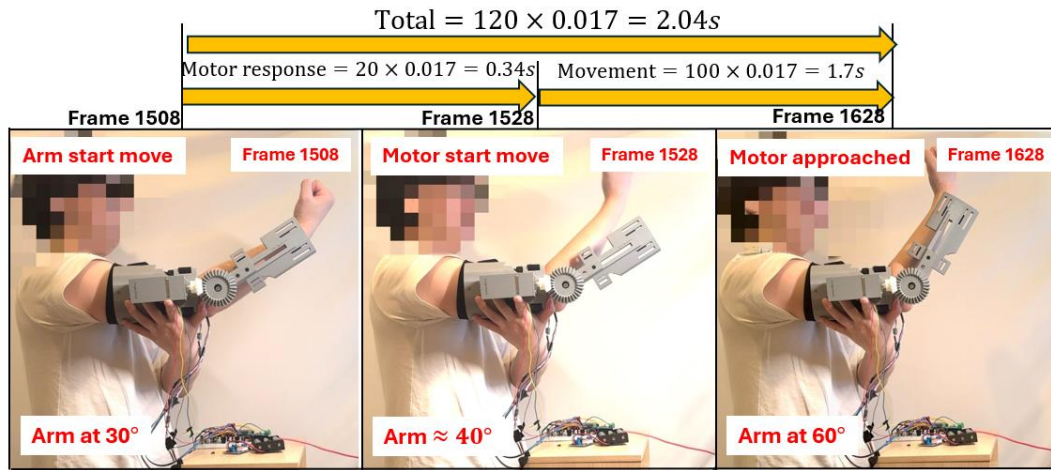


Figure 53. System response frame with time

Figure 53 shows the motor response time is about 0.34s (20 frames) And the total time for exoskeleton move to the target position used 2.04s for  $30^\circ$ . The test result is slightly larger than theory of 0.2s, which might because of the time needed for MCU calculate control degree and.... And the 2.04s total time for 30degree is longer than expectations.

Although the motor response delay of 0.3s is within the required 0.5s, the maximum exoskeleton move time is significantly higher than the 0.5s which might still be an issue. Therefore, to reduce the delay caused by signal processing, but considering the much high sampling frequency might cause overheat of the motor as discussed in motor control Section 3.3.4, the sampling time was adjusted from 200ms to 100ms, Kalman Filter `errorEstimate` Parameter was increased to 1 and the motor speed was increased from 20 to 30. With the updated data, the following section evaluates the improved overall system latency.

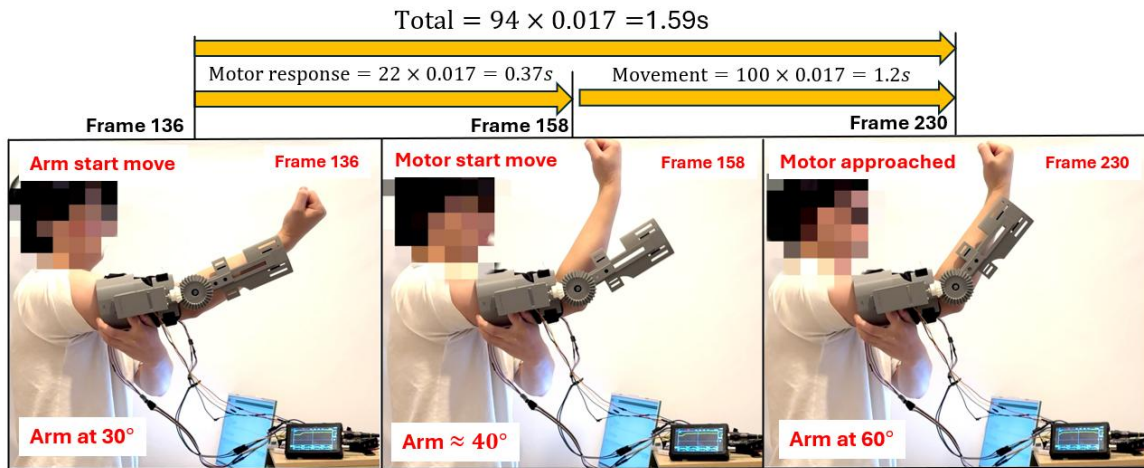


Figure 54. Improved system response frame with time

To reassess the system latency after these adjustments, the same video based frame comparison method was applied, and the results are shown in Figure 54.

After the improvement, the system still showed a delay of about 20 frames, equivalent to a delay of 0.3 s. However, the total driving time of the exoskeleton was shortened to 1.59s, including signal acquisition, filtering, angle mapping and motor driving.

### 4.3 Specification Compliance Review (Conclusion and Limitations)

In conclusion, the integrated exoskeleton system was designed to meet key functional and performance goals, including reliable muscle signal detection, accurate motor control, low response latency, and safe, wearable construction. Based on the results of the testing, the prototype met most of these targets and showed a satisfied performance as a low cost upper limb optical sensor rehabilitation device.

During testing, the optical sensor was able to detect biceps contractions consistently, and the system responded by driving the motor to assist elbow movement. Under controlled conditions, the exoskeleton followed the user's intended motion with reasonable accuracy ( $\pm 6.1^\circ$ ), and the delay between signal detection and motor response was kept within the design goal of 0.5 seconds. Mechanically, the 3D printed structure was lightweight and comfortable to wear with the soft addons, meeting safety and usability requirements.

However, several limitations were observed. One of the main challenges is that the system must be carefully adjusted and calibrated before use. Small differences in how the sensor is positioned, such as strap tightness, exact sensor location, or initial arm posture, can significantly affect the signal range. This is because the control algorithm uses a simple linear mapping based on the highest and lowest voltages measured during an initial calibration phase. If the setup changes, for example from arm held horizontally to arm hanging down, the signal pattern also changes, which can cause errors in control. As a result, if the device is removed and worn again without recalibration, the same muscle action may not produce the same motor response.

Despite this, once properly calibrated, the system showed good repeatability and reliable performance across multiple test cycles. Accuracy was highest at extreme angles like  $0^\circ$  and  $90^\circ$  and in mid range, while slightly larger errors were observed around edge positions such as  $60^\circ$ , likely due to non-linearities in muscle signal behaviour that the linear mapping cannot fully capture. There are some practical limitations to the mechanical design. The motor housing is very compact, limiting heat dissipation. And because there is no feedback loop, the system lacks damping, resulting in slightly jerky motion. However, these deficiencies are acceptable within the scope of the project, as real-time response takes precedence over smooth motion. Future improvements may include adaptive signal processing, better motor control strategies, and more pose-independent calibration methods.

However, the one of the limitations is all the testing was conducted on only one healthy person, with a limited number of trials. As a result, the data obtained may not fully represent the performance of the system across different users or in real-world rehabilitation scenarios. Variations in muscle, skin condition, and wearing consistency could all affect sensor readings and control accuracy. Therefore, while the test results validate the system functionality, further experiments with a broader participant group and more diverse conditions will be necessary to fully evaluate the generalizability and robustness of the system.

In the end, a summary of how the system met each of its specification is provided in Table 18.



Table 18. Specification Compliance Summary

Specification	Achieved	Explanation
Optical sensor detects muscle contraction	Yes	System uses photodiodes + IR LED to detect contraction, signal patterns correlate with motion
Optical signal accuracy $\geq 70\%$ or clearly reflects activity	Yes	Signal shows consistent, repeatable patterns ( $\pm 6.1^\circ$ ), detailed sEMG comparison not performed due to scope
TIA + filter circuit produces clean, stable voltage signal	Yes	Noise reduced, and signal clearly visible and readable (slight 50Hz noise), and second stage amp and 0.6Hz HPF added
Real-time ADC sampling and digital processing	Yes	Also added a Kalman + 50Hz LPF filtering
Muscle activity data library with $\geq 50$ samples	Partially	Control algorithm changed to real-time calibration and thresholding
PID control for motor movement	No	PID not implemented due to the time, but system works well
Motor response delay $< 0.5$ s	Yes	Motor begins movement within 0.3 s, but full motion slower
<b>Stretch goal:</b> Exoskeleton design and 3D printing	Yes	Fully built, tested, and refined, mechanical gear reduction included
<b>Stretch goal:</b> Advanced control algorithm	No	Current logic sensitive to sensor placement/posture, machine learning Method needed for improvement

## 5 Conclusion

### 5.1 Project Conclusion

This project developed a prototype of smart exoskeleton system for upper-limb rehabilitation, capable of assisting elbow movement based on voluntary muscle activation. The core concept was to explore the feasibility of using a non-invasive, low-cost optical sensing method to detect biceps contraction and translate it into real-time motor control rather than traditional sEMG method. To achieve this, the system was first designed an optical sensing unit using infrared photodiodes and a transimpedance amplifier circuit, then a signal processing and motor control algorithm based on Kalman and low-pass filtering, and a lightweight 3D-printed exoskeleton that provides 1DOF at the elbow joint were developed. Each subsystem was developed, integrated, and tested. The final prototype, built with a total component cost of approximately £100, was able to detect muscle activity reliably, map the signal into control angles, and actuate a stepper motor via a bevel gear mechanism to assist elbow flexion in real time. It successfully demonstrates the feasibility of optical sensing in wearable assistive devices.

A detailed review of the system's performance and specification compliance is presented in Section 4.3. Table 18 summarizes each requirement from the original project proposal and provides justification for any adjustments made. Overall, the system have met most of the goals. It achieved real-time sensing and actuation with acceptable accuracy ( $\pm 6.1^\circ$ ) and latency (0.3s), offered safety and comfort, and demonstrated stable functionality under controlled calibration.

However, the limitations are also obvious. The most significant issue lies in the complexity of muscle behaviour and the sensitivity of optical sensing to physical placement. This system only performs reliably when the arm is held in a fixed posture during calibration and operation. Any change in posture (arm hanging versus horizontal) alters the signal range and invalidates the linear mapping used for control. Furthermore, the control system remains open-loop and lacks torque feedback. A closed loop control with torque sensing and more advanced control strategies, such as machine learning models, would significantly improve accuracy and robustness. Other constraints include the single DOF implementation and limited testing with only one healthy tester under controlled conditions.

As an undergraduate project, although the initial goals were conservative, a lot of time and efforts were spent on it, and there were many more factors to consider than originally thought during the development process. For the project integrity, this project eventually realized a prototype of the smart upper limb rehabilitation exoskeleton. This project certainly has some limitations, but these inadequate also proves clear directions for further development. The project will in certain to achieve better results and performance if more resources are invested.

## 5.2 Future Improvements

Since the project aims to develop a prototype of the smart optical exoskeleton and is trying to demonstrate a functional platform that confirms the feasibility of optical sensing in wearable assistive devices. During the development of the project, some possible improvements were considered. One of the key limitations is the complexity of capturing optical signals from human arm muscles. The upper limb consists of numerous muscle groups and, due to its 7 DOF, has a wide variety of movement patterns. Therefore, a large amount of data is required to understand and model the signal behaviour for different actions and users. To address this issue, future versions may introduce machine learning to analyse and classify the collected signals. With a sufficiently large and diverse dataset, it may be possible to isolate key features from the muscle signals and improve control accuracy. This would enable the exoskeleton to adapt to different users and usage conditions, reduce reliance on current fixed posture calibration, and enable smarter and more responsive control.

Based on more robust and adaptive sensing, the exoskeleton can also be expanded to support more degrees of freedom. For example, for patients severely impaired by stroke, a multi-joint assistive device with for example 5 DOF (including elbow, wrist, and finger movements) could provide more comprehensive support. In addition, more efficient, bio-inspired actuation methods, such as artificial muscle-like actuators [30], could be considered in the future.

## 5.3 Consideration of System within the Wider Context

The initial motivation behind this project was to support patients recovering from stroke or neuromuscular injuries by helping them regain basic arm muscle function. Specifically, the goal was to assist elbow flexion through muscle-driven control, enabling users with weakened upper-limb mobility to gradually restore movement through repeated, intention-based rehabilitation. Although the current prototype cannot yet fully achieve this aim in clinical settings, it successfully demonstrates the feasibility of using optical sensing and low-cost hardware to build a wearable assistive device.

With a total system cost of around £100, the device provides an affordable alternative to conventional rehabilitation robots, which are often bulky, expensive, and restricted to hospital environments. The lightweight, non-invasive design and simple signal calibration process make it particularly suited for

home use or in low-resource settings, where access to regular therapy is limited. This makes the system especially valuable in the context of growing global healthcare pressures.

Looking beyond its initial goal, the system also shows promise for broader applications such as assisting elderly individuals with basic daily arm movements. As populations continue to age, the demand for personal support devices that can help older adults maintain mobility, independence, and muscle condition is steadily increasing. With future improvements—such as adaptive control algorithms, more degrees of freedom, and personalized calibration—the system could be expanded into a smart wearable assistant that adjusts its assistance based on user strength and behaviour. This would help address not only rehabilitation needs but also age-related decline in muscle control and coordination.

Furthermore, the modularity and use of open-source components mean this system could serve as a research or educational platform for those working on low-cost biomedical devices. It aligns well with the trend of democratizing medical technology by making it accessible to underserved populations, enabling more inclusive and sustainable healthcare solutions in the future.

## 5.4 Reflection on Project Management

The project significantly strengthened research and development capabilities in managing a technical engineering process from initial concept to prototype implementation. Through this experience, project planning, prioritisation, communication, and troubleshooting skills were developed. At the same time, a range of real world challenges were overcome, such as delays, component failures, and time misjudgment. These issues highlighted the importance of adaptability and effective risk management. Although the project objectives were ultimately achieved, the outcome relied heavily on continuous problem-solving and iterative replanning.

Reflecting the project progress, the management process began with a clear division of the system into three main parts: optical sensor circuit, control algorithm with motor drive, and exoskeleton hardware. At the outset of the project, extensive background literature was reviewed prior to each weekly meeting. Summaries, questions, and notes from previous group meetings were documented systematically. This approach significantly facilitated early familiarisation with the project, while also supporting a clearer understanding of key challenges and task prioritisation. A Gantt chart was then created to outline the key milestones and deadlines (Appendix II), and buffer time was reserved for each major stage. According to the plan, the sensor and control system are scheduled to be completed in the first semester, the exoskeleton is expected to be completed in the second semester, and March 3 is the deadline for the final system integration.

Despite careful planning, the project encountered significant issues early on. As documented in the first and second review forms (24/10/2024 and 03/12/2024) in Appendix I, the university system upgrade caused unexpected delays in obtaining essential components, significantly affected planned schedule. Because this project depended heavily on practical lab-based testing, this delay was a major concern. To adapt, task priorities were rearranged, deciding to begin developing the signal processing and motor control algorithms first, since these tasks did not immediately require hardware components. In addition, some components were borrowed from supervisor, including the Feather M4 MCU and a stepper motor, allowing to familiarise with the programming environment and hardware interfaces in advance. During discussions with workshop staff, it was revealed that component ordering could be facilitated through the RS platform. This enabled the early acquisition of critical components and allowed practical testing to commence by late November. Prior experience in developing a pulse oximeter during the second year of study contributed to the

accelerated progress of the sensor development phase. Initial circuit design and testing were completed by the end of the semester. However, progress was hampered during the winter break due to poor use of time, partly due to delayed execution of tasks. Although buffer time was originally planned, it was not used effectively.

In the second semester, more time is arranged for the project due to a lighter academic load. This allowed a buffer to recover lost time and meet the goals outlined in the third progress review (11/02/2025), where both core subsystems were completed. The project was then moved on to the stretch goal that design and print the exoskeleton before the March 3rd deadline. This careful staging and built-in buffer time proved essential to keeping the project on track. However, writing the dissertation presented another challenge. Despite early encouragement from the supervisor to begin writing, the time required for drafting was underestimated. An attempt was made to produce a complete first draft in a single stage rather than adopting an incremental approach. This strategy proved ineffective, resulting in a significant delay, that although the initial plan targeted a full draft submission by March 27th, substantial progress was not achieved until April. For future projects, a staged writing strategy is recommended to distribute the workload more evenly and mitigate time pressure near deadlines.

One final unexpected issue occurred during system testing. The MCU was accidentally damaged due to high motor holding current at a fast sampling rate. This incident, mentioned in the fifth review form (25/03/2025), caused delays in test data collection. But under the help with supervisor, a replacement MCU was received. In the meantime, I used this setback as an opportunity to improve formatting, including tables and figures, to strengthen the quality of the dissertation.

Several project management strategies proved especially effective and will be valuable for future engineering projects. The early risk identification and flexible task reordering enabled consistent progress despite obstacles. Building in buffer time for every major milestone made the timeline more resilient. However, one area that clearly needs improvement is time management for documentation, especially final reporting, which should have started earlier and been approached iteratively. The MCU failure also emphasised the importance of hardware testing safeguards and redundancy planning.

In summary, this project provided hands-on experience managing a complex technical task with multiple dependencies, risks, and deadlines. The skills in proactive problem-solving, re-prioritisation, and maintaining communication with stakeholders were developed. These lessons will be essential for addressing future engineering challenges with improved confidence, practical awareness, and methodological discipline.

## 6 References

- [1] World Health Organization, "Stroke (Cerebrovascular accident)," *WHO Regional Office for the Eastern Mediterranean*. [Online]. Available: <https://www.emro.who.int/health-topics/stroke-cerebrovascular-accident/index.html> [Accessed: Oct. 17, 2024].
- [2] R. Abbasi, D.-E. Peppas, P. Spyritos, I. U. H. Awan, and M. Shoaib, *Design of an Intelligent Exoskeleton for Patient Rehabilitation Assistance*, Group Design Project Report, Module MAE7003-B, University of Bradford, Apr. 2017. [Online]. Available: <https://www.researchgate.net/publication/328758301> [Accessed: Mar. 7, 2025].
- [3] T. Proietti, E. Ambrosini, A. Pedrocchi, and S. Micera, "Wearable Robotics for Impaired Upper-Limb Assistance and Rehabilitation: State of the Art and Future Perspectives," *IEEE Access*, vol. 10, pp. 106117-106134, 2022, doi: 10.1109/ACCESS.2022.3210514.
- [4] L. Cen, H. Han, and J. Kim, "Optical muscle activation sensors for estimating upper limb force level," in *2011 IEEE International Instrumentation and Measurement Technology Conference*, 10-12 May 2011 2011, pp. 1-4, doi: 10.1109/IMTC.2011.5944228.
- [5] Y. T. Wu, M. K. Gomes, W. H. da Silva, P. M. Lazari, and E. Fujiwara, "Integrated Optical Fiber Force Myography Sensor as Pervasive Predictor of Hand Postures," *Biomedical Engineering and Computational Biology*, vol. 11, p. 1179597220912825, 2020, doi: 10.1177/1179597220912825.
- [6] L. Blanchet, S. Achiche, Q. Docquier, P. Fisette, and M. Raison, "A procedure to optimize the geometric and dynamic designs of assistive upper limb exoskeletons," *Multibody System Dynamics*, vol. 51, no. 2, pp. 221-245, 2021/02/01 2021, doi: 10.1007/s11044-020-09766-6.
- [7] S. Anwer et al., "Rehabilitation of Upper Limb Motor Impairment in Stroke: A Narrative Review on the Prevalence, Risk Factors, and Economic Statistics of Stroke and State of the Art Therapies," (in eng), *Healthcare (Basel)*, vol. 10, no. 2, Jan 19 2022, doi: 10.3390/healthcare10020190.
- [8] F. Molteni, G. Gasperini, G. Cannaviello, and E. Guanziroli, "Exoskeleton and End-Effector Robots for Upper and Lower Limbs Rehabilitation: Narrative Review," *PM&R*, vol. 10, no. 9, Suppl 2, pp. S174–S188, Sep. 2018, doi: 10.1016/j.pmrj.2018.06.005.
- [9] C. Greco, P. Kotak, C. Lamuta, and L. Pagnotta, "The evolution of mechanical actuation: from conventional actuators to artificial muscles," *International Materials Reviews*, vol. 67, no. 6, pp. 575–601, 2022, doi: 10.1080/09506608.2021.1971428.
- [10] J. Pustavrh, M. Hočevár, P. Podržaj, A. Trajkovski, and F. Majdič, "Comparative study of a hydraulic, pneumatic and electric linear actuator system," *Scientific Reports*, vol. 13, no. 1, Nov. 2023, Art. no. 20938, doi: 10.1038/s41598-023-47602-x.
- [11] G. Rau, C. Disselhorst-Klug, and R. Schmidt, "Movement biomechanics goes upwards: from the leg to the arm," *Journal of Biomechanics*, vol. 33, no. 10, pp. 1207-1216, 2000/10/01/ 2000, doi: [https://doi.org/10.1016/S0021-9290\(00\)00062-2](https://doi.org/10.1016/S0021-9290(00)00062-2).
- [12] S. C. F. A. von Werder and C. Disselhorst-Klug, "The role of biceps brachii and brachioradialis for the control of elbow flexion and extension movements," *Journal of Electromyography and Kinesiology*, vol. 28, pp. 67-75, 2016/06/01/ 2016, doi: <https://doi.org/10.1016/j.jelekin.2016.03.004>.
- [13] A.M. Zanchettin, P. Rocco, L. Bascetta, I. Symeonidis, and S. Peldschus, *Kinematic motion analysis of the human arm during a manipulation task*. 2010, pp. 1-6.
- [14] Lybrate, "Arm Muscles (Human Anatomy): Image, Functions, Diseases and Treatments," Mar. 18, 2023. [Online]. Available: <https://www.lybrate.com/topic/arm-muscles-image>
- [15] Apokusay, "Arm muscles structure diagram medical science vector image," VectorStock, Image ID: 48838352, Oct. 2023. [Online]. Available: <https://www.vectorstock.com/royalty-free-vector/arm-muscles-structure-diagram-medical-science-vector-48838352>

- [16] H. Han and J. Kim, "Novel muscle activation sensors for estimating of upper limb motion intention," in *2009 Annual International Conference of the IEEE Engineering in Medicine and Biology Society*, 3-6 Sept. 2009 2009, pp. 3767-3770, doi: 10.1109/IEMBS.2009.5334485.
- [17] R. H. Chowdhury, M. B. I. Reaz, M. A. Ali, A. A. A. Bakar, K. Chellappan, and T. G. Chang, "Surface Electromyography Signal Processing and Classification Techniques," *Sensors*, vol. 13, no. 9, pp. 12431-12466doi: 10.3390/s130912431.
- [18] D. Wu *et al.*, "A Surface Electromyography (sEMG) System Applied for Grip Force Monitoring," *Sensors*, vol. 24, no. 12, doi: 10.3390/s24123818.
- [19] L. Cen, H. Han, and J. Kim, "Optical muscle activation sensors for estimating upper limb force level," in *2011 IEEE International Instrumentation and Measurement Technology Conference*, 10-12 May 2011 2011, pp. 1-4, doi: 10.1109/IMTC.2011.5944228.
- [20] M. Shahmohammadi, B. Guan, R. V. Godoy, A. Dwivedi, P. Nielsen, and M. Liarokapis, "On lightmyography based muscle-machine interfaces for the efficient decoding of human gestures and forces," *Scientific Reports*, vol. 13, no. 1, p. 327, 2023/01/06 2023, doi: 10.1038/s41598-022-25982-w.
- [21] T. Miyake, T. Minakuchi, S. Sato, C. Okubo, D. Yanagihara, and E. Tamaki, "Optical Myography-Based Sensing Methodology of Application of Random Loads to Muscles during Hand-Gripping Training," *Sensors*, vol. 24, no. 4, doi: 10.3390/s24041108.
- [22] S. Hauschild, F. John, H. Hellbrück, and R. Kusche, "Optical Muscle Contraction Detection via Frequency Multiplexed LEDs," in *2024 IEEE International Symposium on Medical Measurements and Applications (MeMeA)*, 26-28 June 2024 2024, pp. 1-6, doi: 10.1109/MeMeA60663.2024.10596742.
- [23] A.Bansal, S. Hou, O. Kulyk, E. Bowman, and I. Samuel, "Wearable Organic Optoelectronic Sensors for Medicine," *Advanced Materials*, vol. 27, 12/01 2014, doi: 10.1002/adma.201403560.
- [24] Adafruit Industries, "Adafruit Feather M4 Express - Featuring ATSAMD51," *Adafruit*, [Online]. Available: <https://www.adafruit.com/product/3857>. [Accessed: Apr.22, 2025].
- [25] Microchip Technology Inc., *MCP6291/2/4: 2.7V to 6.0V, Low-Noise Op Amps with Rail-to-Rail Input and Output*, DS21824F, 2016. [Online]. Available: <https://docs.rs-online.com/2f4a/0900766b813813f6.pdf>
- [26] ExRx.net, "Body Segment Parameters," [Online]. Available: <https://exrx.net/Kinesiology/Segments>. [Accessed: Apr.22, 2025].
- [27] R. Uwamahoro, K. Sundaraj, and F. S. Feroz, "Effect of Forearm Postures and Elbow Joint Angles on Elbow Flexion Torque and Mechanomyography in Neuromuscular Electrical Stimulation of the Biceps Brachii," *Sensors*, vol. 23, no. 19, doi: 10.3390/s23198165.
- [28] PBC Linear, "Stepper Motor Support – Technical Data Sheet," [Online]. Available: <https://pages.pbclinear.com/rs/909-BFY-775/images/Data-Sheet-Stepper-Motor-Support.pdf>. [Accessed: Apr.22, 2025].
- [29] D. Sene, "SimpleKalmanFilter," GitHub, 2019. [Online]. Available: <https://github.com/denyssene/SimpleKalmanFilter>. [Accessed: Apr.27, 2025].
- [30] J. Lee *et al.*, "Intelligent upper-limb exoskeleton integrated with soft bioelectronics and deep learning for intention-driven augmentation," *npj Flexible Electronics*, vol. 8, no. 1, p. 11, 2024/02/10 2024, doi: 10.1038/s41528-024-00297-0.
- [31] H. Liu, J. Tao, P. Lyu, and F. Tian, "Human-robot cooperative control based on sEMG for the upper limb exoskeleton robot," *Robotics and Autonomous Systems*, vol. 125, p. 103350, 2020/03/01/ 2020, doi: <https://doi.org/10.1016/j.robot.2019.103350>.
- [32] A.M. Khan *et al.*, "Estimation of Desired Motion Intention and compliance control for upper limb assist exoskeleton," *International Journal of Control, Automation and Systems*, vol. 15, no. 2, pp. 802-814, 2017/04/01 2017, doi: 10.1007/s12555-015-0151-7.



- [33] Q. Wu, B. Chen, and H. Wu, "Neural-network-enhanced torque estimation control of a soft wearable exoskeleton for elbow assistance," *Mechatronics*, vol. 63, p. 102279, 2019/11/01/ 2019, doi: <https://doi.org/10.1016/j.mechatronics.2019.102279>.
- [34] "Bevel Gear," IQS Directory. [Online]. Available: <https://www.iqsdirectory.com/articles/gear/bevel-gear.html>. [Accessed: Apr.29, 2025].
- [35] I. Cuesta, E. Martinez-Pañeda, A. Díaz, and J. M. Alegre, "The Essential Work of Fracture parameters for 3D printed polymer sheets," *Materials & Design*, vol. 181, p. 107968, 2019/11/05/ 2019, doi: <https://doi.org/10.1016/j.matdes.2019.107968>.
- [36] M. A. Mazlan, M. A. Anas, N. A. Nor Izmin, and A. H. Abdullah, "Effects of Infill Density, Wall Perimeter and Layer Height in Fabricating 3D Printing Products," (in eng), *Materials (Basel)*, vol. 16, no. 2, Jan 10 2023, doi: 10.3390/ma16020695.
- [37] TE Connectivity, *MEAS Detector Assembly EPM-4001: SpO<sub>2</sub> Optical Sensor Component*, Sept. 2017. Accessed: Oct. 25, 2024. [Online]. Available: <https://docs.rs-online.com/d6c0/0900766b81712677.pdf>
- [38] OPTTEK Technology Inc., *OP240/OP245 Series Plastic Infrared Emitting Diode*, Issue A.2, Apr. 2008. Accessed: Oct. 25, 2024. [Online]. Available: <https://docs.rs-online.com/feb3/0900766b8151e48b.pdf>
- [39] Microchip Technology Inc., *MCP6291/1R/2/3/4/5: 10 MHz, 1.0 mA, Rail-to-Rail Op Amp*, DS21812E, Apr. 2007. Accessed: Oct. 25, 2024. [Online]. Available: <https://docs.rs-online.com/2f4a/0900766b813813f6.pdf>

## Appendices

### Appendix I – Project Progress Forms

Project Review Proforma – Review number: 1

Date: 24/10/2024

<b>Summarised Planned State of Project:</b> Understand the content and purpose of the project smart exoskeleton for patient rehab and possible approaches. For example, explore how exoskeletons can help patients in rehabilitation and why optical sensors have advantages over traditional electronic sensors.  Should confirm the project goals and classify their types. Identify the required components and their roles. Complete the project proposal.	<b>Actual Progress Since Last Review</b> Progress is with expectations. I have gained a clear understanding of the project aim and possible approaches. I will using optical sensors to detect bicep activity (using IR light) and processing the muscle signals by TIA and filters, and amplifiers. These signals will then be used to control the motor via a control system, while simultaneously generating a library to record different motor degrees corresponding to muscle activity levels. I will then plan the design of a 1DOF upper arm exoskeleton for system package. The Gantt chart has been completed, and the project proposal, including all necessary sections, has been finalized.
<b>Next Steps and Supervisor Feedback</b> The project is well planned and is about to start. There is a risk of delayed component ordering due to the university system upgrade, which could impact the plan if the optical system components are not received by November 15th. The plan is, proceeded with the plan by starting the signal processing and control system algorithm work in advance to ensure readiness when the components arrive.	

<p><b>Summarised Planned State of Project:</b></p> <p>At this stage, according to the project time plan, I was expected to have completed the basic signal acquisition and processing, as well as the motor control circuit setup and testing.</p> <p>The plan is done the development of the initial setup for capturing muscle activity using the optical sensor system. And the ADC Processing and Filtering by Implementing ADC-based signal acquisition, processing, and applying a 50Hz noise filter to improve signal clarity. Also should develop and test the basic motor control logic using the Feather M4 MCU, ensuring proper response to processed input signals.</p>	<p><b>Actual Progress Since Last Review</b></p> <p>Due to university system maintenance, the ordering of electronic components was delayed,</p> <p>So, I started Implemented ADC-based signal acquisition and filtering in Arduino IDE, using the Feather M4 MCU. And developed and tested the basic stepper motor control logic. Also designed a 50Hz noise filter, which will be further adjusted once real input signals from the optical sensor circuit are available.</p>
<p><b>Next Steps and Supervisor Feedback</b></p> <p>Refining signal processing and motor control algorithms, finalizing the schematic design and simulation of the optical sensor signal acquisition circuit (essential for report), allowing for immediate circuit assembly once components arrive. Validating and optimizing the filtering algorithms, adjusting parameters based on actual signal inputs. Calibrating sensor data and tuning motor control.</p>	

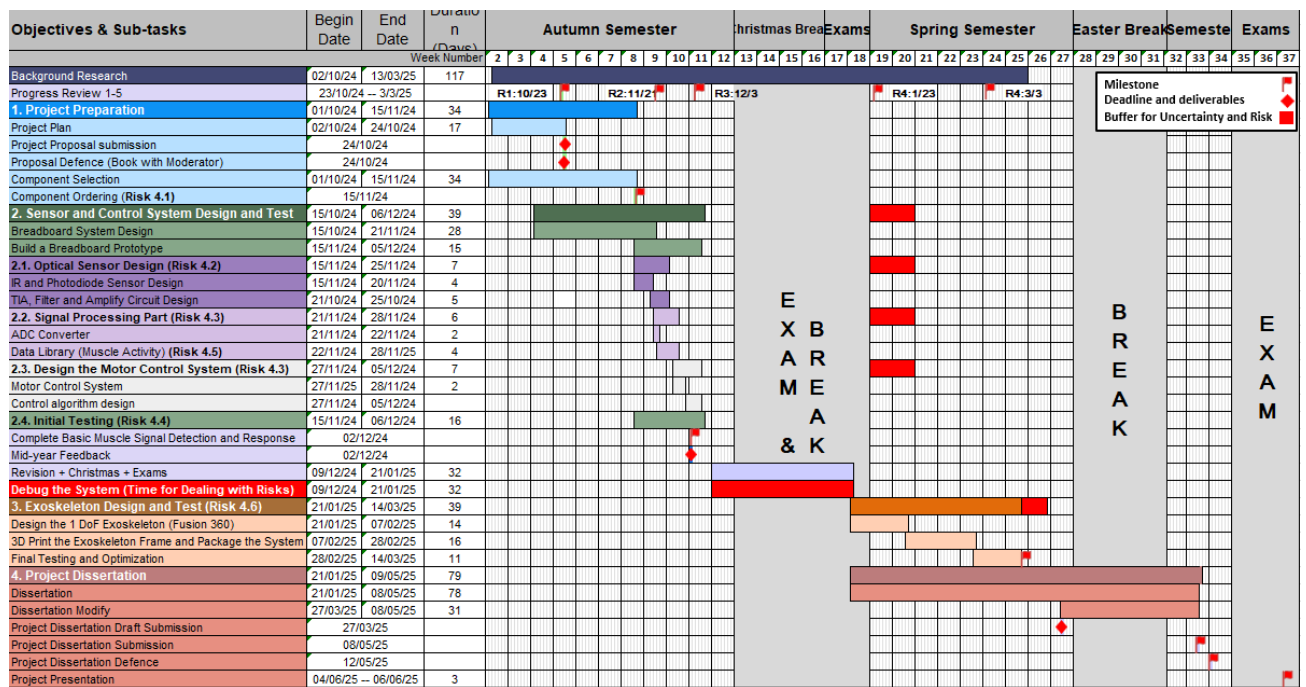
<p><b>Summarised Planned State of Project:</b></p> <p>Complete the implementation and testing of the optical sensor signal acquisition circuit and ADC-based data processing.</p> <p>Ensure that the motor control logic runs smoothly and optimizes the control response based on the processed muscle activity signal.</p> <p>Complete the mechanical design of the exoskeleton, including 3D modelling and structural analysis for 3D printing.</p> <p>In addition, this is also a buffer period for adjustment: before entering full system testing, time needs to be reserved to address possible delays in the previous stages, such as optimizing signal processing, debugging control algorithms, and completing hardware integration.</p>	<p><b>Actual Progress Since Last Review</b></p> <p>During this phase, the signal acquisition, processing, and motor control systems were successfully developed and tested. The optical sensor circuit was built and debugged, with a hardware-based filter replacing the initial digital design for better real-time performance. The ADC processes signals from three photodiodes, averaging their outputs for a more stable control signal. The motor angle (0°-90°) is determined by signal differences, with a 0.5s sampling time, though further optimization is needed. The 1-DoF exoskeleton design has also begun, including 3D modelling and structural planning for integration. The next phase will focus on refining control accuracy and advancing exoskeleton development.</p>
<p><b>Next Steps and Supervisor Feedback</b></p> <p>Junkai has made excellent progress and has already shown an early prototype of the optical and signal processing elements. He's dealt well with challenges as they have arisen and is already beginning to plan for his report. I'm extremely confident in Junkai submitting a very strong project and report.</p>	

<p><b>Summarised Planned State of Project:</b></p> <p>The goal for this stage was to complete the core elements of the system. Completion of the 3D printing of the exoskeleton structure. Functional testing of the optical sensing circuit and control system. Preliminary integration of all modules into a wearable prototype</p> <p>This stage also marks the transition into final system testing, with the intention of assembling all subsystems and preparing for full system validation and performance evaluation.</p>	<p><b>Actual Progress Since Last Review</b></p> <p>Since the previous review, the planned milestones have been successfully achieved. The 1-DoF exoskeleton was fully modelled in Fusion 360 and subsequently fabricated using FDM 3D printing. The printed components were assembled and inspected, confirming the feasibility of the mechanical design.</p> <p>The optical sensing and motor control systems have been refined and are now ready for integration. All hardware modules are prepared, and the system is now entering the final testing phase. Minor hardware modifications were applied to improve thermal dissipation and fit. The control system, including Kalman filter parameters and thresholding logic, is being prepared for final adjustments during full system operation.</p>
<p><b>Next Steps and Supervisor Feedback</b></p> <p>Following discussions with the supervisor, it was agreed that the next priority is to complete the integration of all components and begin final system testing as scheduled. Key tasks will include refining signal stability, tuning Kalman filter parameters, and validating the control system's responsiveness under simulated usage conditions.</p> <p>In parallel, work will begin on preparing the final dissertation. Especially finish the optical sensing part first.</p>	

<b>Summarised Planned State of Project:</b> According to the original project timeline, this should be the time that finishing all the project and have dissertation draft finish. Time for feedback	<b>Actual Progress Since Last Review</b> The project design and implementation have been completed as planned, hardware integration and system testing. However, the writing of the dissertation draft is still in progress and has some delay. The current writing is focused on the optical sensing system section, with remaining sections to follow. However, the project have finished.
<b>Next Steps and Supervisor Feedback</b> The immediate priority is to continue writing and complete the full dissertation draft. Following completion, the supervisor will provide detailed feedback to support revisions and ensure the final version is ready for submission.	



## Appendix II – Project Gantt Chart



## Appendix III – Arduino Control Code

```
#include <Adafruit_MotorShield.h>

// Create the motor shield object
Adafruit_MotorShield AFMS = Adafruit_MotorShield();
Adafruit_StepperMotor *myMotor = AFMS.getStepper(200, 2);

// Define variables
float baseline = 0.0;          // Relaxed voltage
float contractionMin = 3.0;    // Minimum voltage during contraction
const int numSamples = 50;    // Samples for calibration
bool initialized = false;     // Flag for completed calibration
unsigned long lastReadTime = 0;
const int readInterval = 100; // 100 ms sampling interval

// Motor and signal mapping
const float maxAngle = 180.0; // Maximum elbow movement (0-90°)
float currentAngle = 0.0;

// Kalman Filter variables
float estimate = 0.0;
float errorEstimate = 0.1;
float errorMeasure = 0.005;
float kalmanGain = 0.0;

// Low-pass filter variables
float filteredVoltage = 0.0;
const float alpha = 0.5; // LPF smoothing factor

// Function to read average voltage from A0, A1, A2
float readAverageVoltage() {
    int adcA0 = analogRead(A0);
    int adcA1 = analogRead(A1);
    int adcA2 = analogRead(A2);
    float voltageA0 = adcA0 * (3.3 / 1024.0);
    float voltageA1 = adcA1 * (3.3 / 1024.0);
    float voltageA2 = adcA2 * (3.3 / 1024.0);
    return (voltageA0 + voltageA1 + voltageA2) / 3.0;
}

float readVoltage() { //Test input, only A2)
    //int adcA0 = analogRead(A0);
    //int adcA1 = analogRead(A1);
    int adcA2 = analogRead(A2);
    //float voltageA0 = adcA0 * (3.3 / 1024.0);
    //float voltageA1 = adcA1 * (3.3 / 1024.0);
    float voltageA2 = adcA2 * (3.3 / 1024.0);
    return voltageA2;
}

// Kalman Filter function
float kalmanFilter(float measurement) {
    kalmanGain = errorEstimate / (errorEstimate + errorMeasure);
    estimate = estimate + kalmanGain * (measurement - estimate);
    errorEstimate = (1 - kalmanGain) * errorEstimate;
```

```

    if (errorEstimate < 1) {
        errorEstimate = 1;
    }
    return estimate;
}

// Low-pass filter function
float lowPassFilter(float currentInput, float lastOutput) {
    return alpha * currentInput + (1 - alpha) * lastOutput;
}

void setup() {
    Serial.begin(9600);
    while (!Serial);

    Serial.println("Initializing Motor Shield...");
    if (!AFMS.begin()) {
        Serial.println("Motor Shield not found. Check wiring.");
        while (1);
    }
    Serial.println("Motor Shield initialized.");
    myMotor->setSpeed(30); // Motor speed 20 RPM

    // --- Calibration Phase ---

    // Step 1: Relaxed - Measure Baseline
    Serial.println("Hold your arm relaxed for 5 seconds...");
    float totalRelaxed = 0.0;
    for (int i = 0; i < numSamples; i++) {
        totalRelaxed += readVoltage();
        delay(100); // (5s total)
    }
    baseline = totalRelaxed / numSamples;
    Serial.print("Baseline Voltage (Relaxed): ");
    Serial.println(baseline, 3);

    delay(1000);

    // Step 2: Contracted - Measure Minimum
    Serial.println("Fully contract your muscle for 5 seconds...");
    for (int i = 0; i < numSamples; i++) {
        float sample = readVoltage();
        if (sample < contractionMin) {
            contractionMin = sample;
        }
        delay(100); // (5s total)
    }
    Serial.print("Contraction Min Voltage: ");
    Serial.println(contractionMin, 3);

    estimate = baseline; // Initialize Kalman estimate
    filteredVoltage = baseline; // Initialize LPF output
    initialized = true;
}

```

```

    delay(2000);
}

void loop() {
    if (!initialized) return;

    unsigned long currentTime = millis();
    if (currentTime - lastReadTime >= readInterval) {
        lastReadTime = currentTime;

        float rawVoltage = readVoltage();
        float kalmanVoltage = kalmanFilter(rawVoltage);
        filteredVoltage = lowPassFilter(kalmanVoltage, filteredVoltage);

        // Calculate mapped angle
        float range = baseline - contractionMin;
        float delta = baseline - filteredVoltage; //filteredVoltage;
        float targetAngle = (delta / range) * maxAngle;

        // Constrain angle
        if (targetAngle > maxAngle) targetAngle = maxAngle;
        if (targetAngle < 0) targetAngle = 0;

        Serial.print("Mapped Target Angle: ");
        Serial.print(targetAngle/2);
        Serial.println(" degrees");
        Serial.print("Current Voltage: ");
        Serial.print(filteredVoltage);
        Serial.println(" V");

        // Stepper motor control
        int targetSteps = targetAngle / 1.8;
        int currentSteps = currentAngle / 1.8;
        int stepDifference = targetSteps - currentSteps;

        if (stepDifference > 0) {
            Serial.println("Moving FORWARD");
            myMotor->step(abs(stepDifference), FORWARD, DOUBLE);
        } else if (stepDifference < 0) {
            Serial.println("Moving BACKWARD");
            myMotor->step(abs(stepDifference), BACKWARD, DOUBLE);
        } else {
            Serial.println("Holding Position");
        }
        delay(100);
        currentAngle = targetAngle; // Update
    }
}

```